NOISE EFFECTS, EMITTANCE CONTROL, AND LUMINOSITY ISSUES IN LASER WAKEFIELD ACCELERATORS

by

SERGEY VALERIEV CHESHKOV, B.S.

DISSERTATION

Presented to the Faculty of the Graduate School of

The University of Texas at Austin

in Partial Fulfillment

of the Requirements

for the Degree of

DOCTOR OF PHILOSOPHY

THE UNIVERSITY OF TEXAS AT AUSTIN

May 2001

NOISE EFFECTS, EMITTANCE CONTROL, AND LUMINOSITY ISSUES IN LASER WAKEFIELD ACCELERATORS

APPROVED BY
DISSERTATION COMMITTEE:

Supervisor: _____

_____

_____

_____

_____

Acknowledgements

There is a number of people I wish to thank for their encouragement, help, and friendship during my years as a graduate student at UT. I am thankful to my advisor Toshi Tajima for guiding my thesis research in Laser Wakefield Acceleration and exposing me to new and exciting ideas. I learned a tremendous amount from him in the process of working on my Ph.D.

I wish to thank the people I collaborated with throughout my studies at UT: Toshi Tajima, Charles Chiu, Wendell Horton, Michael Downer of UT; Kaoru Yokoya of KEK; Pisin Chen and Ronald Ruth of SLAC. I really enjoyed our collaborative work on various aspects of advanced accelerators.

Special thanks to the experimentalists of Michael Downer's femtosecond group: Erhard Gaul, Paul LeBlanc, Andy Rundquist for the fruitful discussions. I want to acknowledge my current and former office mates and friends: Edmund Yu, Bernhard Rau, Nikhil Padhye, Koichi Noguchi, Evstati Evstatiev, Nikola Petrov, Hani Kaldass, Bo Hu, Tom Yudichak, Frank Breitling for their friendship and willingness to discuss physics and other things at any time.

I wish to thank my committee members Wendell Horton, Charles Chiu, Michael Downer and Rafael de la LLave who advised me while working on my dissertation.

I thank my whole family, especially my parents Katinka and Valeriy and

my brother Cvetan for encouraging me to pursue my graduate studies and for constantly asking me about my graduation date.

I am grateful to my wife Gergana Drandova for for all her love and help during these years.

Lastly, I would like to acknowledge the support of the US Department of Energy (grant # DE-FG03-96ER40954), a Japan Atomic Energy Research Institute grant, Institute for Fusion Studies, and the Physics Department of UT throughout my studies.

NOISE EFFECTS, EMITTANCE CONTROL, AND LUMINOSITY ISSUES IN LASER WAKEFIELD ACCELERATORS

Publication No. _____

Sergey Valeriev Cheshkov, Ph.D.
The University of Texas at Austin, 2001

Supervisor: Toshiki Tajima

To reach the new high energy frontiers (higher than a TeV center of mass energy) new acceleration methods seem to be needed. Plasma based wakefield accelerator is one possible candidate which can provide an ultra high gradient acceleration and thus make the total acceleration distance reasonable. However, the final energy is not the only requirement. The accelerator should maintain an excellent beam quality to meet the luminosity requirements at the Interaction Point (IP). One of the most important figures of merit which describe the quality of the beam is its emittance. We study the particle dynamics in laser pulse-driven wakefields over multi-stages in a several TeV range center of mass energy e^+e^- collider. The approach is based on a map of phase space dynamics over a stage of wakefield acceleration induced by a laser pulse (or electron beam). The entire system of the collider is generated with a product of multiple maps of wakefields, drifts, and magnets, etc. This systems map may include offsets of various elements of the accelerator, representing noise

and errors arising from the operation of such a complex device. We find that an unmitigated strong focusing of the wakefield coupled with the alignment errors of the position (or laser beam aiming) of each wakefield stage and the unavoidable dispersion in individual particle betatron frequencies leads to a phase space mixing and causes a transverse emittance degradation. The rate of the emittance increase in the limit of constant energy is proportional to the number of stages, the energy of the particles, the betatron frequency, the square of the misalignment amplitude, and the square of the betatron phase shift over a single stage. The accelerator with a weakened focusing force in a channel can, therefore, largely suppress the emittance degradation. To improve the emittance we introduce several methods: a mitigated wakefield focusing by working with a plasma channel, an approximately synchronous acceleration in a superunit setup, the "horn" model based on exactly synchronous acceleration achieved through plasma density variation and lastly an algorithm based on minimization of the final beam emittance to actively control the stage displacement of such an accelerator.

We analyze the IP Physics luminosity and background issues in a high beamstrahlung parameter regime using the Yokoya's Monte Carlo code "CAIN". The possibility for delivering polarized electron and positron beams at the collision point as an additional leverage to control the complicated background situation is also investigated. We prove that the initial beam polarization is not degraded significantly by the beam transport and acceleration in the plasma based wakefield accelerator and by the beamstrahlung at IP.

Finally, we propose a beam driven acceleration scheme which can provide an ultra high acceleration gradient (greater than 100 GeV/m). This scheme is based on a reasonable modification of current SLAC beam parameters.

Table of Contents

List of Figures

List of Tables

Chapter 1

Introduction

1.1 Linear Collider Future and Plasma Wakefield Acceleration

In the quest for exploring the fundamental properties of matter, high energy accelerators are essential. There has been a continuous progress in technology leading to higher particle energies, better beam quality and handling. The size and correspondingly the cost of these machines has been also increasing. As an example, the Next Linear Collider design [1] considers an acceleration distance of 30 km. It seems that a large technology jump is needed in order to keep future accelerator parameters within reasonable limits. Naturally, a high acceleration gradient can reduce the total accelerator size. The gradients achievable in today conventional radio frequency (RF) cavities are limited by the metal surface electric breakdown. The idea of using plasma waves (plasma wakefields) excited by laser beams for electron acceleration, first proposed by Tajima and Dawson [2] in 1979 provided a way to overcome this limit. At the time no suitable lasers were available to experimentally investigate the subject. With the advance of the Chirped Pulse Amplification technique (CPA) [3] very powerful femtosecond lasers are now available. The technology still has a long way to go, but there have already been proof of principle wakefield

experiments in many laboratories around the world [4, 5, 6], including at UT-Austin. We are now witnessing a second generation of wakefield experiments [7] with much better controlled wakefield properties. Many variants of the wakefield acceleration method are currently under consideration: plasma beat wave accelerator (PBWA) [8], where the wakefield is excited by beating two lasers with slightly different frequencies; laser wakefield accelerator (LWFA) [2, 5, 6] in which a femtosecond laser pulse generates the wakefield; plasma wakefield accelerator (PWFA) [9, 10] which uses an electron driver beam. These schemes use different methods to excite the wakefield or accelerating structure, but the basic idea is common. Thus, a common mathematical treatment of the acceleration process is possible when it is considered as an element of a system of a large scale high energy accelerator. An important feature of plasma based accelerators (for a review of properties, problems and limitations, see [11]) is their ability to sustain extremely large acceleration gradients ($\sim 100\,\mathrm{GV/m}$). In principle, it means several orders of magnitude higher energy gain than the ones achieved by the RF technology. For an accelerator in high energy physics the energy is one of the important parameters, but many others are also crucial for the successful operation of such an accelerator. Since the cross-sections decrease generally in inverse proportion to the squared energy of the beams, high luminosity is required to detect new physics. The requirement for luminosity, in turn, demands for low beam emittance. The geometrical luminosity is given by

$$\mathcal{L} = \frac{f_c N^2}{4\pi\sigma_x\sigma_y} = \frac{\gamma f_c N^2}{4\pi\sqrt{\epsilon_x\beta_x^*}\sqrt{\epsilon_y\beta_y^*}} \ , \tag{1.1}$$

where f_c is the collision frequency, N is the particle number per bunch, σ_x and σ_y are the r.m.s. beam sizes at the Interaction Point (IP), β_x^* and β_y^* are the

betatron lengths at the IP, ϵ_x and ϵ_y are the normalized transverse emittances of the beams, and γ is the Lorentz factor of the beams. The event rate for a particular process is obtained multiplying the luminosity by the cross-section of that process. Thus, the analysis of the performance of laser wakefield accelerators should consider all relevant beam parameters, such as emittance, in addition to the beam energy [12]. Emittance is a measure of the phase space volume of the beam so that it is directly related to the entropy of the beam (through a logarithm). A complex collider system, such as the laser wakefield collider, is bound to generate entropy over multiple stages of acceleration. Thus, the understanding of the emittance degradation and possible ways to suppress it is of principal importance for improving the discovery potential of such machines.

Yet, another problem comes from the Interaction Point (IP) physics considerations. Severe beam distortion and radiation loss might occur within microns of the collision point. Thus, the collective particle behavior during the collision needs to be studied and optimized as well. Typically, a collider based on wakefield plasma acceleration is pushed into a high beamstrahlung parameter regime [12] which is significantly different from the conventional collider operation. Systematic studies of this subject started in [12] are continued in this dissertation via use of the K. Yokoya's Monte Carlo based code "CAIN" [13]. A full manual is available on line, so here we just mention the most important physics processes included in the code and some details from the mentioned manual important for the present work.

"CAIN" is a FORTRAN Monte-Carlo code for the interaction involving high energy electrons, positrons, and photons. The objects that might be used

are two particle beams, lasers, and constant external fields. The interactions treated are:

- Classical interaction due to Coulomb field.
- Luminosity between electrons, positrons, and photons.
- Beamstrahlung and coherent pair creation by high energy photons in the beam field.
- Interactions with laser field.
- Classical and quantum interactions with an external field.
- Incoherent e^+e^- pair creation.

Polarization can be included in most of the effects.

1.2 Dissertation Outline

The chapters of this dissertation are self contained and the outline is as follows. Chapter 1 is the present introduction. In Chapter 2 we study the dynamics of particles in laser pulse-driven wakefields over multi-stages in a collider. The approach is based on a map [14, 15, 16] of phase space dynamics over a stage of wakefield acceleration induced by a laser pulse (or electron beam) and a particle tracking FORTRAN systems code based on this map. Most of this work was published in [16]. The entire system of a collider is generated with a product of multiple maps of wakefields, drifts, and magnets, etc. This systems map may include offsets of various elements of the accelerator, representing noise and errors arising from the operation of such a complex device. We find that

an unmitigated strong focusing of the wakefield coupled with the alignment errors of the position (or laser beam aiming) of each wakefield stage and the unavoidable dispersion in individual particle betatron frequencies leads to a phase space mixing and causes a transverse emittance degradation. The rate of the emittance increase [16] in the limit of constant energy is proportional to the number of stages, the energy of the particles, the betatron frequency, the square of the misalignment amplitude, and the square of the betatron phase shift over a single stage.

To improve the emittance we introduce in Chapter 3 several methods: a mitigated wakefield focusing by working with a hollow plasma channel [16], an approximately synchronous acceleration in a superunit setup [17], the "horn" model [18] based on exactly synchronous acceleration achieved through plasma density variation, and lastly an algorithm based on minimization of the final beam emittance [19] to actively control the stage displacement of such an accelerator. All these methods provide better emittance control and appear promising.

In the next energy frontier of an electron-positron (electron-electron) linear collider the demand for both extreme high energy and high luminosity leads to a high production of beamstrahlung photons, coherent and incoherent e^+e^- pairs, and W^+ W^- (W^- particles). In Chapter 4 we study the luminosity distributions and QED backgrounds via "CAIN" code simulations. Since these backgrounds are strongly oriented along the beam line of the colliding particles it seems relatively easy to avoid them by properly placing the particle detectors around the final focus region. In order to delineate processes of interest, it is also advantageous to polarize the electron and positron beams, as this tends

to suppress the W production processes and thus heightens the sensitivity to the sought-after processes. We investigate the possible depolarization of the electron (positron) beams in the acceleration stages as well as at the collision point. We take the example [20] of the laser wakefield accelerator design at 5 TeV center of mass energy of colliding beams. We find that in this design the spin depolarization due to the stage jitter noise is certainly negligible, and the depolarization at the collision point is still tolerable. We also consider the luminosity properties in several lower energy scenarios as they might be possible to achieve in a single beam driven acceleration stage.

In Chapter 5 we propose a single stage electron beam-driven plasma wakefield acceleration scheme which can provide an acceleration gradient in excess of 100 GeV/m based on a reasonable modification of the existing Stanford Linear Collider parameters.

We summarize the results of this work in Chapter 6 and indicate future research goals.

Chapter 2

Particle Dynamics in Plasma Wakefield Based Multi-stage Collider

2.1 Approach

The essence of calculations in this chapter is to extract a map from the particle dynamics in phase space over one wakefield stage and then to multiply over as many elements as there are in the system to yield the final overall map. The properties of this map are generically the same for many schemes of the wakefield based accelerators, as mentioned in Chapter 1. We first derive the ideal map in which no disturbance or noise is present in each element of the accelerator. We analyze the mathematical properties of the ideal map. Then we go on to study a realistic or non-ideal map in which the disturbance or noise from the ground shake, plasma noise, collisions, laser misalignment, etc. is incorporated. To make our discussion concrete, we take in most of our discussions the example of laser wakefield, following the approach described in [14, 15, 16].

We note that with a short pulse laser driver the whole acceleration process takes place over a period too short for plasma ions to move. Therefore the analysis is limited to considering electron motion only in a background of immobile ions. This not only simplifies the analysis, but (generally speaking)

stabilizes the system. In most scenarios the desired final energy of accelerating particles ($\sim$ TeV) cannot be achieved over a single acceleration stage. Thus we need to evaluate the effects associated with multistaging and to analyze the complete acceleration process. In the present investigation we limit ourselves to the linear regime of wakefield generation.

A major simplification arises from the separate treatment of beam electrons and plasma electrons. The plasma electrons are supporting the wakefield but not trapped by it. On the other hand, the beam electrons are affected (accelerated and focused) by the wakefield. To formulate our map approach, we need analytical expressions for the wakefields in a homogeneous plasma for the ideal case. Following [21] we obtain the longitudinal and radial wakefields in the case of cylindrical geometry. Several simplifying assumptions valid in the ultrarelativistic case allow us to integrate the single particle motion for the accelerated beam particles. Based on these results, we derive a map for a multistage LWFA which is used as a base for orbital tracking in Sec. 2.3. This ideal map preserves the normalized transverse emittance of the accelerated beam. In Sec. 2.4 we introduce random errors in the accelerator stage alignment. We consider their effects on the transverse r.m.s. beam emittance over multiple stages through our map code for different conditions. These errors combined with the spread in individual particle betatron frequencies can lead to a considerable emittance growth. To understand, optimize and improve the performance of the LWFA based collider, it is necessary to study the statistical mechanics behavior of these particle dynamics. From this we obtain analytical expressions of normalized transverse emittance degradation in the accelerator map in Sec. 2.5.

2.2 Wakefield Model

A femtosecond high power laser pulse propagating in a plasma excites wakefields. The plasma response can be obtained from the cold fluid equations ([21]):

$$\tfrac{d}{dt}\mathbf{v} = -\tfrac{e}{m_e\gamma}\left\{\mathbf{E} + \tfrac{1}{c}\mathbf{v}\times\mathbf{B} - \tfrac{1}{c^2}\mathbf{v}(\mathbf{v}\cdot\mathbf{E})\right\}, \tag{2.1}$$

$$\tfrac{\partial}{\partial t}n + \nabla\cdot n\mathbf{v} = 0, \tag{2.2}$$

where n is the electron density and γ is the Lorentz factor. These equations may be solved perturbatively, assuming that the density perturbation is relatively small. In the leading order the motion of the plasma electrons is governed by the ponderomotive force

$$\mathbf{F} = e\nabla\Phi_l(r,z,t)\,, \tag{2.3}$$

where the ponderomotive potential Φ_l is related to the laser vector potential A_l:

$$\Phi_l(r,z,t) = -\frac{m_e c^2}{2e}a^2(r,z,t)\,,$$
$$a = \frac{eA_l}{m_e c^2} \tag{2.4}$$

and a is the normalized vector potential. In general, when $a \ll 1$ the plasma response is linear.

Using a Gaussian laser pulse of the form (with a pulse standard deviation σ_l, spot size r_s)

$$a^2 = {a_0}^2\exp\left(-\frac{\xi^2}{\sigma_l^2}\right)\exp\left(-\frac{2r^2}{r_s^2}\right)\,, \tag{2.5}$$

where $\xi = z - v_g t$ and the group velocity v_g is very close to the speed of light, the maximum electric field in the z-direction, behind the pulse ($\xi^2 \gg \sigma_l^2$) is

$$E_z(\xi,r) = -a_0^2\sqrt{\frac{\pi}{2e}}E_0\exp\left(-\frac{2r^2}{r_s^2}\right)\cos k_p\xi, \tag{2.6}$$

where $E_0 = \frac{m_e w_p c}{e}$ is the so-called wavebreaking field and we used the approach of [22]. The maximum field (2.6) is reached when the resonance condition [11] is satisfied: $\sigma_l = \lambda_p/(\pi\sqrt{2})$, where λ_p is the plasma wave wavelength $2\pi c/\omega_p$. A transverse electric field E_r and magnetic field B_θ are generated according to the Panofski–Wenzel theorem [23]:

$$\frac{\partial E_z}{\partial r} = \frac{\partial (E_r - B_\theta)}{\partial \xi}, \tag{2.7}$$

leading to

$$(E_r - B_\theta) = 4\frac{a_0^2}{r_s^2}\sqrt{\frac{\pi}{2e}}\,\frac{E_0}{k_p}\,r\exp\left(-\frac{2r^2}{r_s^2}\right)\sin k_p\xi. \tag{2.8}$$

For a charged relativistic particle ($v_z \approx c$) the transverse force is proportional to $(E_r - B_\theta)$ and there is a region in the wake (quarter period) where a relativistic electron (or positron) experiences simultaneous acceleration and focusing. This feature of the LWFA makes it different from the conventional accelerators. The wakefield structure of this model is common to other sisters of wakefield accelerators such as PBWA and PWFA (See, for example, [24]). In general, it is a typical feature of plasma based accelerators that the accelerating field is independent of the transverse coordinates (up to second order) and the focusing force is linear in transverse coordinates (up to third order):

$$E_z \propto -\cos\Psi\,, \quad E_r - B_\theta \propto r\sin\Psi\,. \tag{2.9}$$

We assume that we have an electron injector which can be used as a charged particle source for our accelerator. Designing such an injector is a task in itself (e.g. [25], [26], [27]), but we are not going to investigate it here. Motion of the high energy electrons of the beam in the plasma wakefield is analyzed based on the following assumptions:

1. The phase space area occupied by the beam particles is small (we will specify the exact conditions later).

2. The wakefield is not affected by the beam (however, the beam loading can be included [15]).

3. The particles in the beam are highly relativistic and move predominantly in the z-direction (which is the direction of propagation of the laser pulse):

$$\dot{z} \gg \dot{x}, \dot{y}$$

$$\dot{z} \approx c\,.$$

4. The particle motions in x and y are decoupled and can be considered independently.

5. There is no interaction among the beam particles.

6. The laser pulse does not evolve. In other words, it is stationary in the co-moving frame. For strongly focused laser a guiding mechanism is required [28, 29, 30, 31]. Otherwise the laser beam will diffract over the Rayleigh range $L_R = \pi w^2/\lambda$, where w is the waist size and λ is the laser wavelength, and thus limit the total acceleration distance. For small waist size this can be severe: for $w = 20\mu$m, $\lambda = 1\mu$m the Rayleigh length $L_R \approx 1\,$mm. In this work we will assume that a certain guiding mechanism is present when needed. See also Sec. 3.3. Various instabilities [11] that the laser pulse might suffer are not investigated in the present dissertation.

Nevertheless it is important to ascertain mathematical and physical properties of a simplified accelerator system first in order to isolate and gain insight into the essential mechanism of the emittance degradation. To lift some of these assumptions is relatively straightforward and work in progress on the problem will relax some of them. The wakefield generated by the beam can be included in the considerations using the results in [32]. Assumption 5 is justified for high energy particles and relatively low currents, because the space charge force diminishes by a factor of $1/\gamma^2$. Assumption 6 is related to the pump-depletion problem [33] and will be taken into account in the next chapter. Starting with the single particle equation of motion $\frac{d\mathbf{p}}{dt} = -e\left(\mathbf{E} + \frac{\mathbf{v}\times\mathbf{B}}{\mathbf{c}}\right)$ and assuming that the beam particles are close to the z-axis, we obtain the following basic system of differential equations for the longitudinal motion

$$\frac{d\gamma}{dz} = k_p \Phi_0 \cos\Psi\,, \tag{2.10}$$

$$\frac{d\Psi}{dz} = k_p(1 - \frac{\beta_p}{\beta}), \tag{2.11}$$

where $\Psi = k_p\, z - \omega_p\, t(z)$ is the particle phase with respect to the wakefield and $\gamma = 1/\sqrt{1-\beta^2}$ is the particle Lorentz factor. For the transverse motion

$$\frac{d\hat{p}_u}{dz} = -\frac{4\Phi_0}{r_s^2}\hat{u}\sin\Psi\,, \tag{2.12}$$

$$\frac{d\hat{u}}{dz} = \frac{\hat{p}_u}{\gamma}\,, \tag{2.13}$$

where

$$\beta_p = v_p/c\,, \quad \Phi_0 = \sqrt{\frac{\pi}{2e}}a_0^2, \tag{2.14}$$

$$\hat{u} = u\,, \quad \hat{p}_u = \frac{p_u}{m_e c}\,. \tag{2.15}$$

Here $E_0 = cm_e\omega_p/e$, $k_p = \omega_p/c$, v_p is the phase velocity of the wake and u and p_u stand for transverse variables x and p_x or y and p_y. After convenient normalizations, the important points are that we use z as our time coordinate and the energy and the phase of the particles with respect to the wake are our "longitudinal" variables. Equations (2.10), (2.11) decouple from (2.12) and (2.13) and we can consider these two sets independently. The first set is conveniently analyzed using the following one-dimensional Hamiltonian [34]:

$$H = k_p\gamma(1 - \beta\beta_p) + k_p\Phi(\Psi), \tag{2.16}$$

where

$$\Phi(\Psi) = -\Phi_0 \sin\Psi. \tag{2.17}$$

In the phase space formed by the first pair of variables (γ, Ψ) we have stable fixed points: $\gamma = \gamma_p$ and $\Psi = \pi/2 + 2n\pi$ and unstable fixed points: $\gamma = \gamma_p$ and $\Psi = -\pi/2 + 2n\pi$, where $\gamma_p = 1/\sqrt{1-\beta_p^2}$ is the Lorentz factor corresponding to the phase velocity of the plasma wave. There are two phase space regions – the trapped region, where the particles execute bounded motion and the untrapped one, where the motion is unbounded in Ψ direction (see Fig.2.1). Because we are primarily interested in high energy physics applications of LWFA here, we consider the untrapped case, where the particle orbits are well above the separatrix. We can further simplify the equations of motion for γ and Ψ by putting in the right hand side of Eq. (2.11) $\beta = 1$ for ultra-high energy particles to obtain:

$$\frac{d\gamma}{dz} = k_p\Phi_0 \cos(\Psi)\,, \tag{2.18}$$

$$\frac{d\Psi}{dz} = \frac{k_p}{2\gamma_p^2}. \tag{2.19}$$

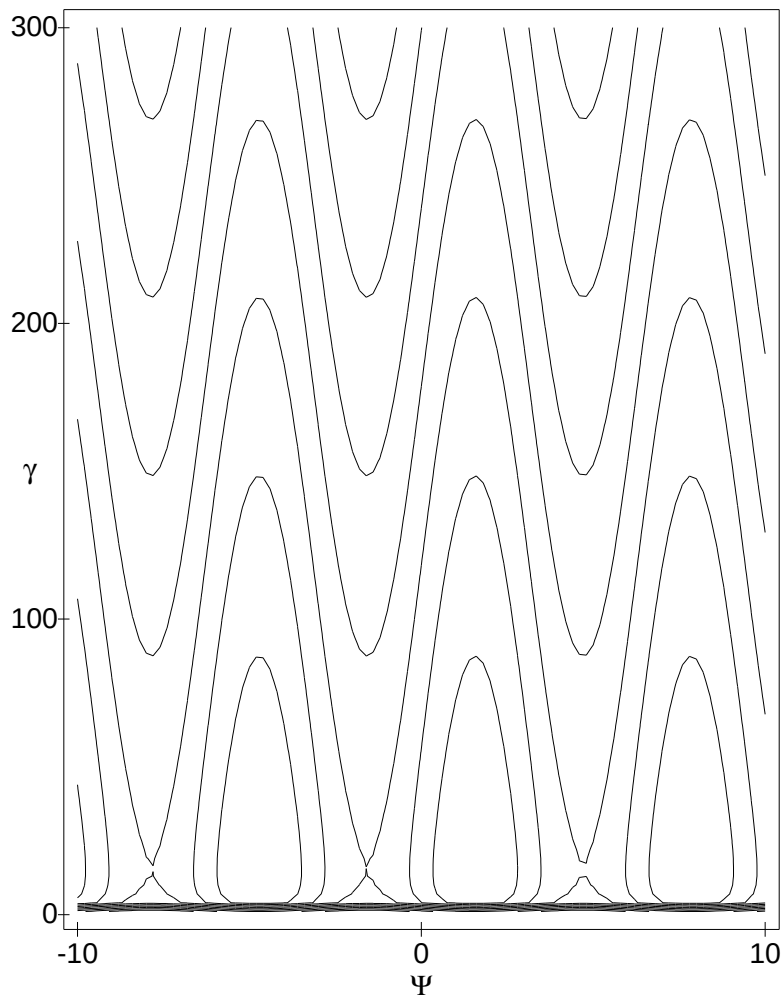

Figure 2.1: The longitudinal phase space: electron Lorentz factor γ vs. its phase with respect to the wakefield Ψ. Parameters used: $\gamma_p = 15$, $\Phi_0 = 0.2$.

These equations are integrated directly to give

$$\Delta\gamma = 2\Phi_0\gamma_p^2(\sin\Psi - \sin\Psi_0)\,, \tag{2.20}$$

$$\Psi = \Psi_0 + \frac{k_p z}{2\gamma_p^2}\,, \tag{2.21}$$

where Ψ_0 is the initial phase of the particle with respect to the wakefield. First we observe that the maximum energy gain (limited by the particle dephasing[1]) in Eq. (2.20) is $2\Phi_0\gamma_p^2$ (corresponding to $\Psi - \Psi_0 = \pi/2$). We call this an energy gain per unit stage. In order to gain more energy, we need multiple stages. Taking typical values of the parameters $\Phi_0 = 0.2$ (which corresponds to $a_0 = 0.5$, corresponding to the intensity of about $3 \cdot 10^{17}$ W/cm^2 for 1 micron laser wavelength) and $\gamma_p = 100$ (plasma electron density of 10^{17}cm^{-3}) we see that the above gain is about $4 \cdot 10^3$ in units of electron's rest energy, or about 2 GeV. This energy is achieved over a distance z of about 50 cm. We take $a = 0.5$ to be still in the "controlled" linear regime. The actual gain is smaller if the pump depletion [33] is taken into account. Lastly we note that by properly choosing Φ_0, r_s and γ_p we can analyze other plasma based accelerators, e.g. PWFA.

2.3 Multistage Acceleration and the Map

If we are to accelerate particles to TeV energies, we need to investigate problems associated with multistaging. Such a design for a 5 TeV center of mass energy based on the LWFA acceleration method has been devised in [12] to satisfy all the known accelerator physics constraints. In order to analyze the properties and efficacy of such an accelerator we characterize the beam dynamics to obtain a map which describes the one to one correspondence between the entrance phase space coordinates and the exit coordinates of the beam particles during the propagation of the beam through each accelerating stage and concatenate

[1]Here we also require that the particles are always in the focusing region of the wake. This makes the maximum useful phase range equal to $\pi/2$.

these maps over many stages. We use the multiple product of maps to build a systems code for a LWFA collider. As in the standard RF linac theory [35],[36] we have a reference particle moving along the ideal (design) orbit. All other particles in the bunch are described by their position with respect to the reference one.

The linearized equations of motion for the longitudinal degrees [2] of freedom are:

$$\delta\Psi_{n+1} = \delta\Psi_n \ , \tag{2.22}$$

$$\delta\gamma_{n+1} = 2\gamma_p^2\Phi_0(\cos(\Psi_s+\Delta)-\cos(\Psi_s))\delta\Psi_n + \delta\gamma_n, \tag{2.23}$$

where the subscript n enumerates the stage (n the entrance and n+1 the exit), Ψ_s is the "synchronous" phase, Δ is the phase slippage per accelerating stage (actually it can also depend on n). Because of the fact that we are considering extremely high energy particles ($\gamma \sim 10^5 - 10^7$) the equation (2.22) is decoupled from (2.23). Formally the equations look the same as in standard linac theory when the synchrotron oscillation frequency approaches zero. However, the physical regime of operation for the LWFA is different from the RF linac – we have a significant phase slippage over a stage (it is precisely this slippage which gives us the energy gain). And it also limits the maximum possible gain per stage. This difference comes from the fact that the plasma wave is relatively slow ($\gamma_p \approx 100$, instead of ∞). For the PWFA, however, the Lorentz factor of the driver can be much higher (for instance, the current SLC beam energy [1] corresponds to a Lorentz factor of about 10^5) and then the dephasing is not significant. From equations (2.22) and (2.23) we see that in the approximation

[2] We suppress the particle label in these formulas for brevity.

we are working in the relative phases of the particles do not change and the absolute energy spread increases linearly with the stage number (actually this is the beginning of a very slow synchrotron oscillation which happens on a time scale much greater than the time it takes a particle to travel the whole accelerator). The longitudinal beam emittance which up to a constant is the r.m.s. area in (γ, Ψ) space occupied by the beam is conserved due to the area preserving nature of the transformation in Eq.(2.22) and Eq.(2.23). Before concentrating on the transverse particle motion we also note that the phase Ψ_s is assumed to have the same value for all stages.

Now let us consider the transverse motion. If we assume that the particle energy does not change significantly over a single stage (which is valid in our case), this motion is described by

$$\ddot{\tilde{u}} + \left[\omega_\beta^2 \sin\left(\omega_s z + \Psi_s + \delta\Psi_n\right) - \frac{1}{2}\frac{\ddot{\gamma}}{\gamma} + \frac{1}{4}\frac{\dot{\gamma}^2}{\gamma^2}\right]\tilde{u} = 0\,, \tag{2.24}$$

where

$$\omega_s = \frac{k_p}{2\gamma_p^2}\,, \tag{2.25}$$

$$\omega_\beta = \left(\frac{4\Phi_0}{\gamma r_s^2}\right)^{1/2} \tag{2.26}$$

are the "slippage" and maximum possible betatron frequencies, respectively, in units of 1/m, and $\tilde{u} = \sqrt{\gamma}\, u$. In the high energy regime the third term in the square brackets in (2.24) is negligible and the second term is usually also small because of the proportionality to $1/\gamma_p^2$. Still, in the cases of very weak focusing we have to take it into account (for instance, in a hollow plasma channel).

An analytic solution can be found when some additional approximations are made. The simplest and first thing to do is to approximate the sine function

in (2.24) by some constant value (known as the "smooth" approximation) and then the equation describes just a simple harmonic oscillator (we always operate in the focusing phase region). Consider the following:

$$\ddot{x} + f(t)\, x = 0 \ , \tag{2.27}$$

where $f(t+T) = f(t)$ and $f(t)$ is positive for any t. If the betatron phase changes slowly on the timescale determined by T, we can instead consider the equation:

$$\ddot{x} + \Omega^2\, x = 0 \ , \tag{2.28}$$

where $\Omega^2 = \int_0^T f(t)\, dt/T$. For reasons to become clear in the next sections we are mostly interested in exactly this type of weak focusing scenario which is well described by the above "smooth" approximation. In this chapter we also assume a free drift (in vacuum) of the particles between the stages. The transformation matrix for the gap space in this case is

$$M_{\text{gap}} = \begin{pmatrix} 1 & L \\ 0 & 1 \end{pmatrix} . \tag{2.29}$$

Instead of this drift we can have magnets. Some examples are given in the next chapter (see Figure 2.2). Here we just note that if pairs of convergent and divergent quadrupole magnets are placed between the wakefield sections the gap transformation is

$$M_{gap} = \begin{pmatrix} 1 + \frac{s}{b} - \frac{as}{b^2} & [1 - \frac{a^2 s}{b^2}] L_0 \\ -\frac{s}{b^2 L_0} & 1 - \frac{s}{b} - \frac{as}{b^2} \end{pmatrix} , \tag{2.30}$$

where $b = f/L_0$, f is the magnitude of the focal length which is assumed to be the same for both the convergent and the divergent quadrupoles.

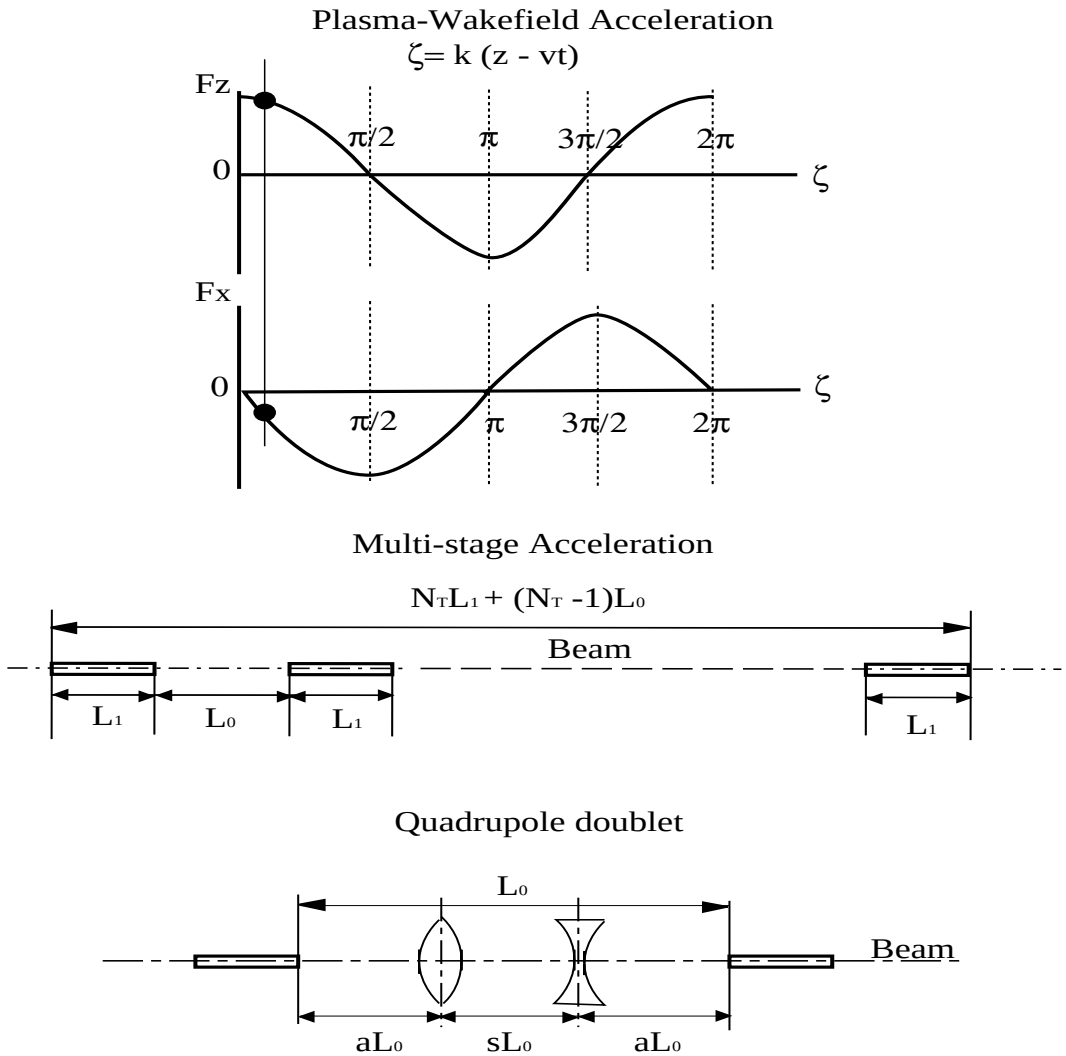

Figure 2.2: Multistage LWFA accelerator setup

Let us forget for a moment that the particles are being accelerated, and that the strength of the focusing force actually depends on the stage even if the stages are physically identical. To get stable solutions, we need to satisfy:

$$|\mathrm{Tr}\, M| < 2, \tag{2.31}$$

where M is the transfer matrix:

$$M = \begin{pmatrix} \cos(\frac{\omega}{\omega_s}\Delta), & \frac{1}{\omega}\sin(\frac{\omega}{\omega_s}\Delta) \\ -\omega\sin(\frac{\omega}{\omega_s}\Delta), & \cos(\frac{\omega}{\omega_s}\Delta) \end{pmatrix} \cdot \begin{pmatrix} 1 & L \\ 0 & 1 \end{pmatrix}, \tag{2.32}$$

where L is the drift distance between the wakefield stages and $1/\omega$ is the betatron length in the wakefield. The matrix (2.32) may be also written as

$$M = \begin{pmatrix} \cos(\frac{\omega}{\omega_s}\Delta), & \frac{1}{\omega}\sin(\frac{\omega}{\omega_s}\Delta) + L\cos(\frac{\omega}{\omega_s}\Delta) \\ -\omega\sin(\frac{\omega}{\omega_s}\Delta), & -L\omega\sin(\frac{\omega}{\omega_s}\Delta) + \cos(\frac{\omega}{\omega_s}\Delta) \end{pmatrix}. \tag{2.33}$$

The transverse map $\mathcal{M}$ for the whole accelerator system is

$$\mathcal{M} = M^N, \tag{2.34}$$

where N is the total number of stages when each stage has identical physical parameters.

When we do not have any drift space, the solutions of orbits are always stable. If we increase L keeping the other parameters fixed, at some point we encounter a "blow-up" of the amplitude of the transverse oscillations. So the maximum distance between the stages is limited. The trace of M is:

$$\mathrm{Tr}M = 2\cos\left(\frac{\omega}{\omega_s}\Delta\right) - \omega L\sin\left(\frac{\omega}{\omega_s}\Delta\right) \tag{2.35}$$

and for stability it should satisfy (2.31). We constructed the map code (2.34). The relation (2.31) is used to check the map code. Up to a some value of L the motion is stable (see Fig.2.3a) and after that we indeed find the amplitude "blow up".

This consideration does not take into account the fact that particles accelerate and ω_β is decreasing ($\omega_\beta \propto \frac{1}{\sqrt{\gamma}}$). Also in reality particles have slightly different (random) energies and different (random) phases with respect

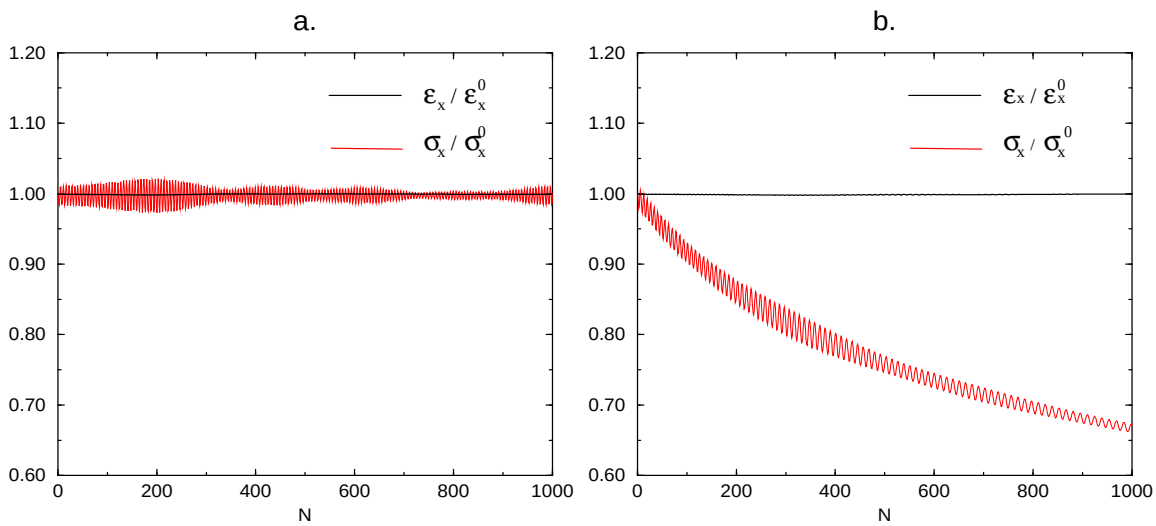

Figure 2.3: (Color) The r.m.s. beam size σ_x and normalized r.m.s. x-emittance ϵ_x vs. stage number N. Parameters used: γ_p=100, drift=17 cm, ϵ_x^0=2.2 nm, r_s=0.5mm, initial relative energy spread $\sigma_{\delta\gamma}/\gamma$=0.01, $\sigma_{\delta\Psi} = 0.01$,
a. no acceleration and no stage dislocations,
b. no stage dislocations.

to the wakefield. Therefore, the above analysis should be carried out for each particle separately, but if the differences in their phases are small, the conditions for stable motion are practically the same for all the particles. In general,

$$\mathcal{M} = M_N M_{N-1} ... M_2 M_1 \,, \tag{2.36}$$

where the transfer matrices depend on the stage number and on the positions of the individual particles in the longitudinal phase space. We note that because of the common structure of the wakefield in all plasma based accelerators, the obtained map with just slight modifications, can be used to analyze their performance as well. We coded the map in the case (2.36). In [12] three sets of scenarios for 5 TeV collider parameters are presented (see also Table 2.1). Case I calls for the tightest emittance, with least driver power. We take this case for most of the time as a concrete example. We also assume that the

Table 2.1: 5 TeV e^+e^-, $\mathcal{L}_g = 10^{35}\text{cm}^{-2}\text{s}^{-1}$ collider parameters according to [12].

Case	P_b(MW)	$N(10^8)$	f_c(kHz)	ϵ_x(nm)	$\beta_x^*(\mu\text{m})$	σ_x(nm)	$\sigma_z(\mu\text{m})$
I	2	0.5	50	2.2	22	0.1	0.32
II	20	1.6	156	25	62	0.56	1
III	200	6	416	310	188	3.5	2.8

accelerated beam is initially matched to the focusing channel of the accelerator. All computer runs in this chapter are done in the limit of full quarter-wave particle dephasing per acceleration stage. This restriction is lifted in the next chapter. Our runs show that when we start with a normalized emittance of $\epsilon_u = \epsilon_x = 2.2\,\text{nm}$ (the case I scenario of [12]), up to some value of the drift space the normalized r.m.s. emittance is well preserved (See Fig. 2.3b) and the transverse particle motion is stable. This does not surprise us because the map is volume preserving, so the phase space area (emittance) is constant. The calculated emittance in the code is the root mean square emittance given by

$$\epsilon_x = \sqrt{(\sigma_{\tilde{x}}\sigma_{\dot{\tilde{x}}})^2 - c^2_{\tilde{x}\dot{\tilde{x}}}}\,, \tag{2.37}$$

where $c_{\tilde{x}\dot{\tilde{x}}} \equiv < \tilde{x}\dot{\tilde{x}} > - < \tilde{x} >< \dot{\tilde{x}} >$.

2.4 Alignment Errors

For a complex system cumulative errors can give rise to an unpleasant result such as emittance dilution. We identify that one of the most important such effects stems from the alignment errors by whatever mechanism of the wakefield with respect to the design particle orbit stage by stage. The problem here is that up to this point we have not considered possible transverse misalignments

of the consequent stages. This, combined with the fact that the focusing force is different for different particles (due to the phase and energy spread), can lead to a severe transverse emittance growth.

Basically, what happens is that the particles rotate at different angular velocities in the transverse phase space and if there is a stage position shift present, we get a characteristic banana (see Fig. 2.4) shaped distribution (it is banana shaped only if the dislocation size is larger than beam size, but in any case the particle distribution gets diluted because of the misalignments). This process critically depends on the magnitude of the betatron frequency spread. This means that the typical strength of the focusing force is of great importance. Of course, additional information can be extracted from the other total phase space cross-sections. See Fig.2.5 and Fig.2.6. However, here we concentrate on the normalized transverse emittance as a figure of merit due to its importance to the final luminosity of the collider. The effect of plasma noise (or other noise, such as laser or the boundary) on the particle dynamics over a stage may be also incorporated in a map similar to the stage-by-stage alignment errors. Such dynamics results in a fuzzy or stochastic [37] map. The longitudinal stage errors may be incorporated in a similar manner. Preliminary analysis shows that their importance is not so critical. We consider the case of transverse stage misalignments. The dislocation of the aligned position of each stage n is given in our code as a stochastic variable $\mathcal{D}_n$ which we impose to have a Gaussian distribution with zero mean and standard deviation $\sigma_{\mathcal{D}}$ which we assume to be independent of the stage number

$$\begin{pmatrix} \tilde{x}_{n+1} \\ \dot{\tilde{x}}_{n+1} \end{pmatrix} = M_n \begin{pmatrix} \tilde{x}_n - \tilde{\mathcal{D}}_n \\ \dot{\tilde{x}}_n \end{pmatrix} + \begin{pmatrix} \tilde{\mathcal{D}}_n \\ 0 \end{pmatrix} , \tag{2.38}$$

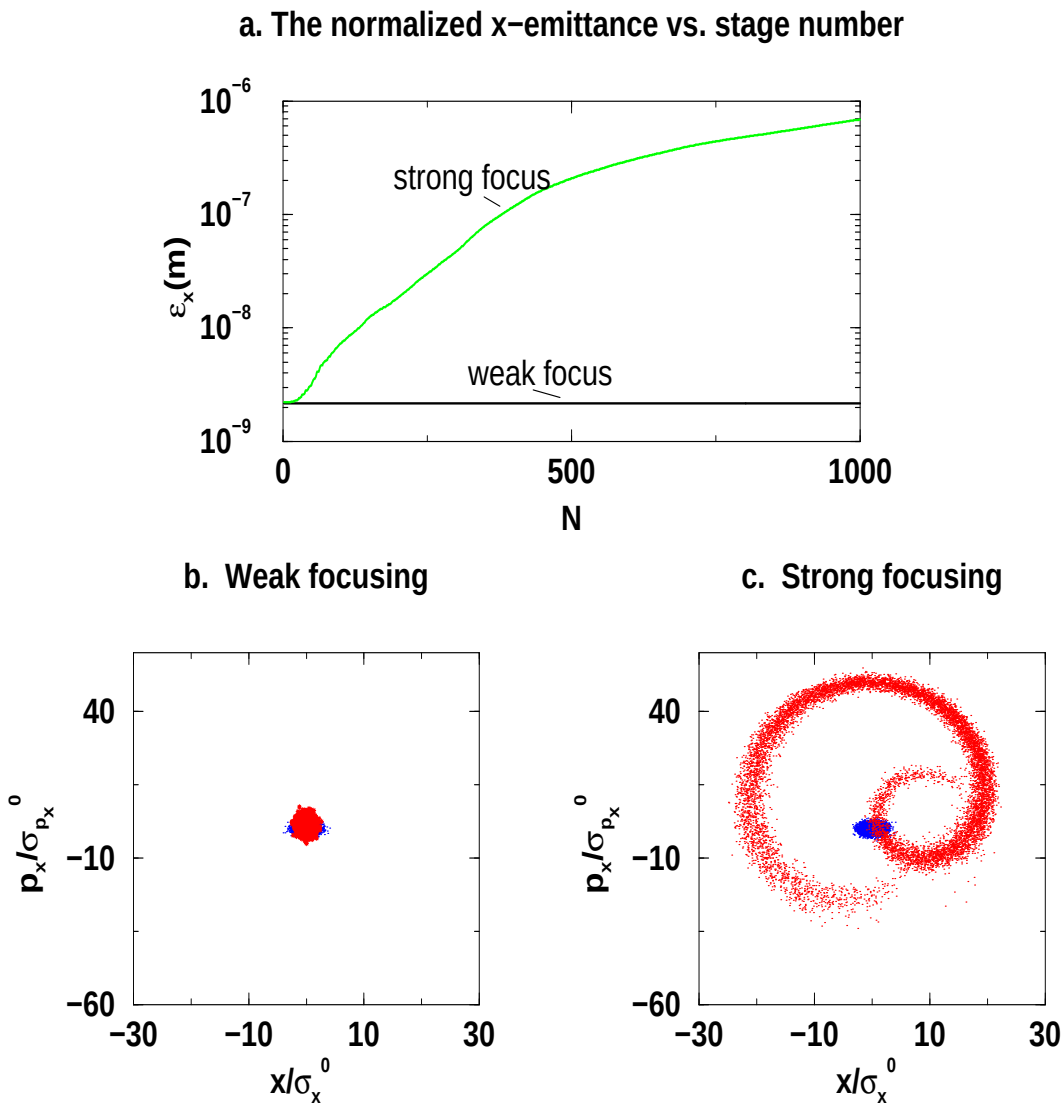

Figure 2.4: (Color) Weak and strong focusing cases for acceleration to 2.5 TeV: a. The normalized x-emittance ϵ_x vs. stage number N. Parameters used for the strong focusing force case: γ_p=100, drift=17cm, ϵ_x^0=2.2 nm, r_s=0.5mm, $\sigma_{\mathcal{D}} = 0.1\mu$, initial particle Lorentz factor $\gamma \approx 10^6$, initial relative energy spread σ_γ/γ=0.01, $\sigma_{\delta\Psi} = 0.01$. For the weak focus case see Chapter 3.
b. The phase space p_x vs. x. for the weak focusing force case.
c. The strong focusing case.
The initial (in blue) distribution (Gaussian and the beam is assumed initially matched to the focusing properties of the channel) and the final (in red) after 1000 acceleration stages.

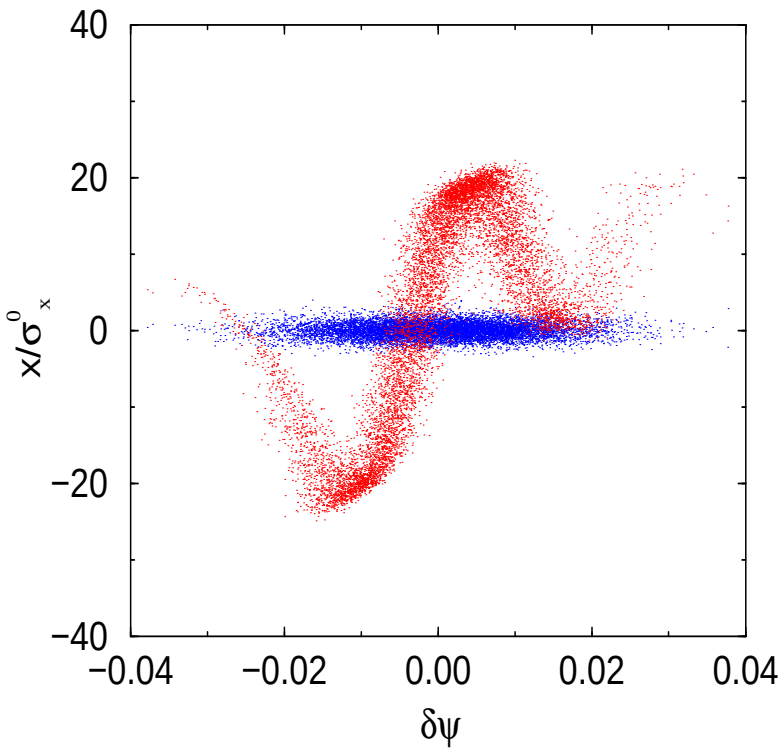

Figure 2.5: (Color) Additional cross-sections of the initial (blue) and final (red) phase space: Transverse coordinate vs. longitudinal phase.

where $\mathcal{D}_n$ is the stochastic misalignment ($\tilde{\mathcal{D}}_n = \sqrt{\gamma_n}\mathcal{D}_n$). The longitudinal degrees of freedom are not affected. For this map to describe realistically the electron motion, we assume that $\sigma_{\mathcal{D}} \ll r_s$. The total transverse map (in the presence of errors) can be written in the form

$$\begin{aligned}\begin{pmatrix} \tilde{x}_{n+1} \\ \dot{\tilde{x}}_{n+1} \end{pmatrix} &= M_n M_{n-1} \ldots M_2 (1 - M_1) \begin{pmatrix} \tilde{\mathcal{D}}_1 \\ 0 \end{pmatrix} + \ldots (1 - M_n) \begin{pmatrix} \tilde{\mathcal{D}}_n \\ 0 \end{pmatrix} \\ &\quad + M_n M_{n-1} \ldots M_1 \begin{pmatrix} \tilde{x}_1 \\ \dot{\tilde{x}}_1 \end{pmatrix} . \end{aligned} \tag{2.39}$$

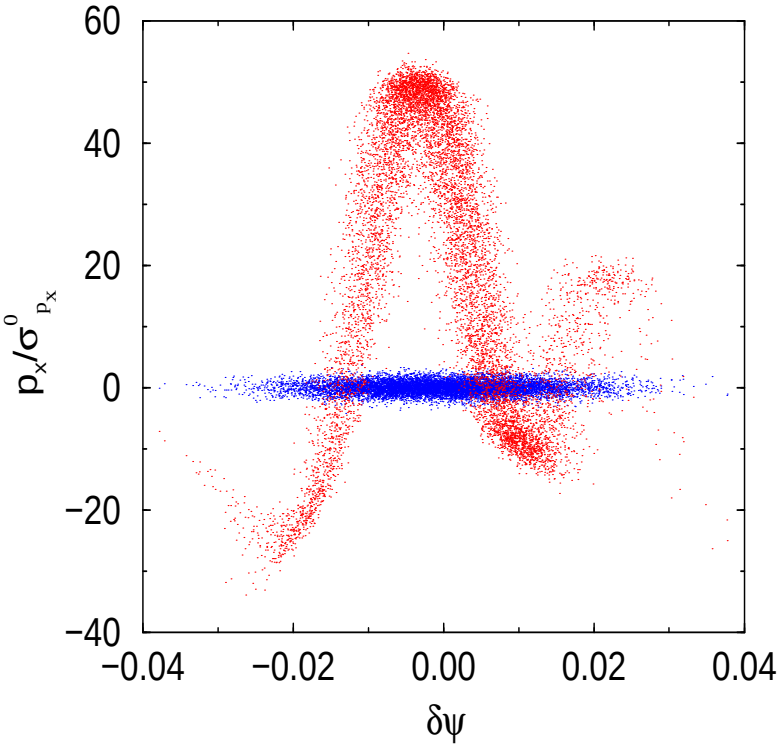

Figure 2.6: (Color) Additional cross-sections of the initial (blue) and final (red) phase space: Transverse momentum vs. longitudinal phase.

2.5 Emittance degradation

The stochastic map (2.39) leads to a transverse emittance degradation. A run with small random dislocations of magnitude $\sigma_{\mathcal{D}} = 1 \cdot 10^{-7}$ m is presented in Fig.2.4a and Fig.2.4c. We see that in this case (which corresponds to design I in [12]) we have a severe emittance growth (the initial normalized emittance is 2.2 nm). A density plot of the initial and final phase transverse space is shown in Fig. 2.7. We have to point out that even though there are cases corresponding to large laser spot sizes which preserve the normalized emittance quite well their practical realization would require a huge laser power probably well above any future experimental limits. Also the efficiency of the accelerator would be

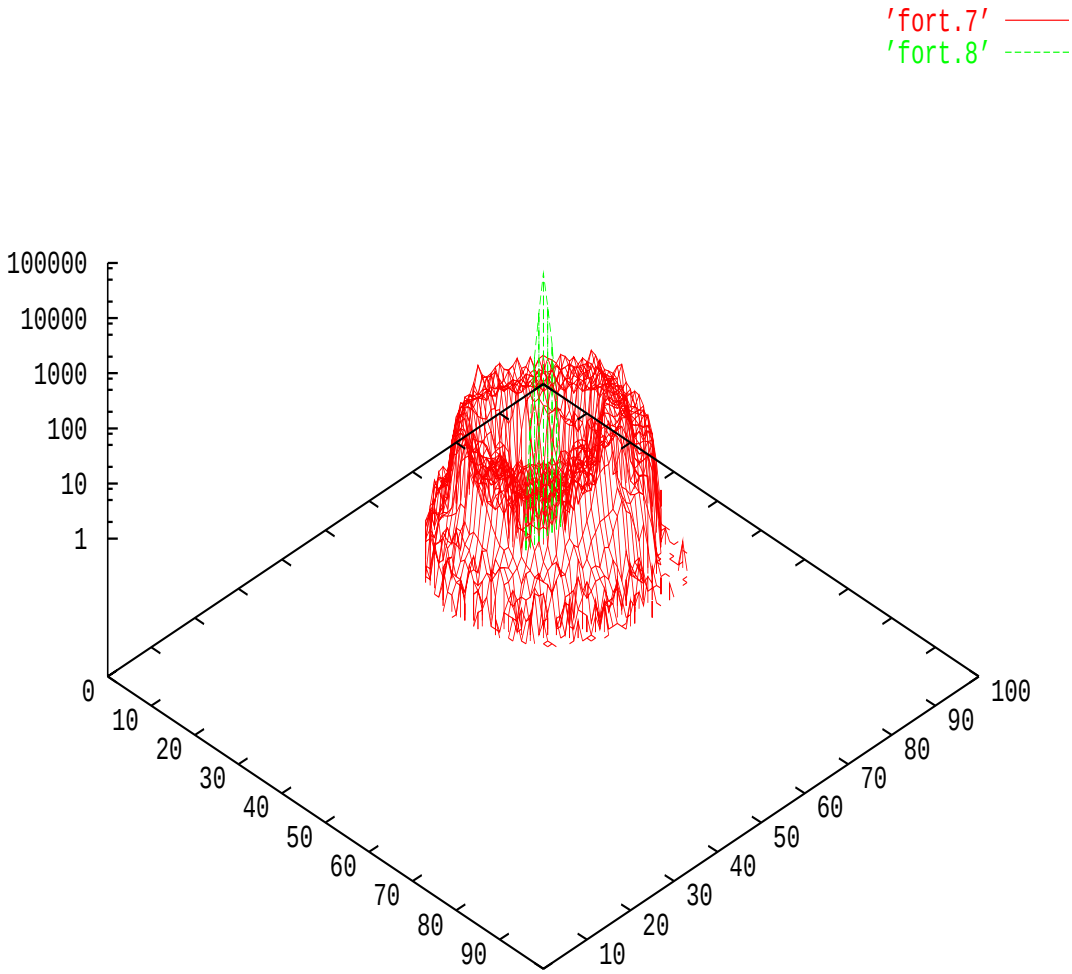

Figure 2.7: (Color) Density plot of the beam particle distribution before and after the acceleration to 2.5 TeV. Phase space plane is in arbitrary units.

unacceptably low. Some alternative approaches to reduce the emittance growth are discussed in [14], [15]. In general, the problem can be cured by decreasing the focusing of the accelerator system. One possible way is to use a plasma channel [38], [39]. It provides a linear weak focusing and we showed in [15] that

its performance in a collider application is promising. In the next chapter we discuss this issue. Here we concentrate on the map properties.

We observe a certain random feature over shorter time scales – runs with different misalignment distributions (just different sequences, otherwise the same macroscopic properties) give different $\epsilon = \epsilon(N)$ behavior. This is due to the fact that the practical number N is too small with respect to the long range stationary behavior of the map. Even though the emittance is a cumulative quantity which characterizes the particle ensemble as a whole, it still has a stochastic nature. Only in the limit of large N and long enough transverse phase space mixing does the final emittance distribution shrink, resulting in an approximately deterministic value for a given set of parameters and $\sigma_{\mathcal{D}}$. For large N we observe a typical diffusion process; the emittance growth is linearly proportional to N (it is correct only in a constant energy approximation, in the case of adiabatic energy increase the dependence is more complicated, see (2.48)).

The dependence of the emittance growth on the betatron frequencies spread is quadratic in the beginning (see Fig.2.9), but if the parameters are such that full phase space mixing occurs:

$$\sigma_{\delta\omega} N l > 2\pi, \tag{2.40}$$

where $\sigma_{\delta\omega}$ is the betatron frequency spread and l is the length of a single stage, then the emittance growth rate is practically independent of the particular value of $\sigma_{\delta\omega}/\omega$. The continuous growth of the emittance is maintained under the presence of betatron frequency spread. In the limit of small betatron frequency ω, namely $\omega\, l < 1$ and small distance between the wakefield stages the map

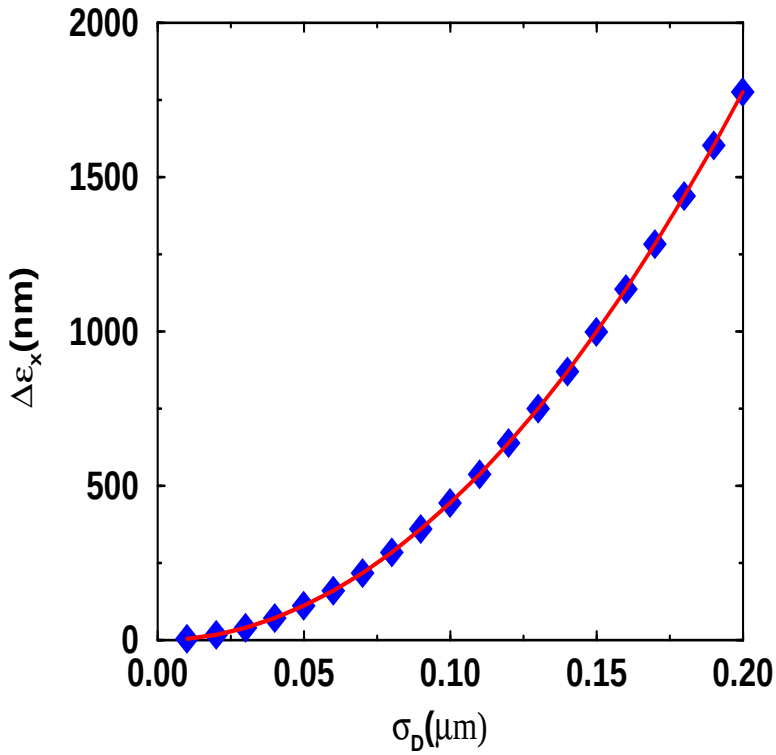

Figure 2.8: (Color) Dependence of the normalized emittance growth $\Delta\epsilon_x$ on the magnitude of the transverse stage offsets $\sigma_{\mathcal{D}}$. Blue diamonds represent the code results and red line is a quadratic fit.

reduces to a stochastic differential equation:

$$\ddot{\tilde{x}} + \omega^2 \tilde{x} = \omega^2 \tilde{\mathcal{D}}. \tag{2.41}$$

The right hand side of the above equation represents the noise (alignment errors) which drives the oscillation. Considering white noise, we observe

$$< \mathcal{D} > \;=\; 0\,, \tag{2.42}$$

$$< \mathcal{D}(z_1)\ \mathcal{D}(z_2) > \;=\; \sigma_{\mathcal{D}}^2\ l\ \delta(z_1 - z_2)\ . \tag{2.43}$$

Applying the theory of random walk of a harmonic oscillator driven by a ran-

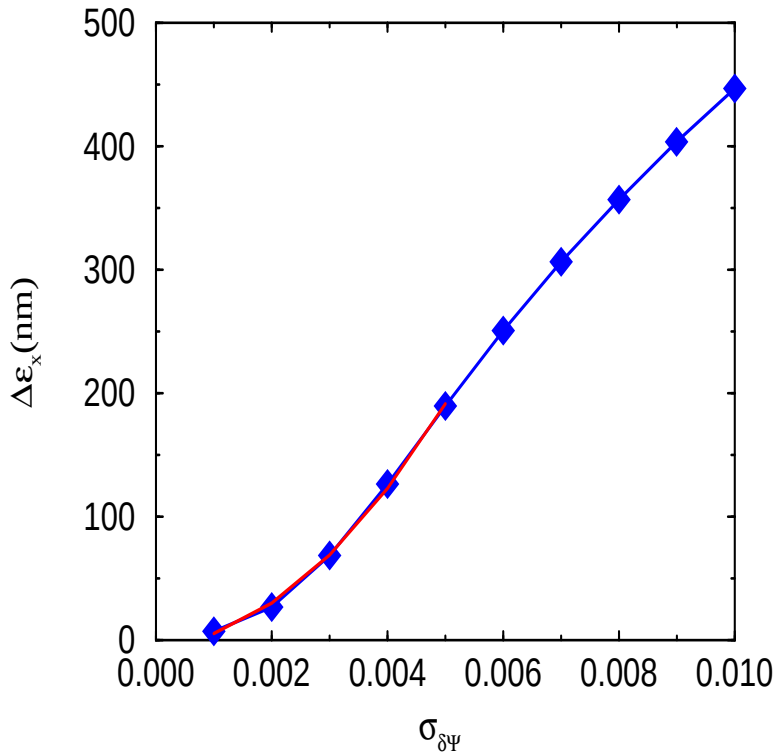

Figure 2.9: (Color) Scaling of the emittance growth with the phase spread. The change is from quadratic to linear dependence and finally saturation.

dom force, we obtain

$$< \tilde{x} > = 0 \ , \ \ < \dot{\tilde{x}} > = \ 0, \ \ < x\dot{\tilde{x}} > = \ 0 \tag{2.44}$$

$$< \tilde{x}^2 > = \ Dz = DNl, \ \ < \dot{\tilde{x}}^2 > = \ D\omega^2 z \ , \tag{2.45}$$

where the diffusion coefficient D is given by:

$$D = \frac{1}{2}\gamma\omega^2 \ l\sigma_{\mathcal{D}}^2 \ . \tag{2.46}$$

We are also assuming that the emittance growth is large (compared to the initial emittance). So, using (2.44) and (2.45) we obtain:

$$\Delta\epsilon \approx \omega D \ z = \frac{1}{2}\gamma\omega(\omega\, l)^2\sigma_{\mathcal{D}}^2 N \ . \tag{2.47}$$

The averages in (2.44) and (2.45) are two-fold: over the particle ensemble and over the noise realizations. However, in the limit of a significant phase mixing and large N the average over the noise realizations can be dropped (in this limit only $\sigma_{\mathcal{D}}$ is important). The alignment errors introduce randomness in the phase space particle positions upon reentry to the next stage, and the differential betatron oscillations mix these positions causing an emittance growth. In fact, the energy increases ($\Delta\gamma$ per stage). In the adiabatic limit we obtain

$$\Delta\epsilon \approx \frac{1}{2}\gamma\omega(\omega\, l)^2\sigma_{\mathcal{D}}^2\left(\frac{\gamma}{\Delta\gamma}\right)^{1/2}\sqrt{N\ln\left(1+\frac{\Delta\gamma N}{\gamma}\right)}\,, \tag{2.48}$$

where γ is the initial particle energy. Typically $\Delta\gamma \approx a_0^2 k_p l$ and $\omega \propto \frac{a_0}{r_s\sqrt{\gamma}}$, so we obtain

$$\Delta\epsilon \propto \frac{l^{3/2}a_0^2\sigma_{\mathcal{D}}^2}{r_s^3 k_p^{1/2}}\sqrt{N\ln\left(1+\frac{\Delta\gamma N}{\gamma}\right)}\,. \tag{2.49}$$

A very important and expected point is the strong dependence of the emittance growth on the magnitude of the betatron frequency[3] (or wakefield curvature). See Fig.2.10. Discrepancy for small r_s (large betatron frequency) between the numerical and analytical results is caused by violation of our $\omega l < 1$ assumption. Of course, better control of the errors reduces the emittance degradation as shown in Fig.2.8 and Fig.2.11. This important issue will be discussed in the next chapter. We can also see from (2.49) that for a fixed final energy reducing the length of a single stage decreases the emittance growth. This point was exploited in Ref.[17] and is also discussed in the next chapter of this dissertation. When the number of stages is relatively small and the phase space mixing

[3]Presumably, the relative betatron frequency spread $\sigma_{\delta\omega}/\omega$ is small due to the smallness of $\sigma_{\delta\gamma}/\gamma$ and $\sigma_{\delta\Psi}$, so as a typical betatron frequency we can use the one of particles with $\delta\gamma = 0$ and $\delta\Psi = 0$, for instance.

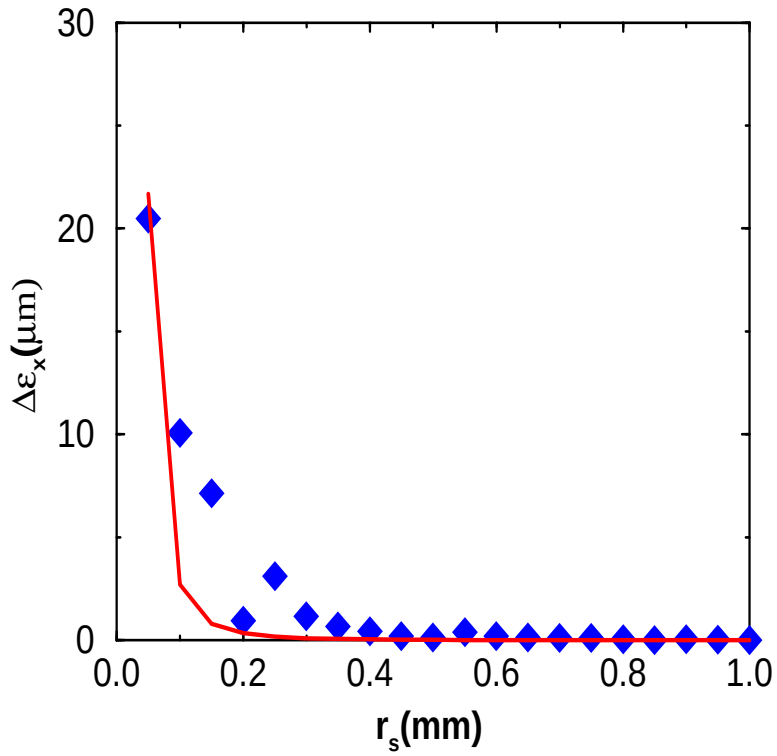

Figure 2.10: (Color) Scaling of the emittance growth with the laser spot radius. The red line fit to the numerical data (blue diamonds) shown is the theoretical prediction $1/r_s^3$.

is not complete, numerical results appear to be the only reliable way to analyze the properties of the map. Analytical estimations are rather difficult. We note that analytical estimations of emittance growth due to stage misalignment valid in the case of full filamentation (phase space mixing) in a single stage can be found in [40]. In this limit (which corresponds to a very strong wakefield focusing), control over the emittance growth can be achieved only by precise handling of the beam (namely error control better than the beam size). The results in this limit can be reproduced in our theory by replacing the factor ωl in (2.47) by unity.

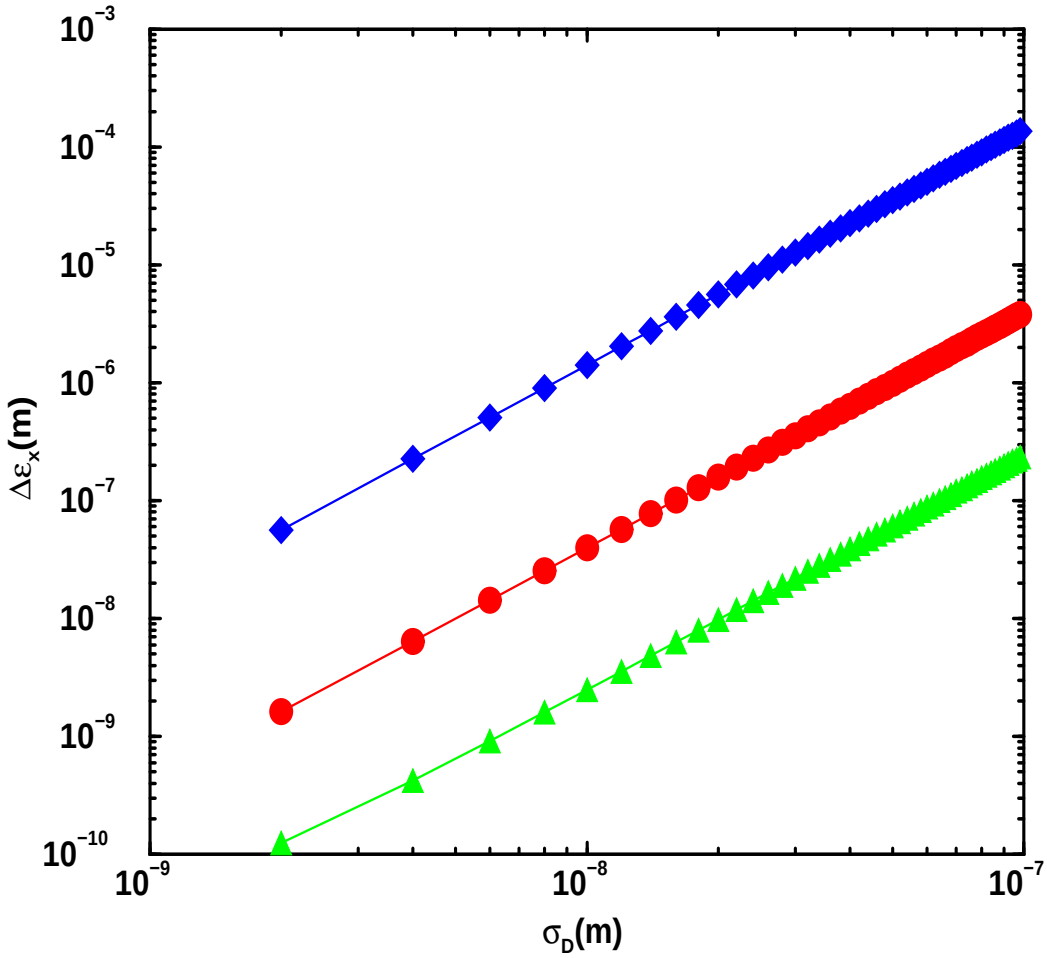

Figure 2.11: (Color) Emittance growth vs. the stage misalignment size for $r_s = 0.05$mm (blue), $r_s = 0.2$mm (red), and $r_s = 0.5$mm (green), respectively.

With the notion of final emittance scaling with the relevant parameters we can start to optimize in the multidimensional parameter space of the future collider. From the computer simulations for the small emittance design [12] for a multi TeV collider the conclusion is that in the case of initially homogeneous plasma it is difficult to avoid a severe emittance growth of the accelerated beam in the presence of small alignment errors stage-by-stage based on reasonable parameters (laser spot size, dislocation size and number of stages). The diffi-

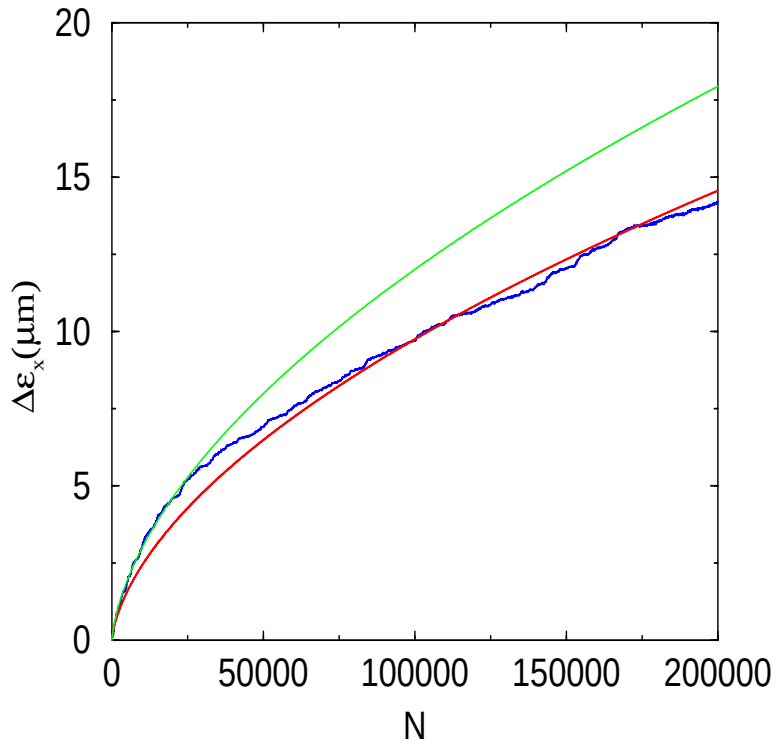

Figure 2.12: (Color) Long range behavior of the emittance degradation. Two fits to the numerical results (in blue): first (red) based only on the derived N dependence and second (green) based on the complete theoretical prediction.

culty is primarily due to the fact that the wakefield focusing force is too large in this case. The above considerations do not include the transverse nonlinear effects which also contribute to the emittance increase.

2.6 Concluding Remarks

We investigated the cumulative effects of the successive acceleration, transport, and focusing in the laser wakefield (or its sister methods) over multiple stages. Such cumulative processes are important for the real world accelerators such as high energy colliders. Errors arising from the misalignments of each stage or

equivalently (in our map approach) the noise in the system can accumulate in such a way to degrade some of the parameters of the beam. The most crucial of these may be the normalized transverse r.m.s. emittance of the beam. We showed that a set of stages with an ideal wakefield acceleration, drift, and focusing can preserve even a very small emittance over a thousand stages.

When we have stochastic variables on the wakefield (we chose the stage errors of the axis of the wakefield, in particular), the emittance can significantly increase over the many stages due to the strong focusing of the wakefield. This is probably the most serious effect on the long range behavior of the beams in this kind of accelerator for high energy applications.

We studied the emittance degradation numerically and analytically obtaining important conclusions about its scalings with respect to the relevant parameters. Based on that we will consider several mitigated focusing scenarios in the next chapter.

Chapter 3

Emittance Control in Laser Wakefield Accelerator

3.1 Initial Considerations

In the previous chapter, a study of emittance degradation in the presence of jitters, associated with stochastic misalignment between the accelerated beam and the wakefields was carried out in the case of a uniform plasma medium and the beam acceleration over a full quarter-wave region (the dephasing limit). We found that the accelerator system is very sensitive to the transverse stage jitter due to the wakefield averaging over the entire accelerating phase and thus typically providing a very strong focusing. In this chapter we are proposing several scenarios which have weaker focusing properties and provide much better transverse emittance control [19].

A possible way to decrease the strong focusing of the wakefield is to use the hollow channel design[38]. We analyze this case and conclude that its weak focusing properties are very favorable from the accelerated beam emittance preservation point of view. There is practically no transverse emittance growth in this scenario. A drawback is that due to the finite density gradient near the wall of the cavity, there is a local plasma frequency which matches the wakefield frequency and leads to a resonance absorption[39]. In [16], numerical models

with beam acceleration over a full quarter-wave-region were considered both without and with the plasma channel, ignoring the resonance absorption effect. The former will be referred to as the CTHY (Cheshkov, Tajima, Horton and Yokoya) model as described in Chapter 2 and the latter as the CTHY1 model which is described in Sec.3.3.

From general considerations, we expect that the emittance degradation should depend on the longitudinal phase-range through which the acceleration occurs. Using two different approaches [17, 18] we explore ways to improve the resilience against transverse stage position jitters through variations of the loading phase and also of the longitudinal phase interval of acceleration. Computer simulations indicate that when the acceleration phase is approximately fixed (the phase slip is small) there is an inverse power behavior (for a fixed final energy of the particles), in particular, the emittance degradation decreases as $1/N_T$, where N_T is the total number of acceleration units. This confirms the theoretical expectation of CTHY model deduced from a statistical theory of the previous chapter. The inverse power law suggests that through the use of small acceleration intervals it might be possible to achieve high system resilience against jitters. The second approach is to develop a synchronous acceleration model, where there is no longitudinal phase slip at all. It was pointed out by Katsouleas[41] over a decade ago that synchronous acceleration can be achieved by varying the plasma density. More specifically, consider the case where the local plasma density along the beam propagation direction is gradually increasing. Then the wavelength of the plasma waves, on which the beam electrons are riding, becomes shorter and shorter. When the rate of the phase-slip of the beam electrons exactly matches the rate of the phase advance

due to the shrinkage of the plasma waves, a continuous acceleration without any phase-slip is achieved. From a study of the hydrodynamics of a nozzle flow [42], we find that in the case of a steady flow opposite to the beam propagation direction, by fine tuning the increase of the nozzle cross section along the beam, one can control the corresponding increase of the plasma density and in turn achieve a synchronous acceleration. Here the acceleration unit has a horn shape and we refer to this model as the "horn model" [18]. Based on the Katsouleas's matching condition, we have derived a set of analytic expressions which have been incorporated in the dynamical map. Our work [18] also takes into account the conservation of energy in the context of the pump-depletion effect [33] and the adiabatic invariance property throughout the acceleration process[43]. The computer simulations for the horn model with a small loading phase show a definite improvement over CTHY model. In the last section of this chapter we propose an active alignment control which can significantly reduce the final emittance of the beam as illustrated by our preliminary numerical results. The analysis is done by introducing a feedback in our multistage systems code which adjusts the accelerator stages based on the calculation of the final emittance only and minimization criteria.

3.2 Multistage Acceleration, Map Approach and Emittance Degradation

In general, TeV center of mass energies of colliding particles require multistage acceleration even if we assume large acceleration gradients typical for the plasma based accelerators. To study such an accelerator system we introduced a map approach described in [14, 15, 16]. A detailed study of the map

and emittance degradation properties was presented in the previous chapter of this dissertation. In the limit of small betatron frequency ω, namely $\omega\, l < 1$ and small distance between the stages and in fixed energy approximation the emittance growth after N acceleration stages was shown to be:

$$\Delta\epsilon \approx \frac{1}{2}\gamma\omega(\omega\, l)^2\sigma_{\mathcal{D}}^2 N \ . \tag{3.1}$$

The alignment errors introduce randomness in the phase space particle positions upon reentry to the next stage, the differential betatron oscillations mix these positions causing an emittance growth. This is valid in the case of a small drift $L \ll l$. If this is not the case, but $L\omega \ll 1$ is still satisfied we can modify the above equation by introducing $\omega' = \omega\sqrt{l/(l+L)}$. Then the betatron phase advance per stage (wakefield and drift) is given by $\omega'(l+L)$ and in all formulas ω should be replaced by ω' and l by $l+L$. The total result would be multiplying Eq. (3.1) by the factor $\sqrt{1+L/l}$.

Since the energy increases Eq. (3.1) needs to be further modified. Denote the Lorentz factor increase per stage by $\Delta\gamma$. In the adiabatic limit we obtain

$$\Delta\epsilon \approx \frac{1}{2}\gamma\omega(\omega\, l)^2\sigma_{\mathcal{D}}^2\left(\frac{\gamma}{\Delta\gamma}\right)^{1/2}\sqrt{N\ln\left(1+\frac{\Delta\gamma N}{\gamma}\right)} \ , \tag{3.2}$$

where now γ is the initial particle Lorentz factor and ω is the initial betatron frequency. Typically $\Delta\gamma \approx \frac{ea_0^2E_0 l}{mc^2} = a_0^2 k_p l$, where E_0 is the nonrelativistic wavebreaking field, and $\omega \propto \frac{a_0}{r_s\sqrt{\gamma}} < \sin\Psi >^{1/2}$ (averaging is over a stage), so we obtain

$$\Delta\epsilon \propto \frac{l^{3/2}a_0^2\sigma_{\mathcal{D}}^2}{r_s^3 k_p^{1/2}}\sqrt{N\ln\left(1+\frac{\Delta\gamma N}{\gamma}\right)} < \sin\Psi >^{3/2} \ . \tag{3.3}$$

For fixed initial and final particle energies the above equation reduces to

$$\Delta\epsilon \propto \frac{\sigma_{\mathcal{D}}^2}{r_s^3 k_p^2 a_0}\frac{1}{N_T} < \sin\Psi >^{3/2} \ . \tag{3.4}$$

3.3 Hollow Channel

A possible way to decrease the wakefield focusing is to base our accelerator design on the "hollow channel" wakefield acceleration [38]. The idea is to use a preformed vacuum channel in an underdense plasma (the overdensed case was studied in [44]). This case offers several important advantages compared to our previous scenario: the focusing force is almost exactly (because the phase velocity of the wakemode is very close to the speed of light) linear and weak in the channel (the weak focusing is a very important improvement over that of a uniform plasma case); there exists a stable propagation solution for the laser mode; the acceleration gradient is very uniform in transverse coordinates within the channel. A drawback is the loss in the magnitude of the accelerating field. The equations for the wakefield in the channel are [38]:

$$E_z(\xi, r) = -k_{ch}^2 \int_\xi^\infty \cos(k_{ch}(\xi - \xi'))\ \Phi_l(a, \xi')\ d\xi', \tag{3.5}$$

$$E_r(\xi, r) - B_\theta(\xi, r) = \frac{k_{ch} r}{4\gamma_p^2} k_{ch}^2 \int_\xi^\infty \sin(k_{ch}(\xi - \xi'))\ \Phi_l(a, \xi')\ d\xi', \tag{3.6}$$

where a is the channel radius, Φ_l is the ponderomotive potential and k_{ch} is given by: $k_{ch} = k_p / \sqrt{1 + k_p a \frac{K_0(k_p a)}{2K_1(k_p a)}}$, where K_0 and K_1 are the modified Bessel functions of zeroth and first order, respectively. For instance, if we choose $k_p a = 1$ then the electric field in z-direction will be reduced by a factor of 0.6 [38] compared to the initially uniform plasma. So, formally there are no major changes to our previous map scheme. There is a reduction in Φ_0 and the magnitude of the focusing changes:

$$\omega = k_{ch} \left(\frac{\Phi_0}{2\gamma\, \gamma_p^2} \right)^{1/2} .$$

Since the γ_p factor is usually large the magnitude of the focusing force decreases significantly. This is the most important point for our beam emittance studies.

We investigate the accelerator performance in this case using the same multistage code approach as in the previous chapter. The run shown in Fig.2.4a and Fig.2.4b indicates a very significant improvement over the previous design. Here we are able to preserve even design I emittance of 2.2 nm. The stage considered is: $\gamma_p = 150$, the channel radius $a = 30\mu$m, the laser spot size $r_s = 50\mu$m, the plasma density (outside the channel) $n = 5 \cdot 10^{16}\text{cm}^{-3}$, the laser wavelength $\lambda \approx 1\mu$m, and the drift space of 0.3 m. The magnitude of the stage dislocations is larger than before – $\sigma_{\mathcal{D}} = 0.5\mu$m. From the graphs we see that the emittance growth of the accelerated beam is now much smaller and the design is more promising. Experimental production of such long channels needs to be further investigated and experiments are currently underway [29, 30, 45]. Unfortunately, there is an additional difficulty: because in reality we will always have a finite density gradient in the channel walls there will be a resonant absorption where the local plasma frequency matches the wakefield frequency. This effect has been studied in [39], where an expression for the quality factor of the hollow channel is derived. Possible low values of this factor limit the acceleration of multiple bunches in a single shot created wakefield.

Another way to decrease the wakefield curvature is through the use of transversely shaped laser pulses. A "flat top" laser pulse would produce a small curvature wakefield and correspondingly small focusing force. Creation and propagation of such pulses needs to be studied. In the case of PWFA the density shaping of the driver electron bunch can be achieved by using octupole magnets. See also Chapter 5.

The most reasonable scenario at present might be the following. We note the results in [46] for monomode laser guiding in a hollow capillary dielectric

tubes. A femtosecond 10^{16} W/cm^2 laser pulse is guided over 10 cm with low losses. The transverse intensity profile of such a pulse is $\propto J_0^2(\alpha_{n,0}r/a)$, so the focusing force on the trailing bunch would be proportional to $-\frac{\alpha_{n,0}^2}{a^2}r$. Small focusing force requires a large fiber radius $a \approx 0.5 - 1.0$ mm. The normalized vector potential corresponding to $I = 10^{16}$ W/cm^2 is $a_0 \approx 0.1$ which is relatively low. We can achieve required wakefield by a train of properly spaced pulses [47]. The power of a single pulse is $P \approx 20 - 80$ TW. There are other technical difficulties. Design I, for instance, requires a collision repetition rate of 50 kHz. Even loading multi bunches in a single shot wakefield still requires high laser repetition frequency. In addition to this, the efficiency of the production of TW pulses is currently low – about 10^{-4}. This figure needs to be improved by at least 2 orders of magnitude to keep the operating cost of the collider in reasonable limits.

3.4 Design Issues, Approximately Synchronous Acceleration, Horn Model

The material discussed in this section is a collaborative work [17, 18] with C. Chiu and T. Tajima, with C. Chiu having the leading role.

3.4.1 Accelerator with superunits, chips and magnets

In this subsection we investigate the effect on the emittance degradation of a reduction in the phase range of acceleration. Since we fix the total acceleration energy, as the acceleration interval per stage decreases, the number of acceleration stages will accordingly increase. The approach is the same as in the CTHY model, except that here we allow for variations of both the tube (wakefield sec-

tion) length and the gap-width. Fig. 3.1 shows emittance degradation vs. total number of stages for two sets of gap widths and various jitter parameters at a loading phase $\Psi_s = 0.15$ rad. All the graphs are given in log-log-plots.

There is a general trend that as the number of stages N increases, the average emittance growth decreases persistently. This behavior (see Eq. 3.4) is to be compared with an inverse-law parameterization [18] (valid for fixed final energy and gap to tube length ratio)

$$\Delta\epsilon = \frac{b\sigma_D^2}{N_T}. \tag{3.7}$$

There are two different b values, one for the gap=10tubes cases and one for gap=tube cases. This parameterization is based on the stochastic theory considered in the previous chapter. Here we mention that to derive this form, among other things, one needs to assign a mean acceleration phase Ψ_m. The approximation used here is given by

$$\Psi \approx \Psi_m = \Psi_s + 0.5\Delta.$$

This approximation is good if Δ is small or the number of stages N is large. We will confine our attention mainly to the region where $\Delta \leq 0.05$ rad or $N \geq 20$.

Figure 3.1 shows that for the jitter parameters $\sigma_D = 1\mu$m and 0.5μm, the average rate of fall of data points (solid circles and solid triangles) follows the respective lines reasonably well. There are more pronounced oscillations in the $\sigma_D = 0.5\mu$m case as compared to that in the $\sigma_D = 1.0\mu$m case. We now turn to the $\sigma_D = 0.1\mu$m cases, where points with open circles are to be compared to the respective dashed lines. Again the agreement with the theoretical prediction is reasonable. The overall pattern in Fig. 3.1 suggests

the following: the inverse-law parameterization works approximately for large N which is exactly in accordance with the limits of our theory from the previous chapter[1].

In a such scenario of having a very large number of stages, each stage becomes very short (e.g. of the order of 1 cm) and we are led to consider a superunit which is made out of many short tubes or chips, the wakefield within each chip is created by an independent laser pulse. We consider distances of the order of 1m between adjacent superunits to allow the experimental set up needed to maintain superunits including magnets placed over a certain period of length to ensure the quality of the beam. We have considered the following illustrative system:

- Total energy: 2.5 TeV, which is used as each of the two arms of the 5 TeV collider. The acceleration is from 0.5 TeV to 2.5 TeV.
- Total number of superunits (SU): 500
- Within one super-unit (SU) there are:
  - 100 stages per SU, and
  - gap = tube = 0.83 cm.
- There is a large-gap between two adjacent super-units: 1m
- Length of the accelerator: about 1300 m.

[1]Of course, it will work for any N if we average over many shots using different random sequences describing errors in the system. However, this involves specific assumptions about the time properties of the jitter and it is not pursued in the present work

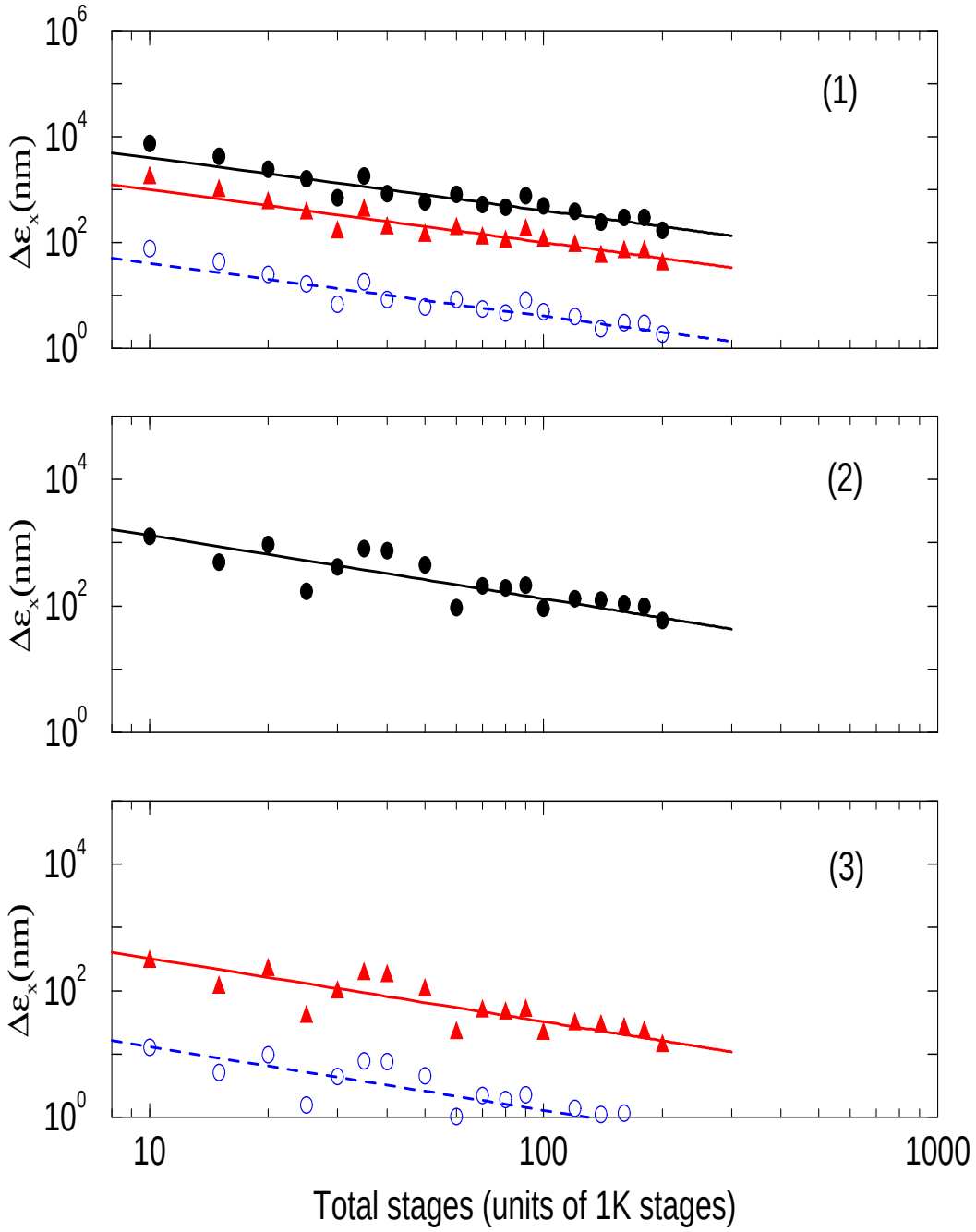

Figure 3.1: (Color) Multistages [17]: (1) Gap=10 tubes, $\sigma_{\mathcal{D}}$=1, 0.5, & 0.1 μm, (2) Gap=tube, $\sigma_{\mathcal{D}}$=1 μm, (3) Gap=tube, $\sigma_{\mathcal{D}}$=0.5 & 0.1 μm. Each case is compared with the inverse power law $1/N_T$. N_T is the total number of stages.

We proceed to look at how emittance degradation varies as a function of the loading phase for the system of superunits with chips. From Eq. (3.1) one expects in some average sense

$$\Delta\epsilon \propto \omega^3 \propto (\sin\Psi_m)^{3/2}, \tag{3.8}$$

where $\Psi_{\rm m}$ is the mean phase of the beam, taken to be $\Psi_m = \Psi_s + 0.5\Delta$. Here Ψ_s is the loading phase and Δ the total phase slip.

Fig. 3.2 shows the final emittance as a function of $(\sin\Psi_m)^{3/2}$ at the default value $\sigma_D = 0.1\mu$m. In the small $\Psi_{\rm m}$ region up to $(\sin\Psi_m)^{3/2} \sim 0.1$ the emittance degradation has an approximately linear behavior superposed by a small oscillation. Beyond this point, the oscillatory behavior becomes violent. This implies that that the resilience of the present system against jitters can be further improved, at least in the small loading phase region, by lowering the loading phase value. We consider two loading phases, i.e. $\Psi_s = 0.15$ rad and $\Psi_s = 0.05$ rad. Figure 3.3 (taken from [18]) shows the interim emittance degradation for three cases. There are 50K stages and all cases are at the final energy of 2.5 TeV. The stochastic theory if applicable implies that the intermediate emittance should grow approximately[2] linearly with the number of stages. Approximate mean linear behavior is observed for curves a and b. For curve c, there is a rapid rise up to about 20% of the total stages, which is followed by an approximately linear mean behavior. To conclude, within the present chip-model the final emittance has been reduced to say less than $2\epsilon_0$, where ϵ_0 is the initial normalized transverse emittance of

[2]This approximate linearity is valid as is Eq. (3.1) only under assumption of a constant typical energy beam transport. Obviously, the linearity is not a good approximation for very large N, when the asymptotic behavior is $\Delta\epsilon \propto \sqrt{N \ln N}$ as seen from Eq. (3.3)

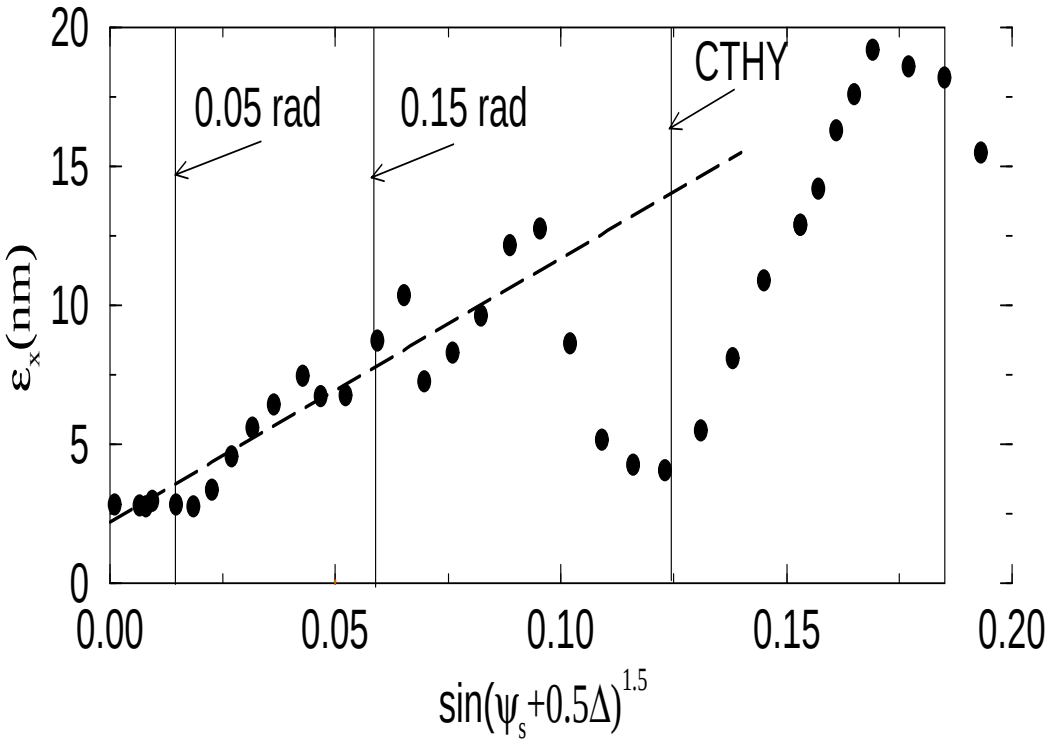

Figure 3.2: A comparison between the numerical results for the chip model and the $(\sin\Psi)^{3/2}$ law.

2.2nm. This is to be compared to the situation in the CTHY model, where the final emittance is beyond $100\epsilon_0$. This, however, is at the expense of introducing 50 times more laser pulses, which increases the power consumption by many folds. Thus it has severe practical limitations. These limitations might be ameliorated by adopting a technique to flip a phase by π by introducing two counterpropagating lasers with slightly different colors (G. Shvets' method[48]).

3.4.2 Synchronous Acceleration

As mentioned earlier for the "horn model" [18], synchronous acceleration may be achieved through a specific variation of the plasma density [41]. Consider a

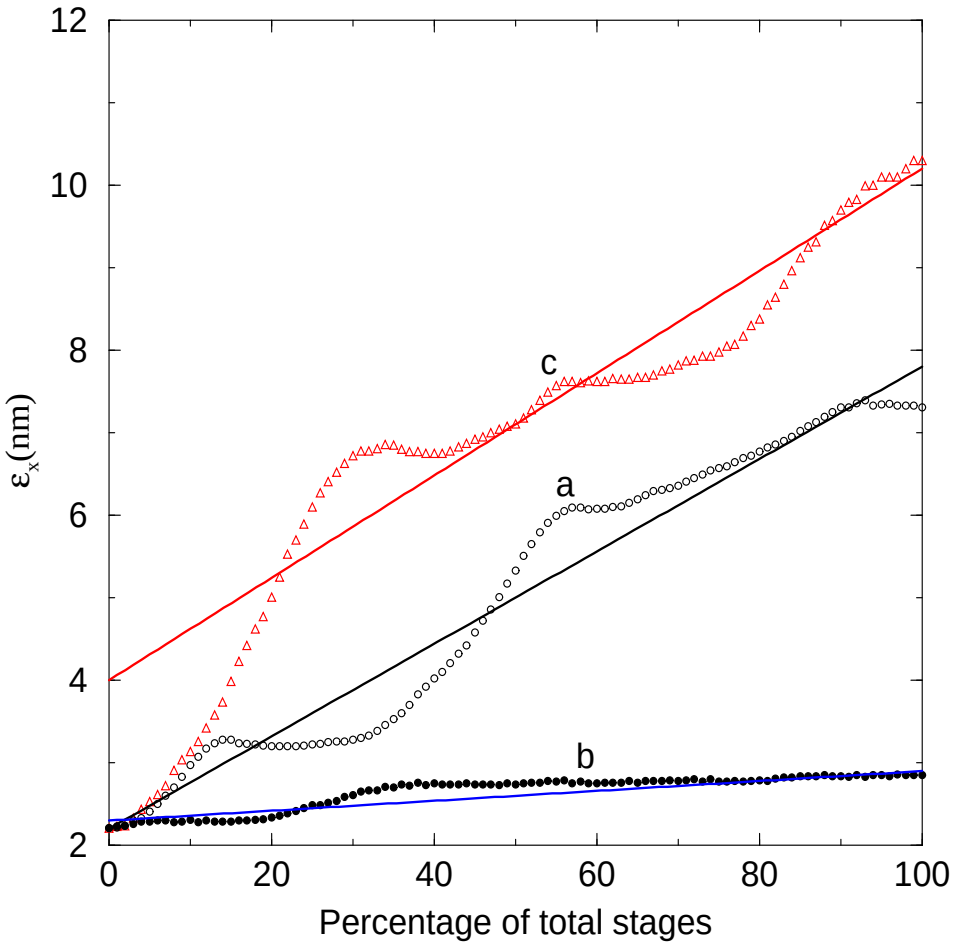

Figure 3.3: (Color) The interim emittance degradation behavior as the beam particles traverse through the system of a chip model for $\sigma_D = 0.1\mu$m. For each case, a solid line of a linear behavior is included to guide the eyes.
Curve a: Total stages: 50K, $\Psi_s = 0.15$ rad.
Curve b: Total stages: 50K, $\Psi_s = 0.05$ rad.
Curve c: Total stages: 20K, $\Psi_s = 0.05$ rad.

steady adiabatic flow of a fluid from a reservoir through a nozzle say in the z direction. Let the static fluid density of the fluid in the reservoir be ρ_0, which will be referred to as the quiescent density. Denote the fluid density at z along the nozzle be $\rho(z)$. In [18] we showed that based on fluid dynamics [42] the

following relation is valid:

$$A(z) = const \left(\frac{\rho(z)}{\rho_o}\right) \sqrt{1 - \left(\frac{\rho(z)}{\rho_o}\right)^{\gamma-1}} \ , \tag{3.9}$$

where γ is the usual ratio of the specific heat at a constant pressure to that at a constant volume. The region of interest is characterized by a subsonic fluid flow (see Figure 3.4a), where there is a one-to-one relationship between the cross sectional area A, and the plasma density ρ. By increasing the cross section along the beam direction in a specified way one may achieve the required density function. Looking down the stream of the beam, the accelerator consists of a system of aligned horns, although in some cases the increase in radius may be slight. This is the reason why we refer to the present model as the "horn model"(see Figure 3.4b). We now come to Katsouleas's matching condition (see Figure 3.4c). Consider the wakefield acceleration of a beam electron which is located at the center of the beam. Let the "loading number" N_{load} be the number of wave crests the electron is lagging behind the laser pulse. If the initial electron phase relative to the local wakefield , as defined earlier, is Ψ_s, then the electron phase relative to the laser pulse defined by the local plasma wave number k_p is

$$k_p s_1 = 2\pi N_{load} - \Psi_s,$$

where s_1 is the distance from the electron to the pulse measured in the rest frame of the pulse. To motivate the matching condition, for the time being imagine the horn has been divided into many segments. We will assume that the density is constant within each segment. For the ith and the i+1th segments, the wave numbers are k_{pi} and k_{pi+1}, respectively. The ith segment has a width

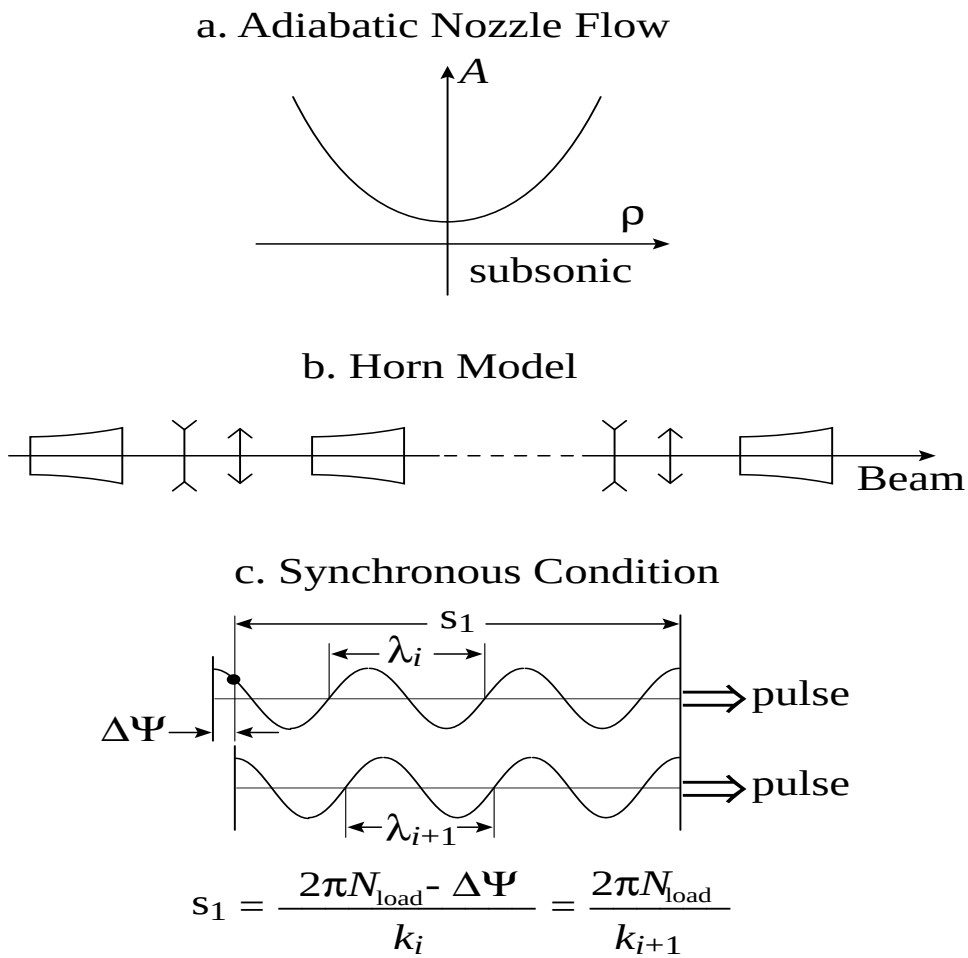

Figure 3.4: The Horn model and the matching condition

Δz and has a phase-slip $\Delta\Psi$. Here its phase relative to the pulse measured by the wave number of the ith segment is $k_{pi}s_1 = 2\pi N_{load} - \Psi_s - \Delta\Psi$. The synchronous condition requires the recovery of the initial phase at the start of the i+1th segment, i.e. $k_{pi+1}s_1 = 2\pi N_{load} - \Psi_s$. In other words, the matching condition is given by

$$\frac{2\pi N_{load} - \Psi_s - \Delta\Psi}{k_{pi}} = \frac{2\pi N_{load} - \Psi_s}{k_{pi+1}}. \tag{3.10}$$

We write $k_{pi+1} = k_{pi} + \frac{dk}{dz}\Delta z$, where Δz is the width of the ith segment. In the continuum limit, after some algebra it leads to

$$\frac{1}{k_p} \cdot \frac{dk_p}{dz} = \frac{1}{(2\pi N_{load} - \Psi_s)} \cdot \frac{d\Psi}{dz} = \frac{1}{2(2\pi N_{load} - \Psi_s)c} \cdot \frac{\omega_p^3}{\omega_0^2}. \tag{3.11}$$

The first equality is Katsouleas' condition for synchronous acceleration. The frequency of the laser pulse is denoted by ω_0. To evaluate the number density variation within the horn, we first recall that the frequency of plasma waves is proportional to the square-root of the number density. Thus the z-dependence of all three quantities: the number density of the plasma medium, the frequency and the wave number of plasma waves, may be specified by a single z-dependent function $\zeta(z)$. In particular, one may write

$$n(z) = n_0\zeta(z)^2,\ \omega_p(z) = \omega_{p0}\zeta(z),\ \text{and}\ k_p(z) = k_{p0}\zeta(z), \tag{3.12}$$

Substituting Eq.(3.12) into Eq.(3.11) gives

$$\frac{1}{k} \cdot \frac{dk}{dz} = \frac{1}{\zeta} \cdot \frac{d\zeta}{dz} = \frac{1}{2(2\pi N_{load} - \Psi_s)c} \cdot \frac{\omega_{p0}^3}{\omega_0^2}\zeta^3, \tag{3.13}$$

To the extent one neglects the pump-depletion effect[33], i.e. the loss of laser pulse energy as it traverses through the horn, the intensity and the frequency

of the laser pulse is assumed to be constant. Integrating over Eq. (3.13) leads to

$$\zeta(z) = \frac{1}{(1 - z/z_0)^{1/3}}, \text{ with } z_0 = \frac{2(2\pi N_{load} - \Psi_s)c}{3} \cdot \frac{\omega_0^2}{\omega_{p0}^3}. \tag{3.14}$$

In a similar fashion pump depletion effect and the adiabatic invariance can be included in our scheme, however it involves significant amount of algebra and is left for [18]. All this leads to modifications in the longitudinal and transverse transfer map. Here we discuss only the numerical results. For the present synchronous acceleration case, there is no quarter-wavelength restriction, so the tube length can *a priori* vary over a range of values. We have verified that the emittance degradation is also not too sensitive to the loading number. Here is an illustrative case [18]. The tube length is 0.35m and the loading number is 5. The density variation per horn is 7%, with the acceleration energy per stage 2.08 GeV, which is comparable to that of the CTHY model. In Figure 3.5 [18], curve-a corresponds to the case where $\Psi_s = 0.15$ rad. Here the final emittance is $\epsilon = 237\text{nm} \sim 108\epsilon_0$, which is in the same ball park as that of the CTHY model. So far we have not gained much ground. The important case is curve-b, which is the case where $\Psi_s = 0.04$ rad. It has a final emittance $\epsilon = 31.7\text{nm} \sim 14.5\epsilon_0$, which is about an order of magnitude reduction compared to that of the CTHY model. The interim emittance for this case [18] is shown in Figure 3.5-1 and with an amplified scale in Figure 3.5-2. The emittance degradation is sensitive to the longitudinal phase spread of the beam which for all cases considered up to now has been taken to be $\sigma_\psi = 0.01$ rad. Curve-c illustrates the case for a negligibly small value of the spread, i.e. $\sigma_\psi = 0.0001$ rad. Here the final emittance is given by $\epsilon = 8.4\text{nm} \sim 3.8\epsilon_0$. See [18] for more details.

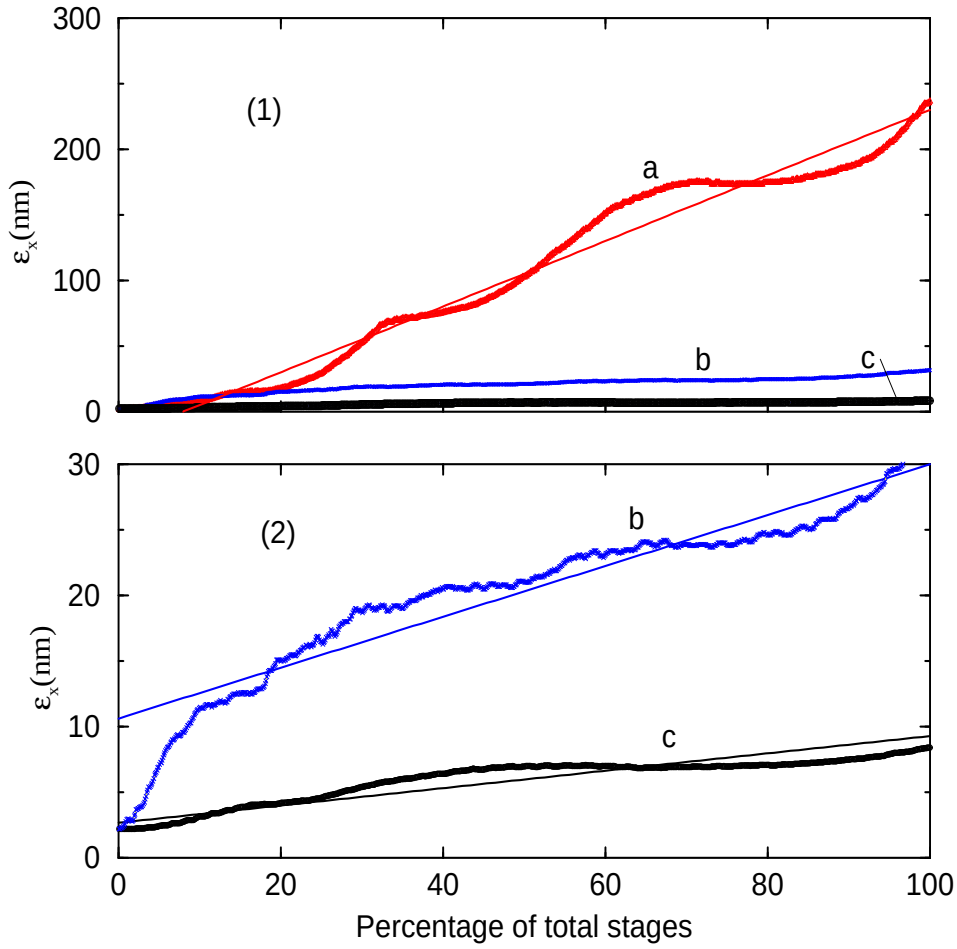

Figure 3.5: (Color) The emittance degradation for three cases of the horn model.
Curve-a: $\Psi = 0.15$ rad
Curve-b: $\Psi = 0.04$ rad
Curve-c: $\Psi = 0.04$ rad and $\sigma_\psi = 0.0001$ rad

3.5 Emittance minimization control of LWFA

In this section we describe preliminary results [19] of our studies on active feedback [49] (and feed forward) control of beams of the LWFA based collider. In the past we introduced the feedforward control of laser optics by the neural net in order to minimize the jitter of the mirror positions [50]. The idea here is

to correct the stage positions based on the measurements of the final emittance only rather than to "measure" more difficult quantities of the beam. This is the entropy minimization strategy. We implemented this strategy in our model CTHY. In our computer code (modified by F. Breitling to include the minimization algorithm), each transverse stage displacement consists of two parts: constant (in time), with a magnitude in the micron range and random (in time), with a magnitude in the submicron range. After each shot a stage is moved transversely by a certain fraction of a micron. If the emittance is decreased the new position is accepted; otherwise the previous position is reset. As a result the emittance can be significantly reduced if the stochastic (in time) jitter is not very large. Typical runs, courtesy of F. Breitling, are shown in Figure 3.6. However, there are several problems: after adjustments the stages are still misaligned (the algorithm finds local minima of the emittance) and correspondingly the beam centroid is usually kicked too much; this method reduces the emittance by a large factor when the emittance growth is large but does not work that well for smaller emittance growth. As a future plan we want to incorporate the beam centroid position in the algorithm and also study the efficacy of the algorithm in different accelerator scenarios.

3.6 Conclusions

Emittance control in a high energy accelerator is of crucial importance. In the previous chapter we identified the main effects that degrade the emittance of the beam in plasma wakefield based collider. In this chapter we considered various methods for emittance control and discussed their efficacy and applicability. A significant improvement over the CHTY model is observed in all mitigated focusing/controlled scenarios. Lastly we note that in the weak

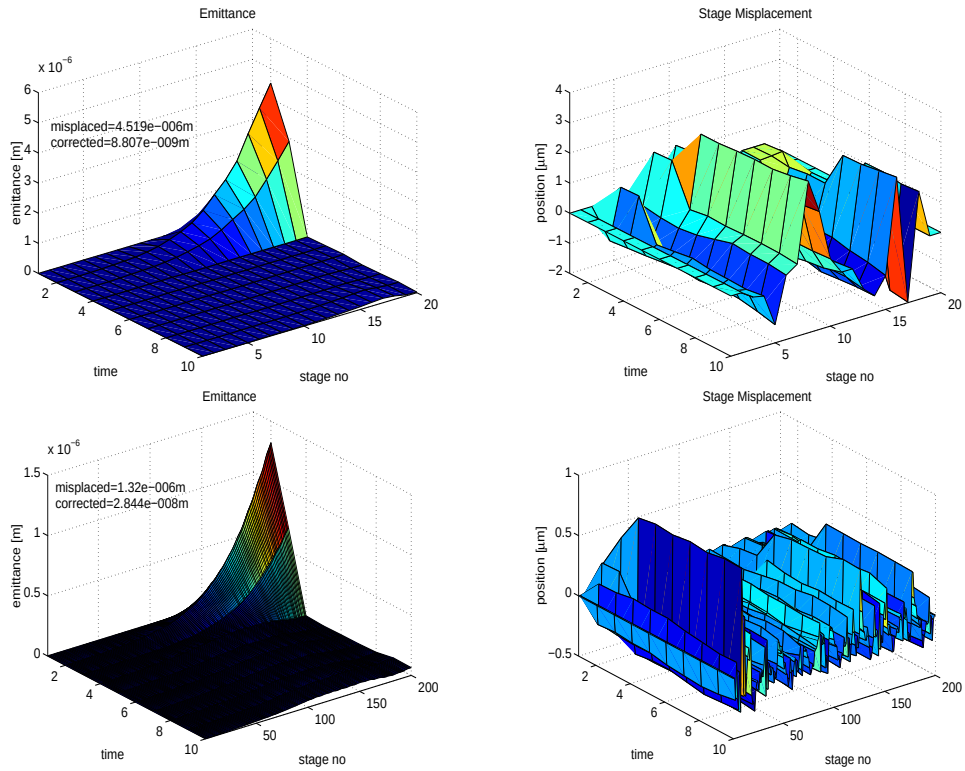

Figure 3.6: (Color) The improved control of emittance by feedback control to minimize beam entropy (final emittance). The transverse normalized emittance and stage positions in 20 (upper row) and 200 (lower row) stage units. Magnitude of the constant in time misalignment is 2μm and of the stochastic one is 0.1μm

focusing cases achieved in plasma the collision-induced emittance degradation becomes important, since it is inversely proportional to the betatron frequency. Correspondingly, there is an optimal wakefield focal strength. We will present the results on this in a follow-up paper. Here let us just make an estimation for a hydrogen plasma. Following [51], we consider the emittance growth rate from the multiple scattering in a hydrogen plasma:

$$\frac{d\epsilon_x}{dz} = \frac{\gamma\beta}{2}\frac{d}{dz} < \Theta^2 >_p \ , \tag{3.15}$$

where

$$\frac{d}{dz} < \Theta^2 >_p = \pi\, n_p \left(\frac{4r_e^2}{\gamma^2}\right) \ln\left(\frac{\lambda_D}{R_0}\right) , \tag{3.16}$$

where $R_0 = 0.7 \times 10^{-13}$cm is the effective radius of the proton and λ_D is the Debye length ($\lambda_{\rm D} = k_p^{-1}\sqrt{kT/mc^2}$). Assuming $\gamma = \gamma_{\rm i} + \gamma' z$ we integrate and obtain

$$\Delta\epsilon_x = \frac{4\pi\, n_p\, r_e^2}{\gamma'} \ln\left(\frac{\lambda_D}{R_0}\right)(\beta_{\rm f} - \beta_{\rm i}) , \tag{3.17}$$

where $\beta_{\rm f}$ and $\beta_{\rm i}$ are the final and the initial betatron lengths, respectively. We used the fact that $\beta \propto \sqrt{\gamma}$. In our CHTY design, for instance, the acceleration gradient is 6 GeV/m which corresponds to $\gamma' \approx 1.2 \cdot 10^4$ m^{-1}. In [51] the electron temperature is chosen to be 5 eV , in our case it might be much higher but the result is very insensitive to this value. In particular for $kT = 5$ eV and $n_p \approx 10^{17}$ cm^{-3} we obtain:

$$\Delta\epsilon_x \text{ [m]} \approx 10^{-8}\,(\beta_{\rm f} - \beta_{\rm i}) \text{ [m]} , \tag{3.18}$$

which gives $\Delta\epsilon_x \approx$ 10nm. This value is several times larger than the design I emittance of [12]. This problem worsens in the weaker focusing scenarios achieved in a plasma. Apparently, it is preferable to have if not completely hollow channel, at least a reduced plasma density on the axis to avoid the multiple Coulomb collisions effect.

This concludes our beam transport and emittance studies. In the future research on this subject many additional problems need to be resolved: the resonance absorption issue in the hollow channel case, possible low efficiency of the relatively large laser spot scenarios. In the next chapter we study additional properties of the LWFA multistage acceleration when applied to polarized electron and (or) positron beams. Additionally we will present IP polarization

and luminosity studies which are important for suppressing the noise at IP and correspondingly for improving the discovery potential of the high energy accelerator.

Chapter 4

Luminosity and Polarization Issues in a High Energy Linear Collider

4.1 Collision Point Physics

In a quest of the next energy frontier an electron-positron linear collider at the energy of 5 TeV has been considered [12, 16]. At this energy many uncertainties exist, including the basic driver. In this chapter we discuss the main Interaction Point Physics issues characteristic of these future machines.

One of the main purposes of the next generation high energy accelerators – the Large Hadron Collider (LHC) and the Next Linear Collider (NLC) is to check the predictions of the weak scale supersymmetry (SUSY) which if correct should lead to the discovery of light Higgs particles and light superpartners. Preservation of beam quality during the acceleration is extremely important, however it is not the only problem we have to solve. There are fundamental difficulties associated with the interaction point (IP) physics. Colliding of beams gives rise to the well known phenomenon of beamstrahlung [52] which is a synchrotron radiation of the particles in the electromagnetic field of the opposing beam. It is often undesirable because it effectively decreases colliding particles energies and can also lead to a possible photon contamination of the detectors. The way to avoid the former is to either work in the classical regime with a

very small beamstrahlung parameter $\Upsilon \ll 1$[1] or to move to the "quantum suppression" regime [12] characterized by $\Upsilon \gg 1$. A very important parameter which characterizes a collider performance is the geometrical luminosity

$$\mathcal{L}_g = f_c N^2 / 4\pi\sigma_x\sigma_y \ , \tag{4.1}$$

where f_c is the collision frequency, N is the number of particles per bunch, σ_x and σ_y are the horizontal and vertical rms beam sizes at the IP, respectively. However, the real luminosity at the IP, in general, is different. Two processes at the IP have a profound effect on the luminosity: the above mentioned beamstrahlung and also the disruption. The beamstrahlung parameter can be calculated in the following way. The beamstrahlung photon energy is $\hbar\omega_\gamma$, where $\omega_\gamma \approx \omega_c\gamma^3$ according to the result for the radiation of an ultrarelativistic charged particle in [53]. The electron (positron) cyclotron frequency ω_c is determined by $\omega_c = \frac{eB}{\gamma mc}$, where B is an effective magnetic field at the IP. Here we assume that the electron (positron) trajectory is approximately circular at the IP. Taking into account that the electron energy is γmc^2 we obtain that the beamstrahlung parameter Υ is given by

$$\Upsilon = \frac{\hbar\omega_\gamma}{\gamma mc^2} = \gamma\frac{B}{B_c} \ , \tag{4.2}$$

where $B_c = m^2c^3/e\hbar = 4.4 \times 10^{13}$ Gauss is the Schwinger's field. It can be also written [52] as

$$\Upsilon = \frac{5r_e^2\gamma N}{6\alpha\sigma_z(\sigma_x + \sigma_y)} \ , \tag{4.3}$$

where σ_z is the rms bunch length, r_e is the classical electron radius and α is the fine structure constant. As analysis in [12] shows in the limit of a large Υ

[1] Υ is defined as the ratio of the classically calculated beamstrahlung photon energy to the beam electron/positron energy.

the radiation losses might be rather small, somewhat counter-intuitively, due to the quantum suppression of the radiation. The radiation losses are most conveniently monitored through the number of emitted photons per electron n_γ given by

$$n_\gamma = 2.54 \frac{\alpha \sigma_z \Upsilon}{\lambda_c \gamma} U_0(\Upsilon) \ , \tag{4.4}$$

where $\lambda_c = \hbar/mc$ is the Compton wavelength, $U_0 \approx 1/(1+\Upsilon^{2/3})^{1/2}$ and the relative electron energy loss δ_E introduced as

$$\delta_E = 1.24 \frac{\alpha \sigma_z}{\lambda_c \gamma} \Upsilon U_1(\Upsilon) \ , \tag{4.5}$$

where $U_1(\Upsilon) \approx 1/(1+(1.5\Upsilon)^{2/3})^2$. The other process of importance is the disruption described by D_y

$$D_y = \frac{2 r_e N \sigma_z}{\gamma \sigma_y (\sigma_x + \sigma_y)} \ . \tag{4.6}$$

Roughly speaking, D_y describes the amount of beam disruption due to the collective field of the opposite beam. In general, for a successful collider operation n_γ, δ_E, and D_y have to be small compared to unity. For large Υ and fixed center of mass energy, geometrical luminosity, available power, and beam aspect ratio (σ_x/σ_y), we can write [12]

$$f_c \sim 1/N \ , \ \ \sigma_y \sim \sqrt{N} \ , \ \ D_y \sim \sigma_z \ , \ \ \Upsilon \sim \sqrt{N}/\sigma_z \tag{4.7}$$

$$n_\gamma \sim (N\sigma_z)^{1/3} \ , \ \ \delta_E \sim (N\sigma_z)^{1/3} \tag{4.8}$$

Now we can see that the performance of the high beamstrahlung parameter collider can be improved by reducing σ_z. Even though Υ increases in this strategy, the real photon radiation actually decreases. Naturally, small σ_z strategy fits well with the plasma based accelerators parameters since the driver wavelength

is very short. Such scenarios are analyzed in [12] and several strawman collider designs were developed. See Table 2.1. An outstanding e^-e^+ luminosity core at the design 5 TeV energy was observed in the "CAIN" simulations. A typical run is shown in Fig. 4.1 (note that a logarithmic scale was used on the y-axis).

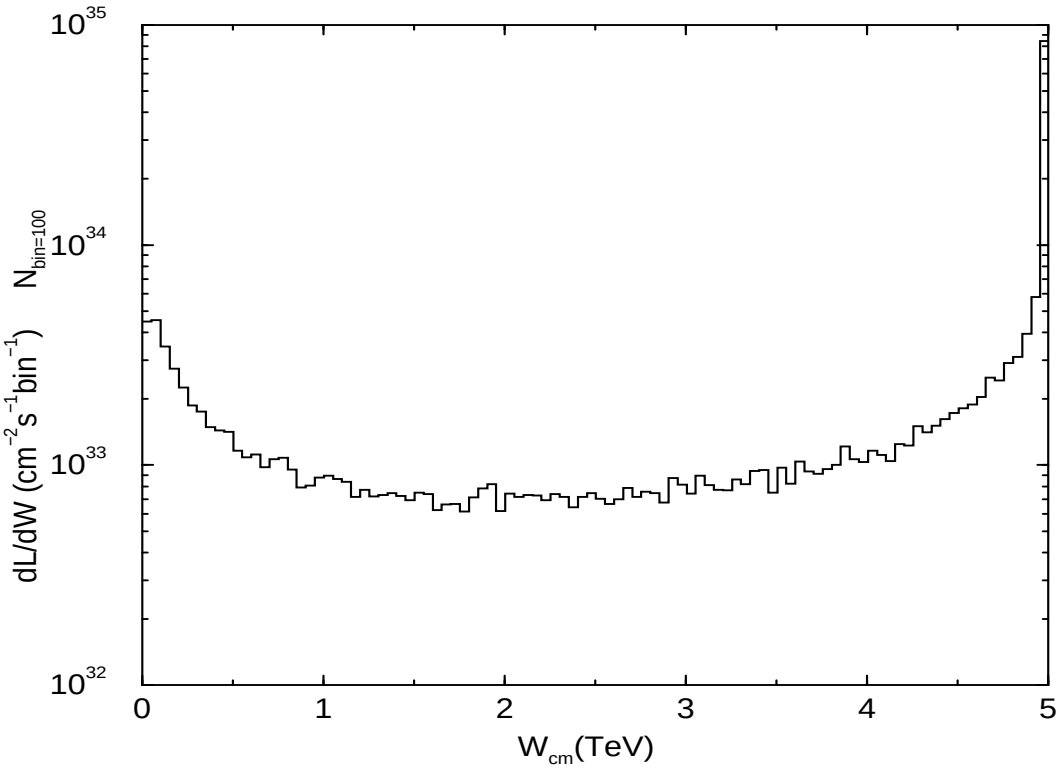

Figure 4.1: Differential e^-e^+ luminosity for the Design I of a 5 TeV electron-positron collider of [12].

We carried out additional QED simulations [15] based on the CAIN code [13], [12]. These simulations show that the photon contamination is relatively easy to avoid due to the fact that the photon angular distribution has a very sharp peak (see Figure 4.2, in this example all the beamstrahlung photons are in a 20 mrad angle around the beam axis) in the forward (backward) direc-

tion (with respect to the beam). Secondary particles created via coherent and incoherent pair production are also sharply peaked in the forward (backward) direction. So we just need to place our detectors at large enough angles.

However, there are additional major obstacles to do discovery physics on such a machine. We should be able to extract the new physics signatures from the experimental data. At these energies, however, there are strong contributions from Standard Model processes which create a significant background to deal with. One of the most important ones, due to the high $\gamma - \gamma$ luminosity (see Figure 4.3), is that of $\gamma\,\gamma \to W^+\,W^-$. We need to impose additional cuts to eliminate background as much as possible and to improve the signal to noise ratio. The analysis presented in [54] shows that in the region of center of mass energies of a few hundreds GeV it should be possible to observe signatures of new physics. We hope to be able to do Higgs physics in this range (if the light Higgs exists) and also to find the lightest supersymmetric partners (if SUSY is correct). A major method to eliminate the background is b-tagging (for Higgs sector). Consider the following example (if $m_h < 2m_Z$): $e^+e^- \to Z \to Z\,h$. The background consists of ZZ and WW and the way to deal with it may be the double b-tagging and jet-jet mass reconstruction followed by visible energy cut. In the search of s-leptons a possible plan is to use polarized electron beams. For instance, $e^-e^- \to \tilde{e}^-\tilde{e}^-$ is practically free of the W-background if we use right handed polarized electron beams [55]. The produced s-electrons can decay in several different modes, all of them ending in neutralino (invisible) production and lepton pairs which leads to a clean missing energy signature of the reaction. High luminosity to be achieved in the high Υ regime is more than welcome in this case. The great opportunity provided by e^+e^- linear machine

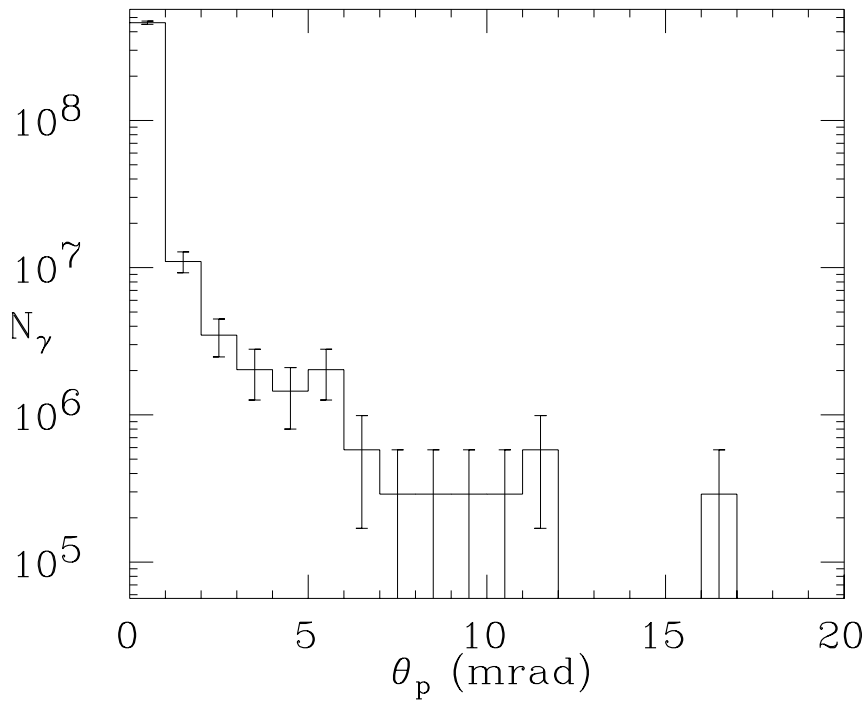

Figure 4.2: The number of photons N_γ vs. θ_p (angle with respect to the beam axis) at IP of a 5 TeV e^+e^- linear collider (parameters used correspond to design III [4]; this and the next graphs are obtained using the "CAIN").

is that it can be relatively easy changed into e^-e^- or $\gamma\gamma$ linear collider. In this sense linear colliders will be of great importance even after the start of LHC. In the TeV range the new physics we can expect is largely unknown. The predictions are strongly model dependent and probably modifications will occur after LHC and NLC become operational. If the light Higgs and superpartners are not discovered at 500 GeV center of mass energy we can hope that moving to TeV range will enable us to do this.

Let us now come back to the polarized beam issues. It is well known that the right and left components of the leptons and quarks exhibit lopsided interactions. Their couplings to the electroweak bosons are different and at high

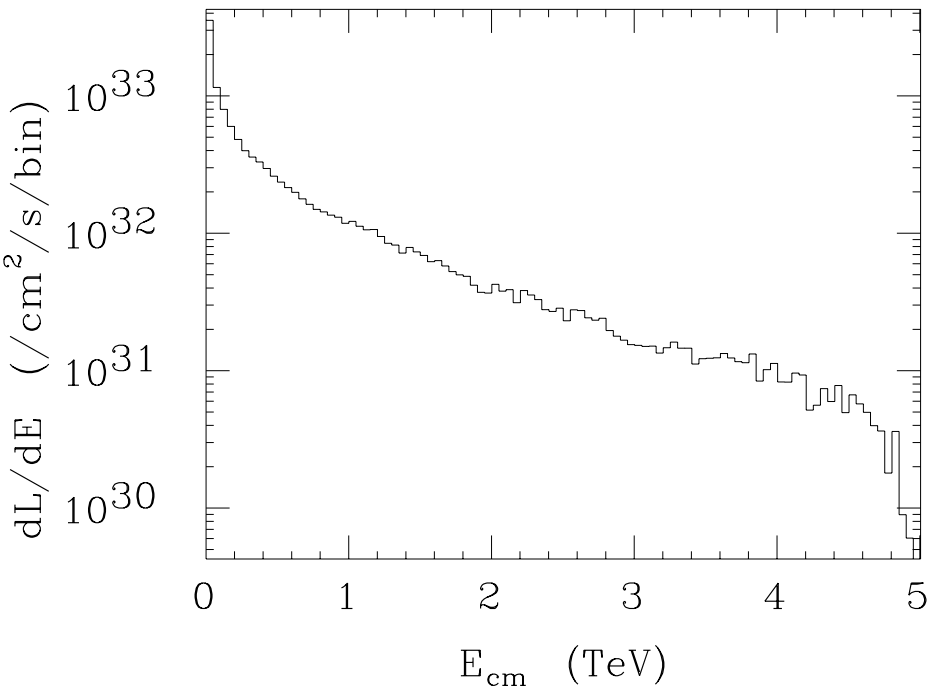

Figure 4.3: The differential $\gamma - \gamma$ luminosity dL/dE vs. the center of mass energy E_{cm} at IP (again design III [4]).

energies (above the electroweak scale) polarization of the particles becomes an extremely important characteristic since R and L components practically do not mix. Because of this in our laser wakefield collider at high energies we can take advantage of these properties to suppress certain branches of reaction which we may deem as "noise" (no new physics). A major concern is the Standard Model background, important part of which is significant W^+W^- production [54] in the e^+e^- case and W^- bremsstrahlung [55] in the case of the e^-e^- collider. It is known that one possibility to suppress partially these processes is via use of polarized electron/positron beams. Correspondingly, it is important to study depolarization effects [20] during acceleration and colliding of the charged particles. Considering a collider based on multiple Laser Wakefield

Accelerator units we estimate depolarization effects due to the focusing and accelerating fields in the main accelerator section. Preliminary results show practical preservation of the initial polarization state, especially in the favorable for many other reasons cases of weak focusing force under ideal focusing and acceleration conditions. Furthermore, we investigate the effect of errors in the accelerating structure by incorporating spin degrees of freedom in our LWFA systems code. We show that in cases which conserve the normalized emittance of the accelerated beam the change in polarization is negligible. To study the depolarization at the Interaction Point (IP) we use again the Quantum Electrodynamics "CAIN" code [13]. We consider high Υ cases which were shown [12] and in this section to be preferential for laser/beam driven plasma wakefield accelerators.

4.2 Depolarization in the Accelerating and Focusing Wakefields

The polarization of a single particle can be described by a vector $\mathbf{s}$ which is equal to the doubled spin value and describes the polarization in the instantaneous rest frame of the particle. The equation of polarization precession [56, 57] is

$$\begin{aligned} \frac{d\mathbf{s}}{dt} &= \frac{2\mu + 2\mu'(\gamma - 1)}{\hbar\gamma}\mathbf{s} \times \mathbf{H} + \frac{2\mu'\gamma}{\hbar(\gamma+1)}(\boldsymbol{\beta} \cdot \mathbf{H})\boldsymbol{\beta} \times \mathbf{s} \\ &\quad + \frac{2\mu + 2\mu'\gamma}{\hbar(\gamma+1)}\mathbf{s} \times (\mathbf{E} \times \boldsymbol{\beta}) \ , \end{aligned} \tag{4.9}$$

where $\mathbf{E}$ and $\mathbf{H}$ are the electric and magnetic fields in the laboratory system, $\boldsymbol{\beta}$ is particle velocity and γ is the Lorentz factor, $\mu = -9.3 \cdot 10^{-21}\text{erg} \cdot \text{Gauss}^{-1}$ and $\mu' = -1.1 \cdot 10^{-23}\text{erg} \cdot \text{Gauss}^{-1}$ respectively. We see that at high energies $\gamma \approx 10^5 - 10^7$ the contribution to the r.h.s. of the above equation from the

classical magnetic moment of the electron becomes negligible. We have to consider only the terms which depend on the anomalous magnetic moment. Equation (4.9) describes the classical precession of the particle polarization. It is applicable when the fields **E** and **H** are not very large and do not vary too rapidly in space. More precisely [56] the fields should vary slightly over distances of the order of the particle wavelength and the Compton wavelength. These requirements are certainly satisfied in the linac portion of the collider. The IP analysis we leave for Sec. 4.4. Neglecting small terms, we obtain:

$$\frac{d\mathbf{s}}{dt} = \frac{2\mu'}{\hbar}\left[\mathbf{s}\times\mathbf{H} + \mathbf{s}\times(\mathbf{E}\times\boldsymbol{\beta})\right] . \tag{4.10}$$

Assuming z is the direction of propagation of the electrons and x and y are the transverse coordinates, in the channeled case of Laser Wakefield Accelerator [38] (ideal hollow channel) we obtain

$$\begin{aligned} \frac{ds_x}{dt} &= \frac{\mu'}{\hbar\gamma_p^2}E_x s_z \ , \\ \frac{ds_y}{dt} &= \frac{\mu'}{\hbar\gamma_p^2}E_y s_z \ , \\ \frac{ds_z}{dt} &= -\frac{\mu'}{\hbar\gamma_p^2}(E_x s_x + E_y s_y) \ . \end{aligned} \tag{4.11}$$

Electrons are considered ultrarelativistic $\dot{z} \approx c$. Assuming that the transverse field can be described by a simple harmonic oscillator restoring force ($E_x = E_0 x/\sigma$, $E_y = E_0 y/\sigma$), the equations of motion of the electron are:

$$x = x_0\cos(\omega t + \phi_x) \ , \tag{4.12}$$

$$y = y_0\cos(\omega t + \phi_y) \ , \tag{4.13}$$

where $\omega = \sqrt{\frac{eE_0}{2\gamma_p^2 m\gamma\sigma}}$ is the betatron frequency (here in units of s^{-1}). So the polarization evolution equations reduce to

$$\frac{ds_x}{dt} = -\Omega\frac{x_0}{\sigma}s_z\cos(\omega t + \phi_x) \ ,$$

$$\begin{aligned} \frac{ds_y}{dt} &= -\Omega \frac{y_0}{\sigma} s_z \cos(\omega t + \phi_y) \ , \\ \frac{ds_z}{dt} &= \Omega \left(\frac{x_0}{\sigma} s_x \cos(\omega t + \phi_x) + \frac{y_0}{\sigma} s_y \cos(\omega t + \phi_y) \right) \ , \end{aligned} \tag{4.14}$$

where $\Omega = \frac{-\mu'}{\hbar \gamma_p^2} E_0$ and σ is the beam transverse size (assuming same in x and y). The transverse field E_0 can be estimated as

$$E_0 = k_p \sigma E_{\text{acc}}, \tag{4.15}$$

where E_{acc} is the acceleration gradient. If we take $E_{\text{acc}} \sim 10$ GV/m and a betatron length of 10 m we obtain $\Omega \approx 4 \cdot 10^3$ s^{-1} which is extremely small compared to $\omega \approx 3 \cdot 10^7$ s^{-1} (in reality ω depends on the energy and we include this in Sec. 4.3). So the corresponding change in the polarization is very small. Let us make some estimations for a single particle. If we take the initial polarization values $s_z = 1$, $s_x = s_y = 0$ and assume $y_0 = 0$ then a closed form solution in this case is $s_z = \cos\left(\frac{\Omega}{\omega} \frac{x_0}{\sigma} \sin \omega t\right)$. As we see from Fig. 4.4 which shows the dependence of the third component of the polarization (which is nearly equal to the longitudinal component of the polarization) of a single particle on the distance traveled in the accelerator, the depolarization in this case is clearly negligible, the amplitude of the small oscillation being approximately $\frac{\Omega^2}{2\omega^2} \frac{x_0^2}{\sigma^2}$. For the case $x_0 = \sigma$ the depolarization is $1 - s_z \approx 10^{-8}$ and for $x_0 = 10\sigma$ it is approximately 10^{-6}. In the case of a uniform plasma, focusing fields are stronger, correspondingly the effect is bigger but still not significant. In the next section we analyze the weak and strong focusing force cases in greater detail for CHTY and CHTY1 models using the systems code approach.

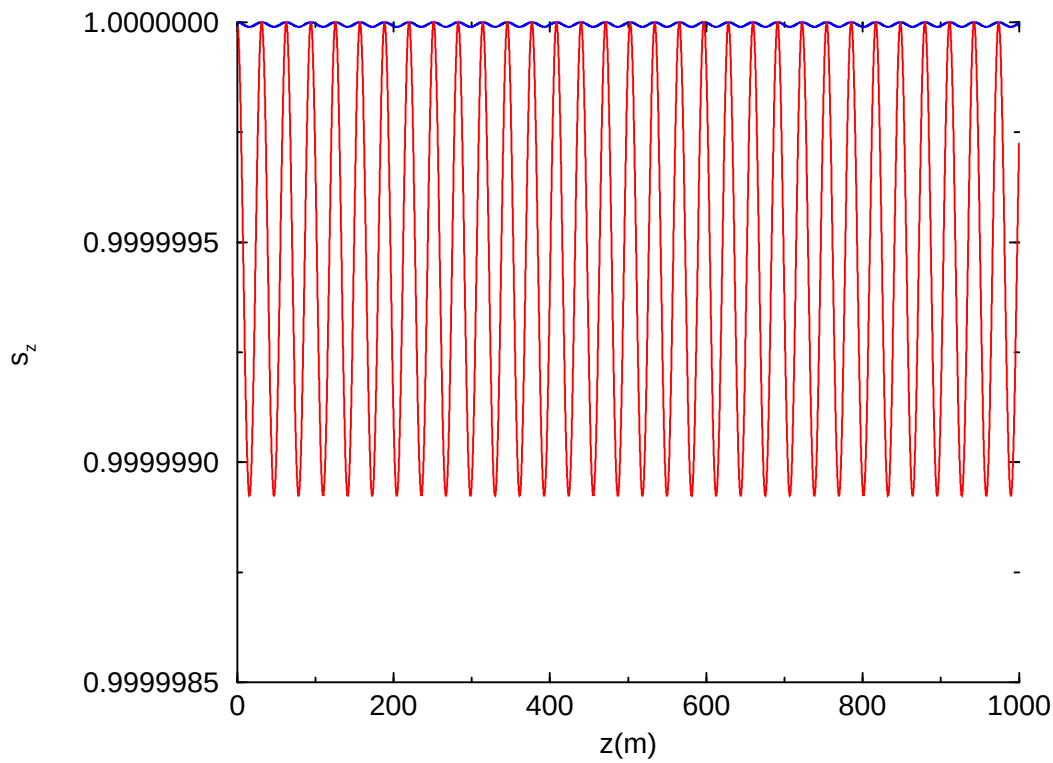

Figure 4.4: (Color) s_z vs. distance (in meters). Blue line is for $x_0 = \sigma$ and red line is for $x_0 = 10\sigma$.

4.3 Accelerator Lattice Errors

It is equally important to study the effect of accelerator lattice errors on the depolarization. In previous chapters we studied the effect of random stage jitter on the beam quality, the beam emittance, in which a weak focusing was crucial in preserving the emittance.

To investigate the jitter effects on spin depolarization during the acceleration, we take the wakefield map of Chapter 2. The model we use again is: N LWFA stages, betatron frequency constant for each stage and each particle; free drift between the stages; stochastic transverse stage jitter.

The transverse map ($\tilde{x} = \sqrt{\gamma}x$, x – the transverse coordinate of the

particle) is

$$\begin{pmatrix} \tilde{x}_{n+1} \\ \dot{\tilde{x}}_{n+1} \end{pmatrix} = M_n \begin{pmatrix} \tilde{x}_n - \tilde{\mathcal{D}}_n \\ \dot{\tilde{x}}_n \end{pmatrix} + \begin{pmatrix} \tilde{\mathcal{D}}_n \\ 0 \end{pmatrix} , \tag{4.16}$$

where $\mathcal{D}_n$ is the stochastic misalignment and

$$M_n = \begin{pmatrix} \cos(\frac{\omega_n}{\omega_s}\Delta), & \frac{1}{\omega_n}\sin(\frac{\omega_n}{\omega_s}\Delta) + L\cos(\frac{\omega_n}{\omega_s}\Delta) \\ -\omega_n \sin(\frac{\omega_n}{\omega_s}\Delta), & -L\omega_n \sin(\frac{\omega_n}{\omega_s}\Delta) + \cos(\frac{\omega_n}{\omega_s}\Delta) \end{pmatrix} ,$$

where ω_n is the betatron frequency in the wakefield (in units 1/m), $\omega_s = \frac{k_p}{2\gamma_p^2}$ characterizes the phase slippage, Δ is the phase slippage and L is the drift space. The map for the longitudinal coordinates is the same as in Chapter 2.

In a similar way we can build a map which describes the evolution of polarization degrees of freedom as beam propagates in the accelerator. Adopting again the scheme with accelerator units and free drift spaces between them we write Eq. (4.14) as (for simplicity we restrict ourselves to a 2-d model)

$$s_x{}^{n+1} = s_x{}^n \cos\theta_n + s_z{}^n \sin\theta_n , \tag{4.17}$$

$$s_z{}^{n+1} = -s_x{}^n \sin\theta_n + s_z{}^n \cos\theta_n , \tag{4.18}$$

where $\theta_n = \frac{\Omega(\dot{x}_n - \dot{x}_{n+1})}{\sigma\omega_n^2}$ and n enumerates the stage. We note that in the absence of stage jitter there is a slight depolarization due to the phase space mixing (different particles have different betatron frequencies and after some characteristic time they "mix"). The precession effect is small for a single particle and correspondingly the depolarization is small for the whole particle ensemble.

In the presence of stage jitter (or any other errors) which has broad frequency spectrum we can expect a resonance phenomenon with the spin precession frequency and depolarization because of this. We add the spin degrees of freedom in our systems multistage code to study the depolarization. Simulations do not show any significant effect arising from the stage jitter. The

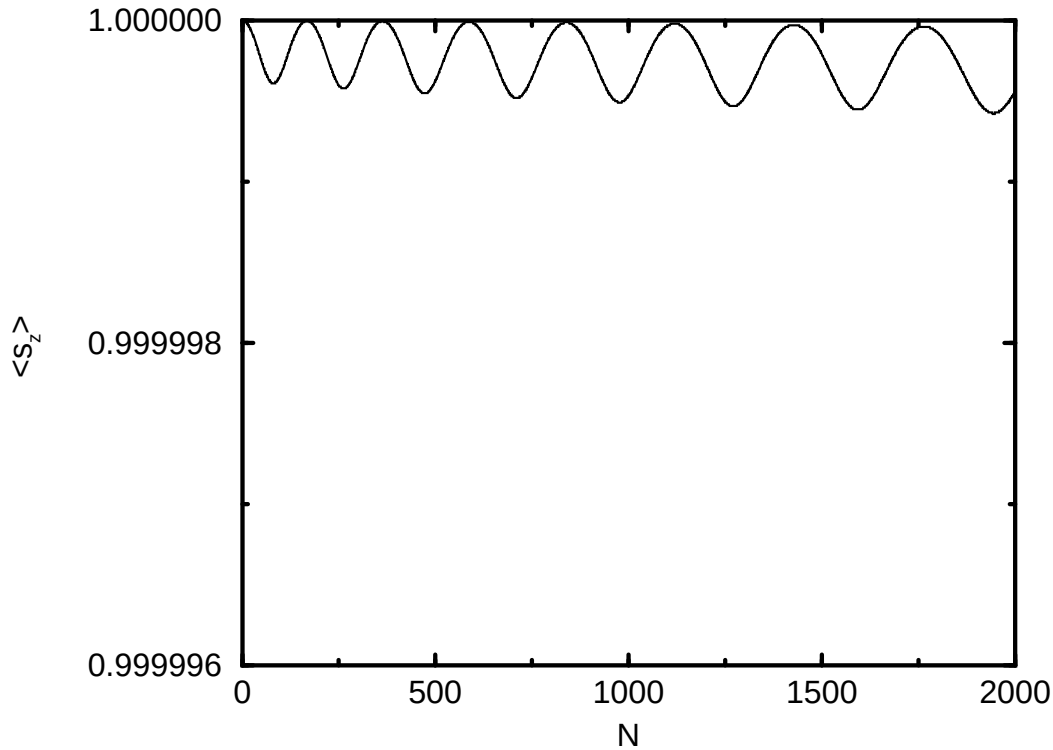

Figure 4.5: Beam polarization vs. stage number. Weak focusing (in a channel) without a transverse jitter.

amount of depolarization during the acceleration process is small in the cases which preserve the normalized beam emittance. Figures 4.5 and 4.6 show hollow channel (weak focusing) runs without and with stage jitter, respectively. The parameters used correspond to design I [12]. The stage considered is: $\gamma_p \approx 150$, the channel radius $a = 30\mu$m, the laser spot size $r_s = 50\mu$m, the plasma density (outside the channel) $n = 5 \cdot 10^{16}\text{cm}^{-3}$ and the laser wavelength $\lambda \sim 1\mu$m. The size of the stage dislocations used was 1.0μm. In the strong wakefield focusing cases (see Fig. 4.7 and 4.8) the depolarization is bigger but still not significant. Initially the beam is completely longitudinally polarized.

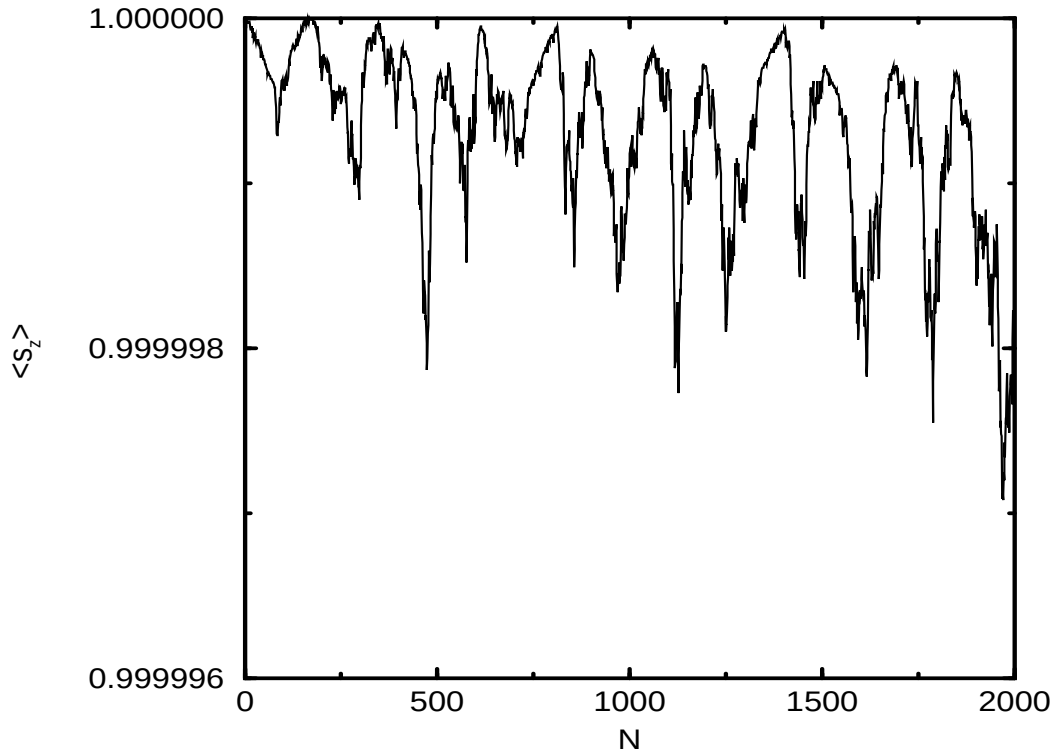

Figure 4.6: Beam polarization vs. stage number. Weak focusing (in a channel) with a transverse jitter.

4.4 Depolarization at the Interaction Point

The depolarization effect maybe more important at the IP [57] because of the extremely large self-fields. The depolarization occurs via two different mechanisms: the first is again the classical polarization precession (but now in the self fields) and the second is purely quantum spin-flip radiation [58]. On the other hand, the anomalous magnetic moment tends to decrease with the field strength therefore in high beamstrahlung parameter Υ regime [12] the depolarization may be rather reduced. Analytical depolarization estimates for SLAC and TLC are given in Ref. [59], here we study this effect using the QED code "CAIN" [13]. This code includes the classical motion of polarization according

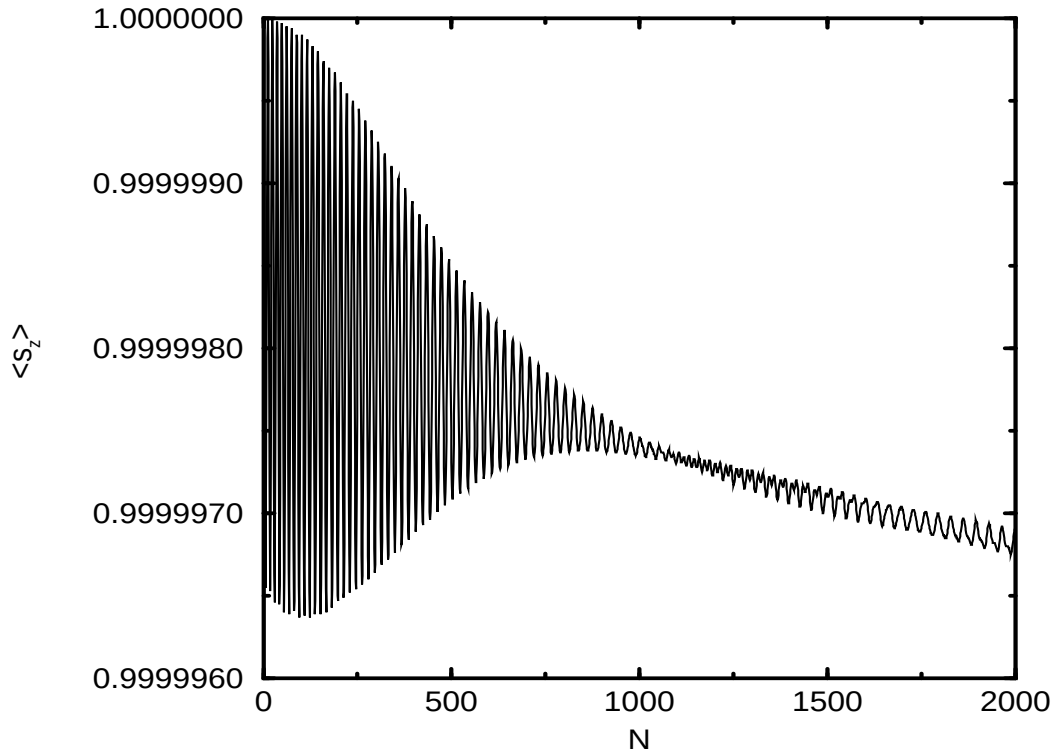

Figure 4.7: Beam polarization vs. stage number. Strong focusing without a transverse jitter.

to the BMT [60] equation with the anomalous magnetic moment now dependent on the field strength (polynomial approximations are used). In addition to that, polarization and changes in it are calculated for the coherent processes at the IP, namely beamstrahlung and coherent pair creation. We first present a simulation based on high beamstrahlung 5 TeV design I [12] of a e^+e^- collider. Table 2.1 contains parameter sets used in the Strawmen's Design of a 5 TeV linear collider [12], namely the beam power P_b, the number of particles per bunch N, the collision frequency f_c, the normalized transverse emittance ϵ_x, the IP betatron length β_x^*, the transverse rms beam size σ_x, and the bunch length σ_z. Initially the beams are assumed perfectly longitudinally polarized

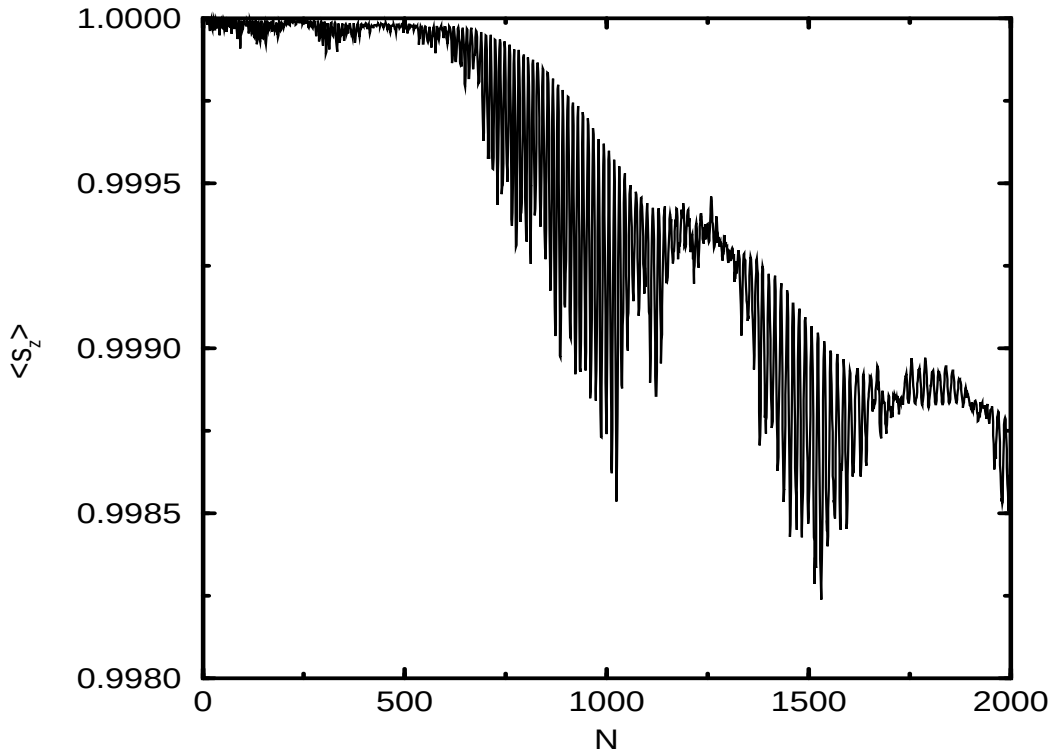

Figure 4.8: Beam polarization vs. stage number. Strong focusing with a transverse jitter.

and we consider the combination $e_R^- \, e_L^+$ (denoted as helicity (+-) in Fig. 4.10). The first observation is that the particles which do not emit beamstrahlung photons keep their initial polarization and the 5 TeV events happen with the "properly" polarized particles. See Fig. 4.9. For instance, if we consider electrons with energies between 2.0 and 2.5 TeV the amount of depolarization is about 0.4 %. Some of the particles which loose energy due to beamstrahlung experience spin-flip which changes their initial polarization but the results (see Fig. 4.10) [2] show that the luminosity of the other helicity combinations of elec-

[2] The luminosity distributions presented in this figure were obtained by much more massive "CAIN" runs (more simulation particles) than the ones we published in [20]. Correspondingly the statistics and resolution are better now.

trons and positrons is much smaller, especially at energies close to the design one. So the conclusion is that the polarization state is well preserved even at the IP and our 5 TeV high Υ collider allows for operation with polarized beams. The choice of beam polarizations does not reduce all of the backgrounds; for instance, it cannot help with $\gamma\gamma \to W^+W^-$ [61]. To deal with the latter some other methods should be used.

Similar conclusions hold in the corresponding e^-e^- scenario. Using right handed electrons in this case would completely eliminate the W^- beamstrahlung and in addition enhance rates for particular super-symmetric processes [55], significantly improving the discovery potential of such a machine.

4.5 Luminosity Comparison Between e^+e^- and e^-e^- Cases at 200 and 500 GeV Center of Mass Energies

In this section we consider different lower energy scenarios of IP. They are also of great interest since the desired final energy of the particles can be achieved in a single plasma wakefield accelerator stage. Such beam driven scenarios are presently under investigation (see next chapter). In this chapter we present just preliminary luminosity studies, leaving detailed systematic study for a future publication. A 200 GeV e^+e^- (e^-e^-) scenario is presented in Table 4.1.

Table 4.1: Strawmen's Design of a 200 GeV , $\mathcal{L}_g = 1.7 \cdot 10^{32}\text{cm}^{-2}\text{s}^{-1}$ e^+e^-/e^-e^- linear collider.

P_b(kW)	$N(10^9)$	f_c(Hz)	$\epsilon_x(\mu\text{m})$	$\beta_x^*(\mu\text{m})$	σ_x(nm)	$\sigma_z(\mu\text{m})$	Υ
100	5	600	2	60	25	0.30	63

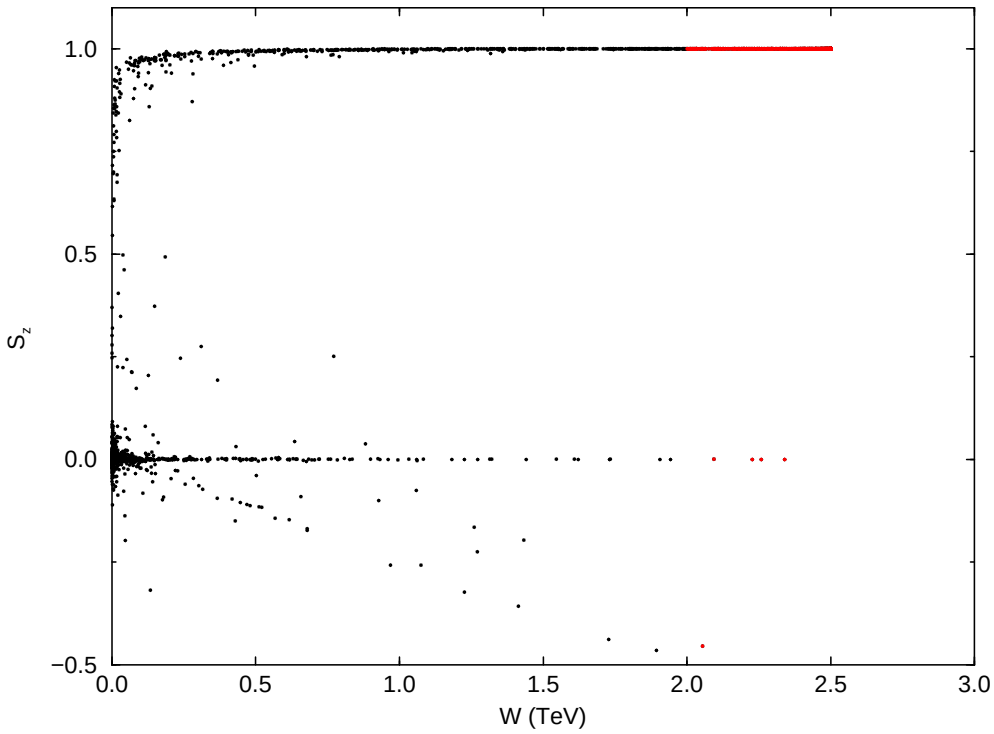

Figure 4.9: (Color) Third component of the particle polarization vs. energy at IP.

The luminosity requirements can be relaxed by almost 3 orders of magnitude compared to the 5 TeV case. Correspondingly this relaxes the restrictions on the transverse beam emittance, beam power and repetition rate. However, we still require same σ_z since the plasma acceleration scheme typically provides very short wavelength driver. Results are similar for e^+e^- and e^-e^- cases and in Fig. 4.11 we present the luminosity spectra [3] (e^+e^- and e^-e^- luminosity, respectively) in both cases. Even though the number of emitted photons per electron n_γ is relatively large (the "CAIN" simulation gives $n_\gamma \approx 1.3$) and the relative energy loss δ_E is about 0.3, the luminosity distribution has a significant

[3] Again we improved the statistics compared to [20].

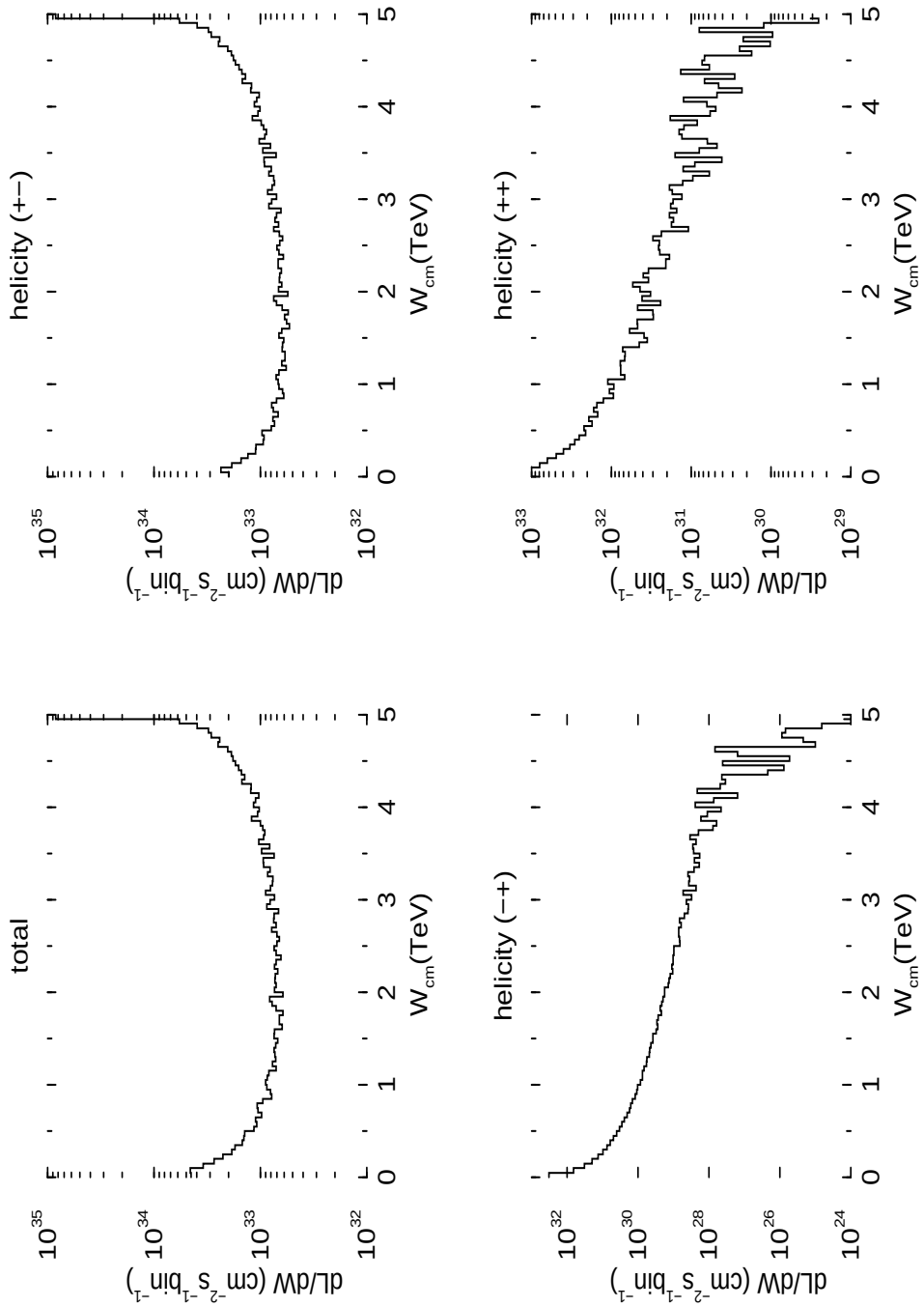

Figure 4.10: Differential e^-e^+ luminosity at IP. Various (e^-e^+) helicity combinations.

core at the design (200 GeV) energy. More specifically $\mathcal{L}(198\,\mathrm{GeV} < W_{\mathrm{cm}} < 200\,\mathrm{GeV})/\mathcal{L}_g \approx 0.6$ and $\mathcal{L}(180\,\mathrm{GeV} < W_{\mathrm{cm}} < 200\,\mathrm{GeV})/\mathcal{L}_g \approx 0.8$. We also

Table 4.2: 500 GeV, $\mathcal{L}_g = 10^{33}\mathrm{cm}^{-2}\mathrm{s}^{-1}$ e^+e^- / e^-e^- linear collider.

P_b(kW)	$N(10^9)$	f_c(Hz)	$\epsilon_x(\mu\mathrm{m})$	$\beta_x^*(\mu\mathrm{m})$	σ_x(nm)	$\sigma_z(\mu\mathrm{m})$	Υ
250	5	600	2	30	11	0.30	393

study the 500 GeV center of mass energy range, again in high Υ regime. Design parameters are given in Table 4.2 and the produced luminosity is shown in Fig. 4.12. Again we see significant fraction of the total luminosity concentrated in the last bin (at 500 GeV). However this high energy luminosity core is not as outstanding as in previous cases: $\mathcal{L}(495\,\mathrm{GeV} < W_{\mathrm{cm}} < 500\,\mathrm{GeV})/\mathcal{L}_g \approx 0.4$ and $\mathcal{L}(450\,\mathrm{GeV} < W_{\mathrm{cm}} < 500\,\mathrm{GeV})/\mathcal{L}_g \approx 0.5$.

4.6 Conclusion

Properly polarized electron/positron beams maybe used to suppress some of the background processes at the IP. We studied changes in the polarization during the acceleration and colliding of the beams. The magnitude of the effect is very small and we conclude that once we prepared an electron/positron beam with a high degree of longitudinal polarization (methods to do this need separate investigation), the main linac portion of the collider and the physics at the IP are not going to significantly affect this polarization state. Additional studies of depolarization in other sections (like magnets, steering systems and damping rings) of the accelerator are necessary. We also investigated different lower energy scenarios for e^+e^- and e^-e^- machines in a high Υ regime and obtained the corresponding luminosity distributions. These results are of interest for the

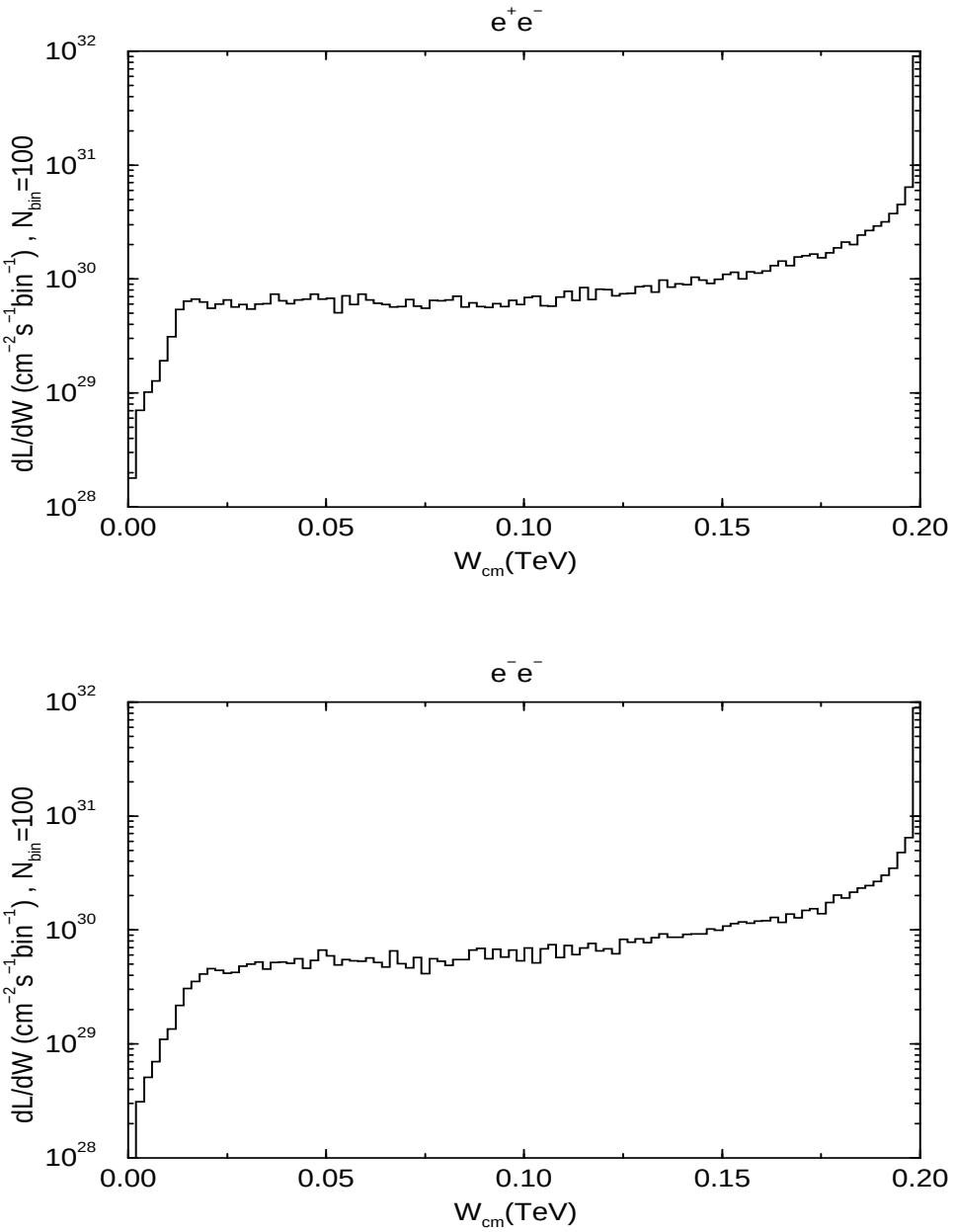

Figure 4.11: Luminosity spectrum of a $\mathcal{L}_g = 1.7 \cdot 10^{32}\,\mathrm{cm}^{-2}\mathrm{s}^{-1}$, 200 GeV e^+e^- / e^-e^- collider.

work on a single stage beam driven plasma wakefield collider. We started this work in collaboration with P. Chen and R. Ruth of SLAC. Main points of it

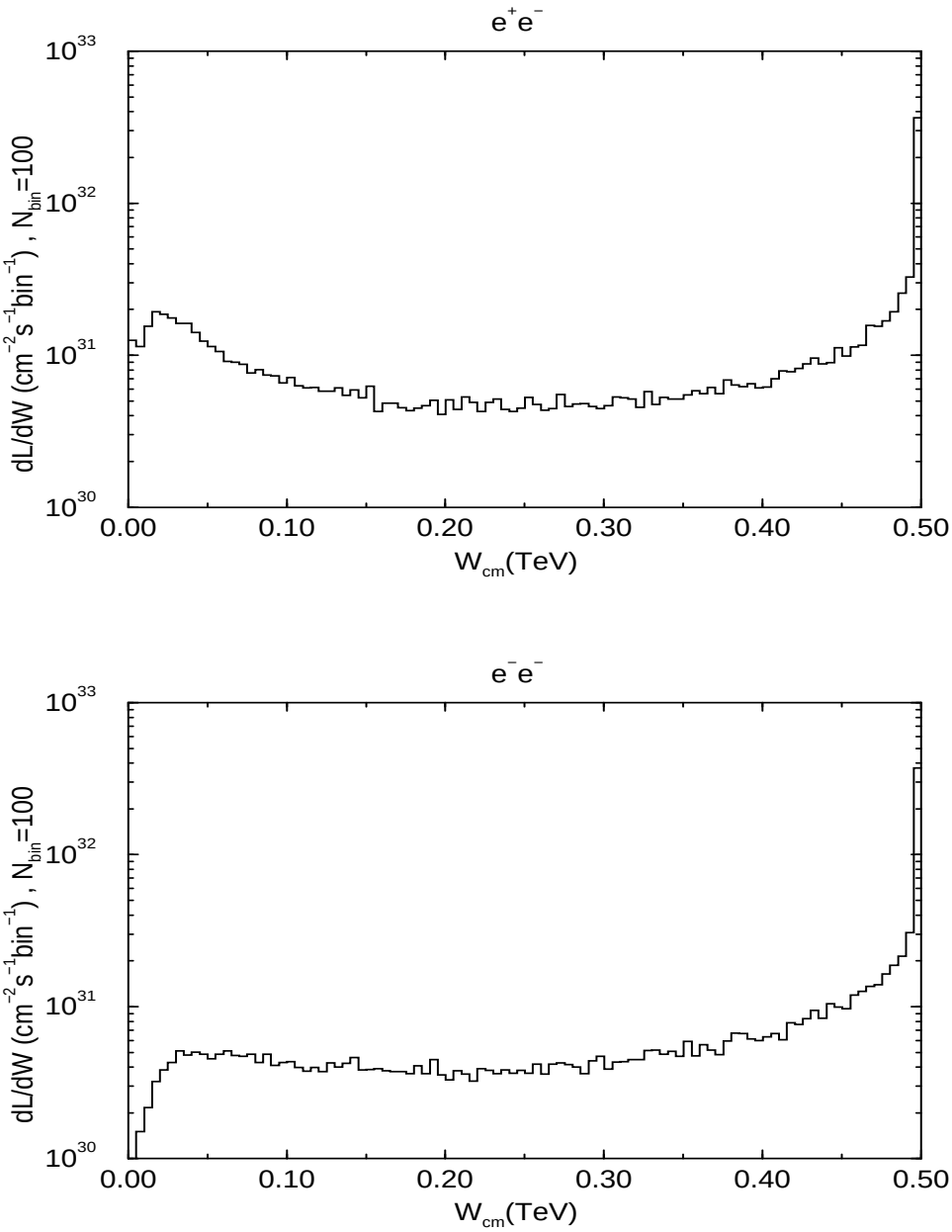

Figure 4.12: Luminosity spectrum of a $\mathcal{L}_g = 10^{33}\,\mathrm{cm}^{-2}\mathrm{s}^{-1}$, 500 GeV e^+e^-/e^-e^- collider.

will be discussed in the next chapter.

Chapter 5

An Ultra High Gradient Plasma Wakefield Booster

5.1 Introduction

In this chapter we present our collaborative study with P. Chen and R. Ruth of SLAC on a Plasma Wakefield Acceleration (PWFA) scheme that can in principle provide an acceleration gradient above 100 GeV/m, based on a reasonable modification of the existing SLAC beam parameters. This work was led by Pisin Chen and will be published in the proceedings of the Advanced Accelerator Concepts 2000 workshop [62]. We also study a possible up-grade of the Stanford Linear Collider (SLC) to hundreds of GeV center-of-mass energy using such a PWFA as a booster. Our study shows that the emittance degradation of the accelerated beams by the plasma wakefield focus is relatively small due to a uniform transverse distribution of the driving beam and the single stage acceleration.

Since the introduction of the plasma accelerator concepts[2, 9], there has been substantial progress both experimentally and theoretically that further advances the schemes[11]. Nevertheless, a macroscopic demonstration of a high gradient plasma acceleration with reasonable accelerated-beam quality, is still lacking. In the case of Laser Wakefield Accelerator (LWFA)[2], very high

acceleration gradients have been observed. But the challenge has been to overcome the laser Rayleigh divergence in the plasma so as to extend the distance of acceleration. The propagation of the laser in a hollow plasma channel appears to be a promising idea[38] combining laser pulse guiding and being very favorable from the accelerated beam emittance preservation point of view. On the other hand, while the electron-beam driven Plasma Wakefield Accelerator (PWFA)[9] can indeed be staged in macroscopic scale [63], the expected acceleration gradient tends to be lower than that in the LWFA scheme unless the driving beam pulse is shaped in either the linear[64, 65] or the nonlinear[66, 67] regime to optimize the *transformer ratio*[64, 65].

We present our study of PWFA parameters based on a reasonable extension of existing beam conditions at the Stanford Linear Accelerator Center (SLAC). We invoke the scheme of a multi-stage bunch compression that would both compress and shape the 50 GeV SLAC beam to tens of micrometers in length. Such high density shaped beams can then excite plasma wakefields that would provide acceleration gradients of more than 100 GeV/m. We also study the beam dynamics of the trailing accelerated beam, the associated beam-beam interaction effects and the luminosity deliverable. Specifically, a rough design is presented for a high energy linear collider built upon adding a PWFA"booster" to the Stanford Linear Collider (SLC). We demonstrate that the collider operation at several hundred GeV center-of-mass energy is possible. It is interesting to note that such a "Plasma Booster" was actually proposed when the PWFA concept[68] was first introduced.

5.2 Plasma Wakefields

Our main motivation is to find a physically realizable parameter set for a linear collider application of the PWFA scheme. The fundamental principles have already been laid down when the concept was originally introduced[68, 9], and studied in some detail[69, 70]. For concreteness, we invoke the existing SLAC beam parameters as our starting point. Several conditions must be satisfied to use the SLAC beam as a driver. Several assumptions are made.

First, we assume that the SLAC beams can be "bunch compressed" to a much shorter length. This is essentially the rotation of the beam in its longitudinal phase space, where the adiabatically damped relative energy spread, $\delta p/p$, is exchanged with the length of the bunch. We second assume that during bunch rotation one is able to shape the beam into an asymmetric head-to-tail density distribution for large transformer ratios, applicable to the linear regime of plasma perturbation, or a uniform distribution from head to tail for the application to the nonlinear regime. Finally, to minimize the transverse focusing of the accelerated beams, we assume that the driving beam is also transversely shaped into a uniform distribution. This can in principle be accomplished by applying proper octupole magnetic fields in the beam line.

The general expressions for the longitudinal and transverse plasma wakefields are[71]

$$W_{\parallel} = -\frac{4\pi e n_b}{k_p^2}\partial_\zeta Z(\zeta)R(r) \ , \tag{5.1}$$

$$W_{\perp} = -\frac{4\pi e n_b}{k_p^2}Z(\zeta)\partial_r R(r) \ , \tag{5.2}$$

where

$$Z(\zeta) = k_p \int_\zeta^\infty d\zeta' \rho(\zeta') \sin k_p(\zeta' - \zeta) \, , \tag{5.3}$$

and $\rho(\zeta)$ is the normalized longitudinal density distribution of the driving bunch. As we assume a uniform transverse distribution, the function $R(r)$ is

$$R(r) = \begin{cases} 1 - k_p a K_1(k_p a) I_0(k_p r)\,, & r < a\,, \\ k_p a I_1(k_p a) K_0(k_p r)\,, & r > a\,. \end{cases} \tag{5.4}$$

Here $\zeta = z - ct$ is the beam comoving coordinate, $k_p = \sqrt{4\pi r_e n_p}$ is the plasma wave number, $r_e = e^2/mc^2$ is the classical electron radius, n_p is the ambient plasma density and n_b is the beam density. K_i's and I_i's are the modified Bessel functions.

For $k_p a \gg 1$ and $r/a \ll 1$ we get

$$W_{\|} = -\frac{4\pi e n_b}{k_p^2} Z'(\zeta) \left(1 - k_p a \sqrt{\frac{\pi}{2k_p a}} e^{-k_p a}\right)\,, \tag{5.5}$$

$$W_{\perp} = \frac{4\pi e n_b}{k_p^2} Z(\zeta) \frac{\sqrt{2\pi}}{4} k_p^{5/2} a^{1/2} e^{-k_p a} r\,. \tag{5.6}$$

We see that the transverse wakefield is exponentially suppressed, whereas the longitudinal wakefield is slightly reduced by the form factor $F(k_p a)$ given by

$$F(k_p a) \equiv \left(1 - k_p a \sqrt{\frac{\pi}{2k_p a}} e^{-k_p a}\right) \approx 1\,. \tag{5.7}$$

There is a quarter-wavelength region in the wake with simultaneous acceleration and focusing, which is the phase suitable for placing the accelerating beam.

5.3 Longitudinal Bunch Shaping

The wakefield acceleration gradient is sensitive to the longitudinal bunch shape of the driving beam. In order to search for the optimal acceleration gradient, we shall consider three representative cases of longitudinal bunch shaping that range from Case A: a parabola beam; Case B: a "doorstep", or optimized,

beam; and Case C: a "flat-top" (uniform density) beam in the nonlinear beam-plasma interaction regime. The first two cases are in the linear regime, where the plasma density is sufficiently higher than that of the beam. In Case A we intend to study the plasma wakefield generated by an unshaped, high energy beam, which is typically in Gaussian distribution. Since mathematically the parabolic density distribution is found to be easier to handle analytically than the Gaussian distribution[70], while the characteristics of the excited plasma wakefields are essentially the same, we shall invoke the parabolic, instead of the Gaussian, distribution, for Case A.

The idea is to use the existing SLC beam with compression and appropriate profile shaping as a driver for the plasma wakefield based accelerator setup in a high density plasma (or gas). This beam is characterized by an energy of 48 GeV, number of particles $N = 2 \times 10^{10}$, normalized emittance $\epsilon_x = 3 \times 10^{-5}$m and $\sigma_z = 700\mu$m. However, to produce tens to hundreds of GeV/m field we need to further shorten the bunch. Such shortening can be achieved by several bunch compression stages utilizing rotation in the longitudinal phase space of the beam. Assuming that the beam energy injected from the Damping Ring into the LINAC is 1.2 GeV, one can in principle achieve a total reduction of the bunch length by a factor of 40 when the beam reaches its final energy of 48 GeV. With the initial bunch length at $\sigma_z = 700\mu$m, the final bunch length would be $\sigma_z = 17.5\mu$m. Of course, when such a Gaussian bunch is further shaped, the total length of the beam will be different from this *rms* value.

Our goal is to achieve an acceleration gradient of the order of a 100 GeV/m. For this purpose we choose a high plasma density. The actual plasma

densities in the following three different cases will be determined by different constraints. Secondly, we wish to maximally reduce the transverse wakefield, i.e., we insist that $k_p a \gg 1$. Thirdly, we want to accelerate the particles over a distance of the order of 1m to achieve significant final energy. When all three constraints are put together, we find it a reasonable compromise to choose $a = 2\sigma_r = 20\mu$m, and the betatron wavelength of the beam becomes $\beta = \gamma\sigma_r^2/\epsilon_x \approx 30$ cm. These should allow us to meet the above requirements.

5.3.1 Case A: Parabola (Linear Regime)

We first examine the wakefield generated by an unshaped beam. As we have explained, it is mathematically simpler to work with a parabolic, instead of a Gaussian, distribution. In this approach, we take the half-length of the parabola, b, to be the *rms* value of the corresponding Gaussian distribution, i.e., $b = \sigma_z$.

The longitudinal beam density profile is given by

$$\rho(\zeta) \equiv \frac{n_b(\zeta)}{n_b} = (1 - \zeta^2/b^2) \ \ , -b \leq \zeta \leq b \tag{5.8}$$

where n_b is the peak density of the driving beam determined from

$$N = n_b \int_0^a \int_{-b}^b 2\pi\, r\, dr d\zeta (1 - \zeta^2/b^2) = \frac{4}{3} n_b \pi a^2 b \ \rightarrow \ n_b = \frac{3N}{4\pi a^2 b}. \tag{5.9}$$

In this case the longitudinal wakefield on axis behind the beam is

$$\begin{aligned} W_{\|} &= 4\pi e n_b F(k_p a) \int_{-b}^b d\zeta' (1 - \zeta'^2/b^2) \cos k_p(\zeta' - \zeta) \\ &= -\frac{16\pi e n_b}{k_p^2 b} [\cos k_p b - \frac{1}{k_p b} \sin k_p b] F(k_p a) \cos k_p \zeta \ . \end{aligned} \tag{5.10}$$

At locations where $k_p\zeta = 2n\pi$, the longitudinal wakefield $W_{\|}$ reaches maxima. We define the maximum value of $|eW_{\|}|$ as the acceleration gradient G.

We want to optimize the acceleration gradient behind the driving beam (with fixed beam parameters) by matching the bunch length with a properly chosen plasma density. This can be determined by demanding $\delta G/\delta(k_p b) = 0$. In our case, this results in a choice $k_p b \approx 2$. Unfortunately this solution would correspond to too large a beam-to-plasma density ratio, $\alpha = n_b/n_p \approx 2/3$, which clearly violates the assumption of linear plasma perturbation. As a compromise (but not much), we choose $k_p b = \pi$ so as to increase the plasma density and reduce α_0. For the given $b = 17.5\mu$m, we find $n_p = 9.2 \times 10^{17}\text{cm}^{-3}$. The density ratio is now reduced to $\alpha = 1/4 \ll 1$. With $a = 20\mu$m, we have $k_p a = 3.6$, and thus $F(k_p a) = 0.93$. Then the acceleration gradient on the axis is

$$G = \frac{16\pi e^2 n_b}{k_p^2 b}[\cos k_p b - \frac{1}{k_p b}\sin k_p b]F(k_p a) \approx 28\text{GeV/m} \ . \tag{5.11}$$

We see that this acceleration gradient, though substantial, falls short of achieving the 100 GeV/m goal.

5.3.2 Case B: "Doorstep" (Linear Regime)

The distribution for a "doorstep" bunch is defined as

$$n_b(\zeta) = \alpha_0 n_p \begin{cases} 1 \ , & 0 < \zeta < \frac{\pi}{2k_p} \ , \\ 1 + k_p(\zeta - \frac{\pi}{2k_p}) \ , & \zeta > \frac{\pi}{2k_p} \ . \end{cases} \tag{5.12}$$

Then the wake potential inside the bunch is

$$Z^- = \alpha_0 \begin{cases} 1 - \cos k_p\zeta \ , & 0 < \zeta < \frac{\pi}{2k_p} \ , \\ 1 + k_p(\zeta - \frac{\pi}{2k_p}) \ , & \zeta > \frac{\pi}{2k_p} \ . \end{cases} \tag{5.13}$$

To find the wake potential Z^+ behind the bunch, we start with the general expression

$$Z^+ = C_1 \cos k_p\zeta + C_2 \sin k_p\zeta \ . \tag{5.14}$$

Matching the boundary conditions at the end of the bunch $\zeta = b$, $Z^-(\zeta = b) = Z^+(\zeta = b)$ and $Z^{-'}(\zeta = b) = Z^{+'}(\zeta = b)$, we get

$$C_1 = \alpha_0 \left\{ -\sin k_p b + \cos k_p b \left[1 + k_p b (1 - \frac{\pi}{2k_p b}) \right] \right\} , \tag{5.15}$$

$$C_2 = \frac{\alpha_0}{\cos k_p b} \left\{ 1 - \sin^2 k_p b + \sin k_p b \cos k_p b \left[1 + k_p b (1 - \frac{\pi}{2k_p b}) \right] \right\} \tag{5.16}$$

An interesting special case is when $k_p b = n\pi$. Then

$$C_1 = \alpha_0 \left[1 + n\pi (1 - \frac{1}{2n}) \right] , \tag{5.17}$$

$$C_2 = \alpha_0 . \tag{5.18}$$

Therefore the transformer ratio becomes

$$R = \frac{W^+_{\|\max}}{W^-_{\|\max}} = 1 + n\pi \left(1 - \frac{1}{2n} \right) . \tag{5.19}$$

The maximum acceleration gradient is

$$G = \alpha_0 \left[1 + n\pi (1 - \frac{1}{2n}) \right] k_p mc^2 F(k_p a) . \tag{5.20}$$

Specifically, let us take $k_p b = 8\pi$. With the total length of the beam assumed to be $b = 2\sigma_z = 35\mu$m, this corresponds to a plasma density of $n_p = 7.2 \times 10^{18}\text{cm}^{-3}$. To ensure self-consistency in the linear approximation of the plasma perturbation, from Eq.(5.12) we require that the ratio of the maximum beam density and the end of the bunch to that of the plasma be much smaller than unity. For definiteness, we set

$$\alpha = 0.5 = \frac{n_b(\zeta = b)}{n_p} = \alpha_0 \left[1 + k_p b - \frac{\pi}{2} \right] , \tag{5.21}$$

and this fixes the parameter $\alpha_0 = 0.02$. Inserting these values into Eq.(5.20), we find

$$G \approx 180\,\text{GeV/m} . \tag{5.22}$$

Note that this gradient is reasonably smaller than the so-called wavebreaking limit, 270 GeV/m, at the given plasma density.

5.3.3 Case C: "Flat-Top" (Nonlinear Regime)

Now we examine the case of a "flat-top" bunch in the nonlinear regime. By this we mean that the longitudinal density distribution of the beam is uniform from head to tail. Such a bunch distribution, though not optimized, can also provide a transformer ratio larger than 2, if the plasma density is matched to be exactly twice that of the beam[66]. One can also shape the beam in a more sophisticated manner to further optimize R[67], similar to that in the linear regime[64, 65]. But for the sake of simplicity, we will consider the uniform distribution only.

Since the density of the uniform beam is $n_b = N/\pi a^2 b \approx 4.5 \times 10^{17}\text{cm}^{-3}$, the matched plasma density, i.e., with $\alpha = n_b/n_p = 0.5$, is $n_p = 2n_b \approx 9 \times 10^{17}\text{cm}^{-3}$, which gives $2k_p b = 6.3 = \tau_f$. Using the results in [66], the maximum accelerating gradient is

$$G = \sqrt{\chi - 1} k_p mc^2 F(k_p a) \ , \tag{5.23}$$

where χ is the solution to

$$\tau_f = \sqrt{\chi}\sqrt{\chi - 1} + \ln\left[\sqrt{\chi - 1} + \sqrt{\chi}\right] \ . \tag{5.24}$$

Eq.(5.24) leads to $\chi \approx 5$ and $G \approx 166$ GeV/m . The transformer ratio in this case is simply

$$R = \sqrt{\tau_f} \sim 2.5 \ . \tag{5.25}$$

Comparing Case B and Case C, we note that operating in the nonlinear regime has the advantage that it achieves the similar level of acceleration

gradient without necessarily invoking a much higher plasma density. The price to pay, however, is that the transformer ratio in the nonlinear case is much smaller. This means with $R = 2.5$, the driving beam with initial energy of 48 GeV cannot sustain more than $L \sim 0.72$m in acceleration length.

The parameters discussed above are listed in Table 5.1.

Table 5.1: Various bunch shapes

Cases	A: Parabola	B: Doorstep	C: Flat-Top
Beam Parameters			
E [GeV]	48	48	48
N [10^{10}]	2	2	2
ϵ_x [10^{-5} mrad]	3	3	3
σ_z [μm]	17.5	17.5	17.5
b [μm]	17.5	35	35
σ_r [μm]	10	10	10
a [μm]	20	20	20
n_b [10^{17} cm^{-3}]	2.4	6.4	4.5
Plasma Parameters			
n_p [10^{17} cm^{-3}]	9	72	9
α	0.25	0.5	0.5
k_p [cm^{-1}]	1800	5000	1800
$k_p a$	3.6	10	3.6
$k_p b$	π	8π	2π
G [GeV/m]	28	180	167
R	2	24.5	2.5
β [cm]	32	32	32

5.4 Beam Dynamics and Beam-Beam Interaction Issues

5.4.1 Beam Dynamics Issues

The emittance of the trailing (accelerated) bunch degrades due to the strong wakefield focusing (combined with structure errors) and binary collisions in the background plasma. To have a reasonable luminosity we need to start with a

high quality beam and to deliver it to the collision point. The trailing bunch needs to be very short for two reasons - the shortness of the driver (PWFA) wavelength and to avoid big losses at the interaction point (IP) ([12]). At present it is not clear if a portion of the driver can be used as a trailing bunch due to the stringent requirements to its quality and parameters. If we use the "doorstep" scenario with $n_p = 7.2 \cdot 10^{18}\text{cm}^{-3}$ plasma density, it gives $\lambda_p = 13\mu$, which makes the useful accelerating period about 3 microns. We can calculate the accelerated bunch betatron length using ("flat top" driver)

$$\beta = \left(\frac{\gamma\, mc^2}{G\, \sin\Psi} \sqrt{\frac{8}{\pi k_p a}} \frac{e^{k_p a}}{k_p} \right)^{1/2} . \tag{5.26}$$

Taking the initial beam energy $\gamma mc^2 = 1$ GeV, $G \approx 180$ GeV/m we obtain $\beta_i \approx 1\text{cm}/\sqrt{\sin\Psi}$. If $\sigma_z = 0.3\mu$m then $k_p\sigma_z \approx 0.15$ so we need to take the phase at least as $\Psi = 0.6$ which gives $\beta_i \approx 1.5$cm. It means that even in a single stage design we need alignment control [14, 15, 16] in the submicron range to preserve the emittance of the accelerated beam (assuming initial normalized emittance of 2 μm, see Table 5.2).

We now estimate the emittance growth from multiple scattering in the plasma in this case. In our design the acceleration gradient is 180 GeV/m which corresponds to $\gamma' \approx 3.5 \cdot 10^5$ m^{-1}. In [51] the electron temperature is chosen to be 5 eV , in our case it might be much higher but the result is very insensitive to this value. In particular for $kT = 5$ eV and $n_p \approx 7.2 \cdot 10^{18}$ cm^{-3}, using Eq. (3.18), we obtain:

$$\Delta\epsilon_x \text{ [m]} \approx 3.2 \cdot 10^{-8} \left(\beta_\text{f} - \beta_\text{i}\right) \text{ [m]} , \tag{5.27}$$

which is clearly negligible compared to the initial emittance.

Table 5.2: Trailing beam parameters at the IP for 500 GeV, $\mathcal{L}_g = 10^{33}\text{cm}^{-2}\text{s}^{-1}$ e^+e^- linear collider.

P_b(kW)	$N(10^9)$	f_c(kHz)	$\epsilon_x(\mu\text{m})$	$\beta_x^*(\mu\text{m})$	σ_x(nm)	$\sigma_z(\mu\text{m})$	Υ	$\frac{\mathcal{L}_{W_{cm}\in 1\%}}{\mathcal{L}_g}$
250	5	0.6	2	30	11	0.30	393	0.4
790	1.6	6	2	30	11	0.30	124	0.6
2500	0.5	60	2	30	11	0.30	39	0.7

5.4.2 Beam-Beam Interaction Issues

In the doorstep case the linear calculation gives $G \approx 180\text{GeV/m}$. The required center of mass energy of 500 GeV can be achieved in a single stage (for each arm) with a length of about 1 m. The luminosity requirement we impose is $\mathcal{L}_g = 10^{33}\text{cm}^{-2}\text{s}^{-1}$ which was considered in the previous chapter of this dissertation. If we are to work with the SLAC driver with repetition rate of 600 Hz, the number of particles in the accelerated bunch needs to be $5{\cdot}10^9$ which would cause severe beam loading issues. To study the luminosity distribution at the IP we again use the "CAIN" code [13]. Figure 5.1 shows three cases (the statistics was improved here compared to [62] via more massive "CAIN" runs) which differ by their repetition frequency at IP and the number of particles in the beam but have the same geometrical luminosity. The corresponding beam parameters: beam power P_b, particle number N, repetition frequency f_c, normalized emittance ϵ_x, IP betatron length β_x^*, IP beam transverse size σ_x, bunch length σ_z, the beamstrahlung parameter Υ, and the relative luminosity in the last simulation bin (within 1% of the design energy), are listed in Table 5.2. Clearly, high repetition frequency is necessary to reduce the number of particles required and to improve the differential luminosity (to achieve a higher peak at

the design 500 GeV center of mass energy). See Table 5.2 and Fig. 5.1. These results indicate the importance of studying multibunch loading in a single shot created wakefield.

5.5 Concluding Remarks, Limitations and Unresolved Issues

The proposed beam driven plasma wakefield acceleration scheme can provide accelerating gradients in excess of 100 GeV/m and opportunity to investigate new processes at 500 GeV center of mass energy of colliding particles. However, several issues need extensive future investigation. Firstly, the proposed SLC upgrade itself and the cost associated with it. Secondly, there might be some stability problems with the driver beam. It is self focused (by its own wakefield), and to avoid the emittance growth due to the phase space mixing it should be matched to the focusing. However, the focusing is different in the head/tail of the bunch, so there is a concern associated with this. The primary beam experiences various instabilities: transverse two-stream [32, 65], Weibel [72], electron-hose [73]. These are summarized in [11] and need investigation for the discussed scenario.

Additionally, stability of the trailing bunch also needs to be studied. It has smaller number of particles but very high density, so the loading issues might be very important.

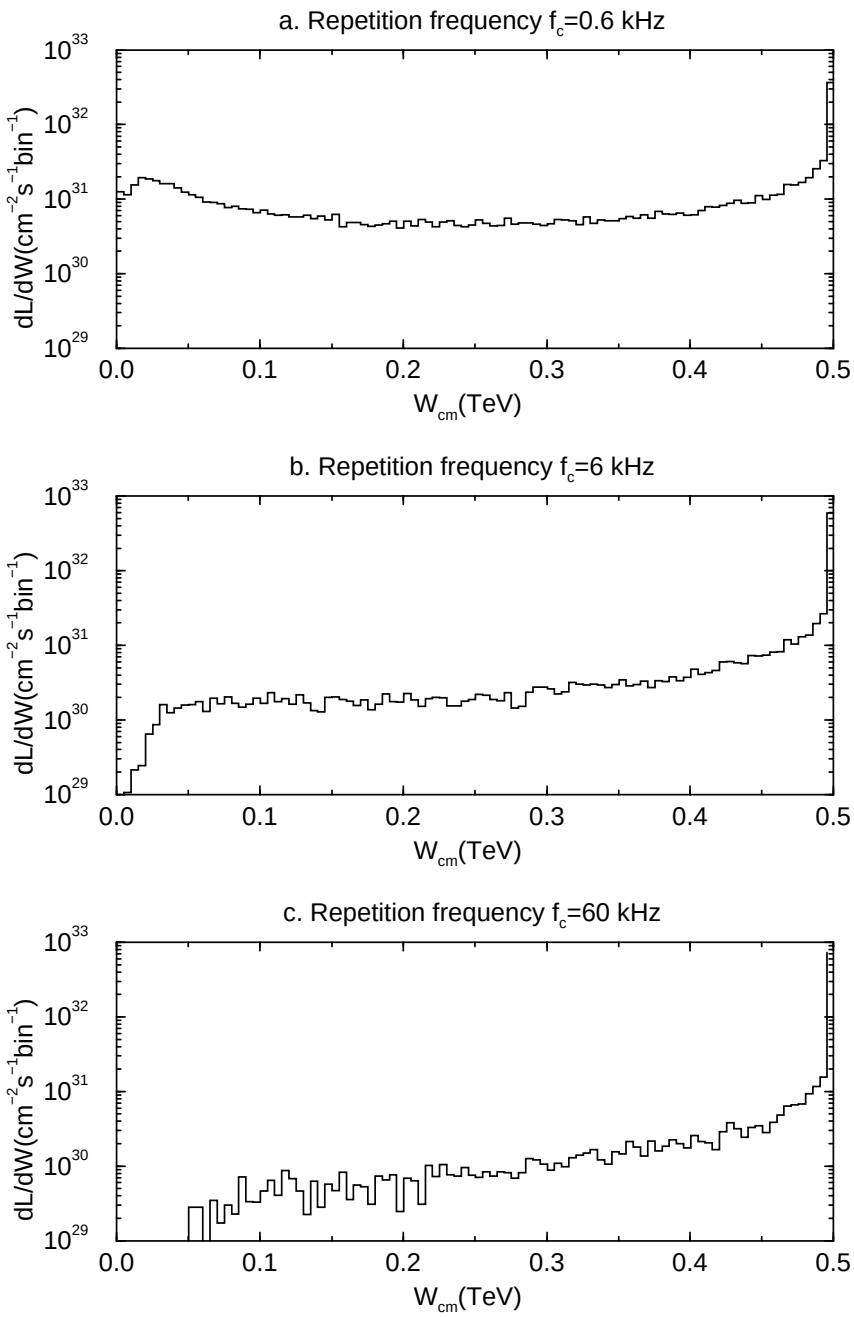

Figure 5.1: Differential luminosity at repetition frequency $f = 0.6$, 6, and 60 kHz, respectively. The geometrical luminosity $\mathcal{L}_g$ was chosen 10^{33} cm^{-2}s^{-1}.

Chapter 6

Conclusion

We investigated the cumulative effects of the successive acceleration, transport, and focusing in the laser wakefield (or its sister methods) over multiple stages. Such cumulative processes are important for the real world accelerators such as high energy colliders. Errors arising from the misalignments of each stage or equivalently (in our map approach) the noise in the system can accumulate in such a way to degrade some of the parameters of the beam. The most crucial of these may be the normalized transverse r.m.s. emittance of the beam. We showed that a set of stages with an ideal wakefield acceleration, drift, and focusing can preserve even a very small emittance over a thousand stages.

When we have stochastic variables on the wakefield (we chose the stage errors of the axis of the wakefield, in particular), the emittance can significantly increase over the many stages due to the strong focusing of the wakefield. This is probably the most serious effect on the long range behavior of the beams in this kind of accelerator for high energy applications.

We studied the emittance degradation numerically and analytically obtained important conclusions about its scalings with respect to the relevant parameters. Based on that we considered several mitigated focusing scenarios in Chapter 3, namely: the hollow channel design, the approximately synchronous

superunit setup and the "horn" model. In all of these scenarios we were able to improve the emittance control and decrease significantly the beam quality degradation. Many important issues need further investigation: experimental channel creation and laser guiding, resonant absorption in the walls, possible low efficiency of the large laser spot scenarios. Using the presented approach, we plan to perform a further optimization in the multidimensional parameter space of a large scale accelerator, taking into account, to our best notion, future experimental limits and restrictions which might come from them.

We studied the collision point physics in the high beamstrahlung parameter regime via theoretical and numerical methods in Chapter 4. Luminosity and QED background distributions at the Interaction Point were analyzed with the help of the Yokoya's Monte Carlo code "CAIN". These collision point studies are not only of interest for plasma wakefield based lepton collider but also for any TeV lepton collider, even if the acceleration is based on some other method, since most probably it will be pushed into the high Υ regime as well.

As a leverage to control some of the Standard Model backgrounds properly polarized electron/positron beams might be used. We studied changes in the polarization during the acceleration and colliding of the beams. The magnitude of the effect is very small and we concluded that once we prepared an electron/positron beam with a high degree of longitudinal polarization (methods to do this need separate investigation), the main linac portion of the collider and the physics at the IP are not going to significantly affect this polarization state. Additional studies of depolarization in other sections (like magnets, steering systems and damping rings) of the accelerator are necessary. We also investigated different lower energy scenarios for e^+e^- and e^-e^- machines in a

high Υ regime and obtained the corresponding luminosity distributions. These results are of great interest for the future work on a single stage beam driven plasma wakefield collider.

Such a single stage high gradient plasma wakefield accelerator based on a reasonable modification of the current SLC parameters was studied in Chapter 5. This SLC upgrade might be possible in near future. The opportunity to study new physics at 500 GeV center of mass energy at relatively low cost is really exciting. Future studies of driver beam instabilities are necessary.

Overall, the Laser Wakefield Acceleration and Plasma Wakefield Acceleration are promising candidates for future high energy physics applications but very significant theoretical and experimental effort and advance are needed to make these schemes possible.

Bibliography

[1] The NLC Design Group and NLC Physics Working Group, *Physics and technology of the Next Linear Collider,* report submitted to Snowmass 96 (1996).

[2] T. Tajima and J. Dawson, Phys. Rev. Lett. **43**, 267 (1979).

[3] D. Strickland and G. Mourou, Optics Communication **56**, 219 (1985).

[4] H. Hamster, A. Sullivan, S. Gordon, W. White, and R. Falcone, Phys. Rev. Lett. **71**, 2725 (1993).

[5] K. Nakajima *et al.*, in *Advanced Accelerator Concepts 6* edited by P. Schoessow, (AIP, New York, 1995), p.145.

[6] C. Siders *et al.*, Phys. Rev. Lett. **76**, 3570 (1996).

[7] M. Kando *et al.*, Japan. J. Appl.Phys. **38**, L967 (1999).

[8] Y. Kitagawa et al, Phys. Rev. Lett. **68**, 48 (1992).

[9] P. Chen, J. Dawson, R. Huff and T. Katsouleas, Phys. Rev. Lett. **54**, 693 (1985).

[10] J. Rosenzweig, D. Cline, B. Cole, H. Figueroa, W. Gai, R. Konecny, J. Norem, P. Schoessow, and J. Simpson, Phys. Rev. Lett. **61**, 98 (1988).

[11] E. Esarey, P. Sprangle, J. Krall, and A. Ting, IEEE Trans. Plasma Sci. **24**, 252, (1996).

[12] M. Xie, T. Tajima, K. Yokoya, and S. Chattopadhyay, in *Advanced Accelerator Concepts 7*, edited by S. Chattopadhyay, (AIP, New York, 1997), p.233.

[13] K. Yokoya *CAIN21e.*
http://www-acc-theory.kek.jp/members/cain/default.html

[14] T. Tajima, S. Cheshkov, W. Horton, and K. Yokoya, in *Advanced Accelerator Concepts 8*, edited by W. Lawson, (AIP, New York, 1999), p.153.

[15] S. Cheshkov, T. Tajima, W. Horton, and K. Yokoya, in *Advanced Accelerator Concepts 8*, edited by W. Lawson, (AIP, New York 1999), p.343.

[16] S. Cheshkov, T. Tajima, W. Horton, and K. Yokoya, Phys. Rev. ST Accel. Beams **3**, 071301 (2000).

[17] C. Chiu, S. Cheshkov, and T. Tajima, Beam Dynamics Newsletter **21**, 2000.

[18] C. Chiu, S. Cheshkov, and T. Tajima, Phys. Rev. ST Accel. Beams **3**, 101301 (2000).

[19] S. Cheshkov, T. Tajima, C. Chiu, and F. Breitling, "Emittance Control in Laser Wakefield Accelerator", to appear in *Advanced Accelerator Concepts 9.*

[20] S. Cheshkov and T. Tajima, J. Mod. Phys. A **15**, 2555 (2000).

[21] E. Esarey, A. Ting, P. Sprangle, and G. Joyce, Comments Plasma Phys. Controlled Fusion **12**, 191 (1989).

[22] L. Gorbunov and V. Kirsanov, Zh. Eksp. Teor. Fiz. **93**, 509, (1987); Sov. Phys. JETP **66**, 290 (1987).

[23] P. Chen, Part. Accelerators **20**, 171 (1985).

[24] B. Breizman, T. Tajima, D. Fisher, and P. Chebotaev, in *Research Trends in Nonlinear and Relativistic Effects in Plasmas*, edited by V. Stefan, (AIP, New York, 1992), p.263.

[25] B. Rau, T. Tajima, and H. Hojo, Phys. Rev. Lett. **78**, 3310 (1997).

[26] D. Umstadter, J. Kim, and D. Dodd, Phys. Rev. Lett. **76**, 2073 (1996).

[27] E. Esarey, R. Hubbard, W. Leemans, A. Ting, and P. Sprangle, Phys. Rev. Lett. **79**, 2682 (1997).

[28] S. Nikitin, A. Alexeev, J. Fan, and H. Milchberg, Phys. Rev. E, **59**, 3839 (1999).

[29] E. Gaul, SP LeBlanc, and M. Downer, in *Advanced Accelerator Concepts 8*, edited by W. Lawson, (AIP, New York 1999), p.377.

[30] E. Gaul, doctoral thesis, UT-Austin, December 2000.

[31] D. Kaganovich *et al.*, Phys. Rev. E **59**, R4769 (1999).

[32] T. Katsouleas, S. Wilks, P. Chen, J. Dawson, and J. Su, Part. Accelerators **22**, 81 (1986).

[33] W. Horton and T. Tajima, Phys. Rev. A **34**, 4110 (1986).

[34] E. Esarey and M. Pilloff, Phys. Plasmas **2**, 1432 (1995).

[35] D. Edwards and M. Syphers, *An Introduction to the Physics of High Energy Accelerators* (John Wiley & Sons, New York, 1993), p.31.

[36] A. Chao and M. Tigner, *Handbook of Accelerator Physics & Engineering: A Compilation of Formulae & Data* (World Scientific, River Edge, 1998).

[37] N. van Kampen, Phys. reports **24**, 171 (1976).

[38] T. Chiou, T. Katsouleas, C. Decker, W. Mori, J. Wurtele, G. Shvets, and J. Su, Phys. Plasmas **2**, 310 (1995).

[39] G. Shvets, J. Wurtele, T. Chiou, and T. Katsouleas, IEEE Trans. Plasma Science **24**, 351 (1996).

[40] R. Assmann and K. Yokoya, Nucl. Instrum. & Methods. A **410**, 544 (1998).

[41] T. Katsouleas, Phys. Rev. A **33**, 2056 (1986).

[42] L. Landau and E. Lifshitz, *Fluid Mechanics*, Pergamon Press,2d Ed., 1987, Sec. 83 and Sec. 97.

[43] H. Kuehl, C. Zhang, and T. Katsouleas, Phys. Rev. E **47**, 1249 (1993).

[44] E. Zaidman, T. Tajima, D. Neuffer, K. Mima, T. Ohsuga, and D. Barnes, IEEE Trans. Nucl. Science **32**, 3545 (1985).

[45] P. Volfbeyn and W. Leemans in *Advanced Accelerator Concepts 8*, edited by W. Lawson, (AIP, New York 1999), p.514.

[46] F. Dorchies, J. Marques, B. Cros, G. Matthieussent, C. Courtois, T. Velikoroussov, P. Audebert, J. Geindre, S. Rebibo, G. Hamoniaux, and F. Amiranoff, Phys. Rev. Lett. **82**, 4655 (1999), and references therein.

[47] D. Umstadter, E. Esarey, and J. Kim, Phys. Rev. Lett. **72**, 1224 (1994).

[48] G. Shvets, N. Fisch, A. Pukhov, and J. Meyer-ter-Vehn, Phys. Rev. E. **60**, 2218 (1999).

[49] J. Seeman *et al.* SLAC-PUB-**5439** (1991), and references therein.

[50] F. Breitling, R. Weigel, M. Downer, and T. Tajima, submitted to Rev. Sci. Instrum.

[51] B. Montague and W. Schnell, in *Laser Acceleration of Particles 2* (AIP, New York, 1985) p.146 (1985).

[52] K. Yokoya and P. Chen, Frontiers of Particle Beams **400**, 415 (1992).

[53] J. Jackson, *Classical Electrodynamics*, second edition (John Wiley & Sons, New York, 1975), p.667.

[54] H. Murayama and M. Peskin, Annu. Rev. Nucl. Part. Sci. **46**, 533 (1996).

[55] F. Cuypers, G. van Oldenborgh, and R. Ruckl, Nucl. Phys. B, **409**, 128 (1993).

[56] V. Berestezky, E. Lifshiz and L. Pitaevsky, *Quantum Electrodynamics* (Moskow, Nauka, 1989), Vol.4.

[57] A. Kushnirenko *et al*, IHEP 93-131, Protvino, 1993.

[58] A. Sokolov and I. Ternov, *Synchrotron Radiation* (Pergamon Press, Oxford, 1968).

[59] K. Yokoya and P. Chen, SLAC-PUB-4692, 1988.

[60] V. Bargmann, K. Michel, and V. Telegdi, Phys. Rev. Lett. **2**, 435 (1959).

[61] H. Murayama, private communication (1998).

[62] P. Chen, S. Cheshkov, R. Ruth, and T. Tajima, "An Ultra High Gradient Plasma Wakefield Booster" to appear in *Advanced Accelerator Concepts 9.*

[63] M. Hogan *et al.*, Physics of Plasmas **7**, 2241 (2000).

[64] K. Bane, P. Chen, and P. Wilson, IEEE Trans. Nucl. Sci. **NS-32**, 3524 (1985).

[65] P. Chen, J. Su, J. Dawson, K. Bane and P. Wilson, Phys. Rev. Lett. **56**, 1252 (1986).

[66] J. Rosenzweig, Phys. Rev. Lett. **58**, 555 (1987).

[67] Y. Yan and H. Chen, Phys. Rev. A **38**, 1490 (1988).

[68] P. Chen, R. Huff, and J. Dawson, "A Plasma Booster for Linear Accelerators", UCLA Report PPG-802, 1984.

[69] R. Ruth, A. Chao, P. Morton, and P. Wilson, Part. Acc. **17**, 171 (1985).

[70] R. Ruth and P. Chen, "Plasma Accelerators", in *Supersymmetry*, SLAC Report No. 296 (1986).

[71] Pisin Chen, Part. Accelerators **20**, 171 (1987).

[72] R. Keinings, and M. Jones, Phys. Fluids **30**, 252 (1987).

[73] D. Whittum, W. Sharp, S. Yu, M. Lampe, and G. Joyce, Phys. Rev. Lett. **67**, 991 (1991).

Vita

Sergey Valeriev Cheshkov was born in Sofia, Bulgaria on December 5, 1970, son of Valeriy and Katinka Cheshkovi. After graduating from the National Nature-Mathematics High School in 1988, and military service from 1988 to 1990, he enrolled in the Sofia University. He graduated in 1995 with Physics Diploma (B.S.) with concentration in "Elementary Particle and Nuclear Physics". In the Fall of 1995 he entered the Graduate School of the University of Texas at Austin. He was employed as a teaching assistant in the Physics Department of UT-Austin from 1995 to 1997 and as a research assistant in the University of Texas Institute for Fusion Studies from 1997 to present. Under the supervision of Prof. T. Tajima he worked on various advanced accelerator concepts based on plasma wakefield acceleration. He married Gergana Drandova in June 1998.

Permanent address: 926E, Dean Keeton St., # 204,
Austin, TX 78712

This dissertation was typeset with LaTeX[‡] by the author.

[‡] LaTeX is a document preparation system developed by Leslie Lamport as a special version of Donald Knuth's TeX Program.